Chapter 1

Introduction

1.1 General Background

What is "nano or nanotechnologies"? Without providing a definite answer to this question, it can be easily found around the environment. Nano has even entered popular culture. It's used as a buzzword in contemporary books, movies and television commercials. For example, in the famous movie, Inner Space (

), its story was related the application of nanotechnology and explored the mystique of human body.

Nano is a popular area of science and technology today. It has attracted the attention of scientists from all walks of life, from physics to chemistry to biology and engineering.

Nanosized particles or nanoparticles (NPs) (sizes between 1 nm to 100 nm) have received much attention, because the chemical and physical behaviors of the particles are unprecedented and remarkably different from those in bulk form. Nanosized materials have great potential applications in the electronic, biological, chemical and mechanical industries, as well as in the related technologies using catalysts, drug carriers, sensors, dyes, also as well as in magnetic, structural and electronic materials.

The mechanical properties of nano-materials have been of great importance in many current engineering science applications depending on their sizes. For example experiments have revealed that forces acting on particle-reinforced composites, torsion of thin wires, bending of thin beams, indentation of a solid, and loads on plates with holes have revealed that a substantial increase in the strength (defined as the maximum load divided by the characteristic cross sectional area of the structure) is achieved by decreasing the particle size, the wire diameter, the beam thickness, the indenter size, and the hole size,

respectively. In other words, with all other properties held constant, the smaller geometrical size is the stronger. The mechanical properties of materials, such as strength or hardness whether in simple tension, torsion, bending, or indentation testing are therefore size dependent. The phenomenon also can be observed that changes of optical, chemical or electronic behaviors of nanosized material depend on the particle size.

Due to the properties of the nanosized materials are determined not only by their compositions, but also by their size. When the particle size of the material is much smaller than its natural radius of the electron-hole pair (Wannier exciton) in a semiconductor, such as Bohr radius (~ 5-10 nm), additional energy is required to confine the excited carriers within the material leading to drastic changes of its electronic and optical properties (as shown in Fig. 1.1). For example, if the size of CdSe quantum dots (QDs) was tuned from 6 nm to 1.5 nm, and emissive color was observed blue shift from red to green (620 nm to 510 nm).

It is well known that using unagglomerated particles with narrow size distribution is the preferred state for applications and technologies, especially for compacting or sintering particles. Large number of techniques for the preparations of nanoparticles that satisfy this requirement have been developed via gas and liquid phase routes. It is important to develop this synthesis method, in which particles having controlled characteristics including size, size distribution, morphology, agglomeration, and composition, can be produced. To be industrially relevant, the process needs to be low-cost and involve both continuous operation and a high production rate. There are two distinct routes to produce QDs. In the "top down", or "physical" approach that QDs are grown by lithographic or molecular beam techniques. In the "bottom up", or "chemical" approach that QDs are synthesized by chemical colloid methods in a organic solvent medium.

The electronic energy levels of nanosized QDs are formed due to the charge

carrier confinement [1]. In very small dots, the spacing of the electronic states is much greater than the available thermal energy (strong confinement). Upon UV-excitation these QDs show strong fluorescence that is a pronounced function of size, providing the advantage of continuous spectral tunability over a wide spectral range simply by changing the size of the nanocrystal (Figure 1.2) [2].

Due to strong luminescence in combination with their high chemical flexibility, luminescent semiconductor nanocrystals are currently investigated as emitting materials for light-emitting devices [3] and biosensor for biological labeling [4]. The synthesis of monodisperse nanocrystals of desired sizes and properties is the first and very important step being a pre-requisite of their further investigation and use in practice. These deal with the development of advanced synthetic routes toward various luminescent nanomaterials. The synthesis and luminescent behaviors of various II-VI and core-shell nanocrystals prepared by chemical colloid methods are discussed in the following chapters.

1.2 Motivations

In 1993, Murray *et al.* [5] reported the synthesis of high-quality cadmium chalcogenides nanocrystals using $Cd(CH_3)_2$ as the cadmium precursor and trioctylphosphine oxide (TOPO) as the surfactants, the synthesis of CdSe QDs using this precursor/surfacant has been well developed. But the cadmium precursor, such as $Cd(CH_3)_2$, is extremely toxic, expensive, unstable at room temperature, and explosive at elevated temperatures by releasing large amount of gas.

In 1993 Honma *et al.* [6] reported that a strong surface-enhanced Raman scattering (SERS) of CdS particles was observed in Ag-CdS colloidal

nanocomposites, indicating novel optical response of CdS fine particles under a strong electric field from the surface plasma excitation of silver particles. Resonance effects in Ag-CdS hybrid aggregates where the band gap of CdS is almost equivalent to the excitation energy of the surface plasmon of Ag attract much interest in fundamental physics as well as device application points of view.

In 1998 Bruchez *et al.* [7] reported a link between biomolecules and core-shell QDs with CdSe as cores and CdS or ZnS as shells, whose surfaces were coated with silica and which were then linked to biomolecules.

In 1998 Chan *et al.* [8, 9] successfully linked proteins to the QD surface through mercaptoacetic acid, causing QDs to transfer and undergo receptor-mediated endocytosis into bio-cells.

In 1998 Nayak *et al.* generated Au-CdSe nanocomposites (NCs) [10] although a large fraction of the particles was found to be a mixture of individual gold and CdSe NPs.

In 2000 Mattoussi *et al.* [11] directly conjugated the protein through a linear polylysine chain onto the negatively charged QD surface through an electrostatic interaction.

In 2001 Peng *et al.* [12] reported the synthesis of high quality cadmium chalcogenides NPs using CdO as precursor. The scheme is reproducible and simple and thus can be readily scaled up for industrial production.

In 2001 Sun *et al.* [13] reported the use of that IgG-conjugated QDs were used to detect the antigen linked to CdSe/ZnS QDs in a readout immuno-assay; and the limit of detection was 10^{-9} M in antigen concentration.

In 2002 Coe *et al.* reported [14] the fabrication of a hybrid OLED, where QDs function exclusively as lumophores.

In 2002 Kulakovich *et al.* [15] have studied the enhancement of luminescence of CdSe/ZnS core-shell quantum dots on gold colloids as a function of semiconductor nanocrystal-metal nanoparticle distance. Using a

layer-by-layer polyelectrolyte deposition technique to insert well-defined spacer layers between gold colloids and quantum dots, a distance-dependent enhancement and quenching of quantum dot photoluminescence has been observed.

In 2003 Yang *et al.* [16] developed for the synthesis of Au@CdS core-shell nanoparticles by a directly self-assembling process. Stable Au@CdS composite colloids were prepared by thiourea, as a double functional reagents acted as the linkage agent between Cd^{2+} ions and gold nanoparticles. The CdS-capped gold composite nanoparticles were successfully integrated into $BaTiO_3$ films. The significant enhancement of nonresonant third-order nonlinear optical nonlinearities of Au/CdS core-shell nanoparticles was reported.

In 2004 Park *et al.* [17] reported experiments on polymer light-emitting diodes made with poly(9,9′-dioctylfluorene)/gold nanocomposites to solve these drawbacks. Blue polymer light-emitting diodes with enhanced luminescent stability were obtained by incorporating 5-10-nm gold nanoparticles as the quenchers of the triplet states of blue emitting polymer. The nanocomposite light-emitting diodes exhibited an enhanced quantum efficiency due to the roughening of the surface onto which the Al cathode is deposited and to balanced charge injection.

In 2004 Chaudhary *et al.* [18] demonstrated a trilayer polymer-quantum dot OLED which was fabricated by sandwiching a CdSe/ZnS QDs layer between films of polyvinylcarbazole (PVK) and butyl-oxadiazole derivative.

In this dissertation, we have succeeded in incorporating luminescent CdSe QDs into a hybrid OLED. The other important target is using luminescent CdSe in fabrication of biosensor. The synthesis of high quality water-soluble CdSe QDs is a very important step. Figure 1.3 presents a simple route that luminescent hydrophobic CdSe QDs through surface modification to form water-soluble CdSe QDs.

1.3 Organizaion of the Thesis

This thesis is divided into six chapters. The contents in each chapter are described as following.

In Chapter 1, a brief introduction of the general background of nanoparticles and luminescent materials (ie. CdSe and CdSe/ZnS) for the current engineering science or bio-technology applications is presented.

Chapter 2 describes the synthesis of various II-VI semiconductor nanocrystals of desired sizes by chemical colloid methods and characterizations of their optical (or physical) properties.

Chapter 3 reports the applications of surface-functionalized CdSe quantum dots in immuno-assay.

In Chapter 4 the interesting enhancement effects of phosphorescence and electroluminescence from triplet emitter by CdSe quantum dot doping are discussed.

Chapter 5 presents the enhanced luminescence of CdSe/ZnS by doping gold noparticles. These results are applied on electroluminescence devices.

Chapter 6 summarizes all experimental results and future work in the dissertation.

1.4 Reference

[1] S. V. Gaponenko, Optical properties of Semiconductor Nanocrystals, Cambridge University Press : Cambridge (1998).

[2] A. P. Alivisatos, J. Phys. Chem. **100** (1996) 13226.

[3] V. L. Colvin, M. C. Schlamp, A. P. Alivisatos, Nature **370** (1994) 354.

[4] M. P. Bruchez, M. Moronne, P. Gin, S. Weiss, A. P. Alivisatos, Science **281** (1998) 2013.

[5] C. B. Murray, D. J. Norris, M. G. Bawendi: J. Am. Chem. Soc. **115** (1993)

8706.

[6] I. Honma, T. Sano, and H. Komiyama, J. Phys. Chem. **97** (1993) 6692.

[7] M. Bruchez Jr., M. Moronne, P. Gin, S. Weiss, A. P. Alivisatos, Science **281** (1998) 2013-2016.

[8] W. C. W. Chan, S. Nie, Science **281** (1998) 2016.

[9] W. C. W. Chan, D. J. Maxwell, X. Gao, R. E. Bailey, M. Han, S. Nie, Biotechnology **13** (2002) 40.

[10] R. Nayak, J. Galsworthy, P. Dobson, J. Hutchinson, J. Mater. Res. **13** (1998) 905.

[11] H. Mattoussi, J. M. Mauro, E. R.Goldman, G. P. Anderson, V. C. Sundar, F. V. Mikulec, M. G. Bawendi, J. Am. Chem. Soc. **122** (2000) 12142.

[12] Z. A. Peng, X. G. Peng: J. Am. Chem. Soc. **123** (2001) 183.

[13] B. Sun, W. Xie, G.. Yi, D. Chen, Y. Zhou, J. Cheng, J. Immunological. Methods **249** (2001) 85.

[14] S. Coe, W.-K. Woo, M. Bawendi, V. Bulovic, Nature **420** (2002) 800.

[15] O. Kulakovich, N. Strekal, A. Yaroshevich, S. Maskevich, S. Gaponenko, I. Nabiev, U. Woggon, and M. Artemyev, Nano Lett. **2** (2002) 1449.

[16] Y. Yang, J. Shi, H. Chen, S. Dai, Y. Liu, Chem. Phys. Lett. **370** (2003) 1.

[17] J. H. Park, Y. T. Lim, O. O. Park, J. K. Kim, J. W. Yu, and Y. C. Kim, Chem. Mater. **16** (2004) 688.

[18] S. Chaudhary, M. Ozkan, W. C. W. Chan, Appl. Phys. Lett. **84** (2004) 2925.
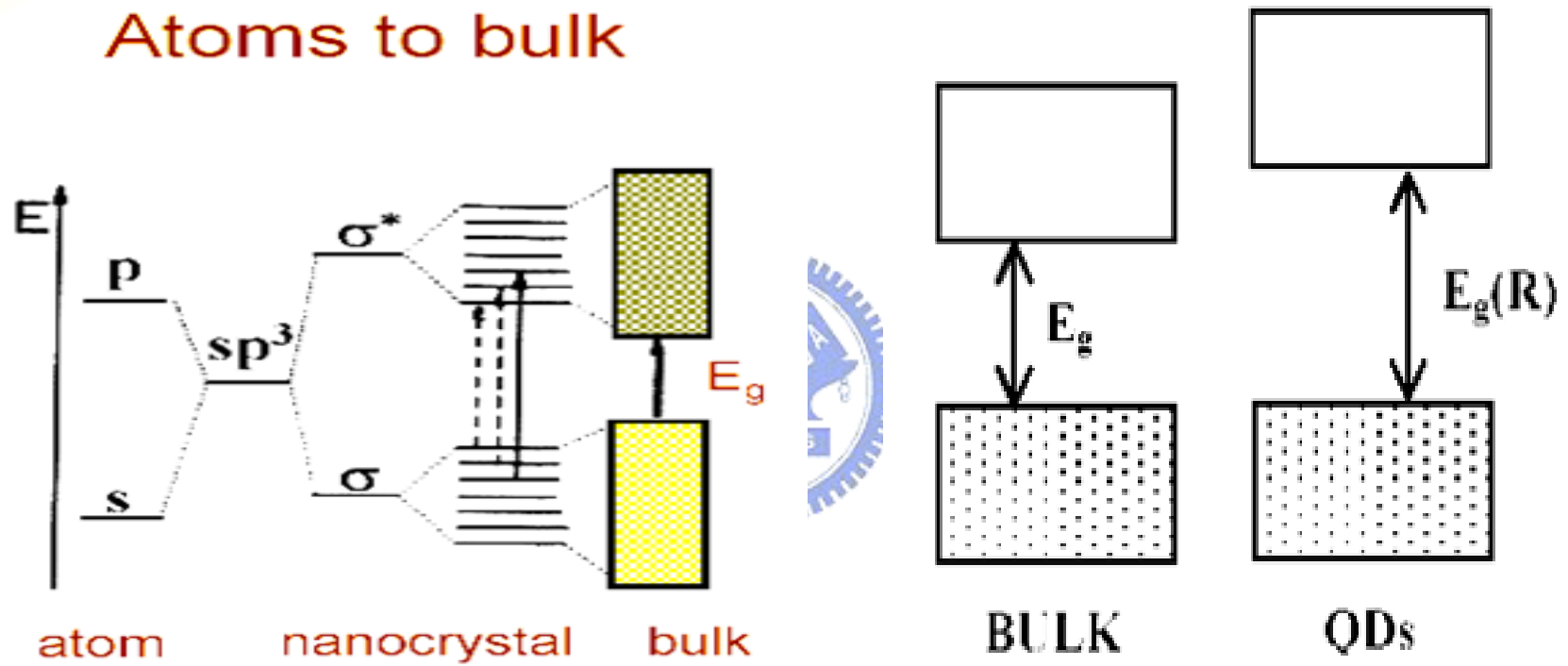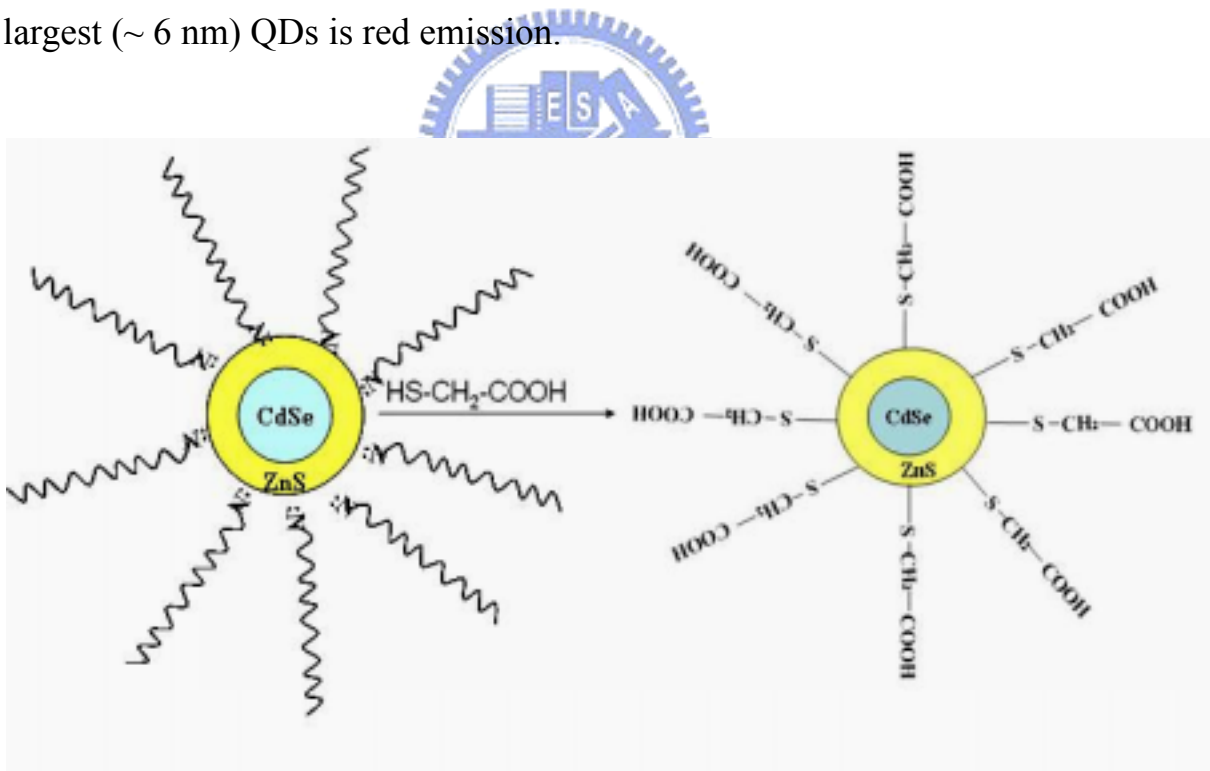
Figure 1.1 The changes of energy levels within atoms and bulk.

Figure 1.2 Size-dependence of the PL color for colloidal solutions of CdSe QDs passivated with a ZnS shell. The smallest (~ 1.7 nm) CdSe QDs emit blue, the largest (~ 6 nm) QDs is red emission.

Figure 1.3 Water-soluble QDs combined with the molecules having specific functional groups (-NH$_2$, -COOH) for technical applications.

Chapter 2

Synthesis and Characterizations of CdSe and Au-CdSe Quantum Dots

Abstract

With a modified synthetic route, we have successfully synthesized a series of monodispersed and high-quality hexadecylamine (HDA)-capped CdSe, CdSe/ZnS and Au-CdSe nanoparticles that exhibit excellent photoluminescence (PL) and photo-stability. The PL QE of the CdSe nanocrystals can be considerably improved by post-preparative surface passivation with an inorganic (ZnS) and organic (amines, HDA) shell. The PL QE of CdSe nanocrystals was increased to ~ 50%. The A strong surface-enhanced Raman scattering (SERS) of semiconductors shell was observed in Au/CdSe colloidal nanocomposites. When the amounts of Au NPs in CdSe NPs (ie., Au-CdSe NCs) were larger than 5%, the XRD peak of Au (2 θ = 38° and 44°) was observed clearly. Due to the SERS effect of Au NPs, the PL quantum efficiency of Au-CdSe/ZnS nanocomposites was increased to ~ 70%.

2.1 Introduction

Colloidal semiconductor nanoparticles (NPs) or QDs have received much attention in fundamental research and technical applications in recently years due to the strong size dependent properties and excellent chemical processibility [1-4]. The size-dependent optical properties of quantum dots with band edge tunable through visible range had received particular interests for fundamental

research and potential applications [5, 6]. Synthesis of high-quality semiconductor QDs has been playing a critical role in this very active field [7]. As the most developed system in terms of synthesis, high-quality CdSe QDs [8] with nearly monodisperse size and shape are in active industrial development for biological labeling reagents [9, 10]. In 1993, Murray *et al.* [11] reported the synthesis of high-quality cadmium chalcogenides nanocrystals using $Cd(CH_3)_2$ as the cadmium precursor and trioctylphosphine oxide (TOPO) as the surfactants, the synthesis of CdSe QDs using this precursor/surfacant has been well developed. $Cd(CH_3)_2$ is extremely toxic, expensive, unstable at room temperature, and explosive at elevated temperatures by releasing large amount of gas. Due to these reasons, the $Cd(CH_3)_2$-related schemes require very restricted equipments and conditions and are not suited for large-scale synthesis. In 2001, Peng *et al.* [12] reported the synthesis of high quality cadmium chalcogenides NPs using CdO as precursor. The scheme is reproducible and simple and thus can be readily scaled up for industrial production. Honma *et al.* [13] reported a strong surface-enhanced Raman scattering (SERS) of CdS particles was observed in Ag-CdS colloidal nanocomposites, indicating novel optical response of CdS fine particles under a strong electric field from the surface plasma excitation of silver particles. Resonance effects in metal-semiconductor hybrid aggregates where the band gap of semiconductor is almost equivalent to the excitation energy of the surface plasmon of metal attract much interest in fundamental physics.

We report here the synthesis of a series of monodispersed CdSe, CdSe/ZnS and Au-CdSe NPs by chemical colloid methods using CdO as a cadmium precursor with HDA and TOPO as capping agents. Using CdO as precursor showed better thermal-stability, safer, cheaper and reproducible on comparison

to that of dimethyl cadmium precursor. Typically, the nucleation temperature need to be 250 ~ 360 °C. Here, different monodispersed and high-quality luminescent CdSe QDs have been synthesized by controlling the low nucleation temperature (160 ~ 220 °C) and Se/TBP injection (< 1 sec).

2.2 Experimental Section

2.2.1 Chemicals

Cadmium oxide (99.5 %), selenium powder (99.5 %) and technical-grade (90 %) trioctylphosphine oxide (TOPO) were all purchased from Aldrich Chemicals (Saint Louis MO, USA). 1-Hexadecylamine (HDA) (98 %) and stearic acid (99 %) and 1-heptanol were purchased from Lancaster (Lancashire, UK). Tri-n-butylphosphine (TBP) was purchased from Showa (Tokyo, Japan). Anhydrous methanol, toluene and chloroform was purchased from TEDIA (Fairfield OH, USA). Hydrogen tetrachloroaurate (III) ($HAuCl_4$) and tetraoctylammonium bromide (TOAB) were purchased from Acros Chemicals Company (Geel, Belgium).

2.2.2 Instrumentations

Furthermore, a JEOL JEM-4000EX transmission electron microscope (TEM) operated at 200 kV was used for morphology determination of QDs. Photoluminescence (PL) excitation and emission spectra were collected at room temperature using a monochromatized Xe light source (300W). The emission spectra of various QDs were obtained using an excitation wavelength (λ_{ex}) of 367 nm. Absorption spectra of QDs were measured with a UV-visible spectrophotometer (Hitachi, U-3010). The concentration of the CdSe samples

for PL and UV-Visible measurements were 20 mg in 5ml chloroform.

2.2.3 Synthesis of TOPO/HDA-cappedCdSe QDs

CdSe QDs were synthesized by dissolving CdO (0.6 mmol), HDA (10 mmol), TOPO (4 mmol) and stearic acid (1.5 mmol) in 20 ml TBP, which was then heated at 250 for 2 h under nitrogen atmosphere. The parent CdSe QDs were readily obtained by reacting Se stock solution with CdO and the reaction mixture was kept for 10 sec at desired temperature (160 ~ 220). The reaction temperature was adjusted to 120 immediately after the injection. The reaction mixture was then allowed to cool to ~ 60 . Purified nanocrystallites are dispersed in 20 ml of anhydrous 1-heptanol forming an optically clear solution. Then anhydrous methanol was added to precipitate the CdSe NPs and excess TBP, TOPO and HDA were removed. The resulting powder is readily dispersed in chloroform.
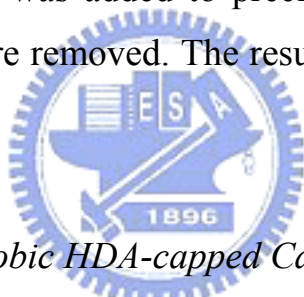
2.2.4 Synthesis of hydrophobic HDA-capped CdSe/ZnS QDs

The core-shell type CdSe/ZnS QDs was synthesized as follows: CdO (0.6 mmol) and 1-Hexadecylamine (HDA) (10 mmol) were dissolved in 20 ml tributylphosphine (TBP), which was then heated at 250 for 2 hrs under nitrogen atmosphere. The parent CdSe QDs were readily obtained by reacting with selenium (Se) stock solution whose 5 ml TBP solution contained 0.6 mmol of Se, and the mixture was reacted at desired temperature (160 ~ 220). The reaction temperature was adjusted to 120 immediately after the injection. The core-shell CdSe/ZnS can then be synthesized by injecting 5 ml of TBP solution containing ZnS (ie., 0.08 mmol of znic acetate and 0.08 mmol of sulfur were dissolved in 5 ml of TBP) stock solution and allow to react for 30 min. The reaction mixture was allowed to cool to 60 . Then anhydrous methanol was added to precipitate the CdSe/ZnS NPs and excess TBP and HDA were removed.

The resulting powder was readily dispersed in toluene.

2.2.5 Synthesis of hydrophobic TOAB-capped Au NPs

A 25 ml aqueous solution of $HAuCl_4$ (0.3 mmol) was added to an 80 ml toluene solution of tetraoctylammonium bromide (1.8 mmol). The transfer of the Au metal salt to the toluene phase was clearly visualized within a few seconds. 25 ml of 0.25 M $NaBH_4$ solution was then added to the stirred mixture, resulting immediately reduction. Then the two phases were separated and the toluene phase was subsequently washed with dilute H_2SO_4, NaOH, and H_2O, and then dried over anhydrous $NaSO_4$.

2.2.6 Synthesis of HDA-capped Au-CdSe nanocomposites

Au-CdSe NPs were synthesized by dissolving CdO (0.6 mmol) and HDA (9 mmol) in 20 ml TBP, which was then heated at 260   for 2 hrs under nitrogen atmosphere. Then 1ml of Au NPs (6 x 10^{-4} M) was injected into the reaction mixture. The parent Au-CdSe QDs were readily obtained by reacting with selenium (Se) stock solution whose 5 ml TBP solution contained 0.6 mmol of Se, and the mixture was reacted at desired temperature (160~260   ) . The reaction temperature was adjusted to 120   immediately after the injection. The reaction mixture was allowed to cool to ~ 60   . Then anhydrous methanol was added to precipitate the Au-CdSe NPs and excess TBP and HDA were then removed. The resulting powder is readily dispersed in pre-dried chloroform.

2.3 Results and discussion

Among all the reactions, stearic acids were determined as the most versatile ligand / solvent. The initial molar ratio of CdO to stearic acid was varied

between 1 : 3 and 1 : 6 and the reddish CdO was found to be soluble and generate a colorless homogeneous solution at about 200 °C.

By adjusting the composition of capping agents of HDA / TOPO, the variation of luminescence intensity of CdSe QDs can be investigated. Figure 2.1 shows a series of PL spectra for CdSe QD stabilized in chloroform and capped with different molar ratio of HDA / TOPO. The nucleation temperature of all the reactions were controlled at 220 °C and reaction time was maintained for 2 minutes. By the same condition, the CdSe QDs capped with only HDA have excellent photoluminescence and photostability. When the concentration of TOPO was increased, the PL luminescent intensity as well as the solubility of CdSe QDs in chloroform was observed to decrease. The interaction between TOPO and CdO is comparatively stronger than the interaction between HDA and CdO, which facilities the formation of HDA capped CdSe QDs and hence stronger emission was observed for the case of HDA capped QDs. Figure 2.2 shows the PL and UV-visible absorption spectra for a green-emitting CdSe QDs with nucleation temperature of 170 °C stabilized in chloroform. The size of the CdSe QDs synthesized by the above procedure was ca. 2 nm. The optimal λ_{ex} was found to be 367 nm, whereas λ_{em} was observed to be 510 nm with full width at half maximum (FWHM) of 30 nm. As indicated in Fig. 2.2, the UV-Vis spectra, the absorption band was found to center at 490 nm, the absorption band was expected to exhibit an apparent red shift, as the size of CdSe increases. The particle size of CdSe QDs based on the wavelength of absorption edge can also be estimated. The TEM image of the green-emitting CdSe QD represented in Fig. 2.3 shows that spherical dots with diameter of ca. 2 nm were identified as CdSe QDs. Figure 2.4 shows powder X-ray diffraction (P-XRD) of the CdSe nanocrystals. In the case of smaller CdSe nanoparticles, the XRD patterns do not allow us to distinguish between the cubic and the hexagonal phases unambiguously.

The room temperature PL quantum efficiency (QE) of as-prepared CdSe

nanoparticles was in the range of 10-25% and has a tendency to decrease with increasing particle size. However, the PL QE of the CdSe nanocrystals can be considerably improved by post-preparative surface passivation with an inorganic (ZnS) or organic (amines, HDA) shell. This is a strong hint that the PL efficiency losses are due to insufficient passivation of surface traps.

In Fig. 2.5, as compared to CdSe NPs, the UV-absorption band of CdSe/ZnS NPs is red shifted by ~12 nm. It is reasonable that the inorganic ZnS-capped CdSe NPs made the effective particle size larger as compared to that of the sole CdSe NPs and hence improved the quantum efficiency. Figure 2.6 shows the PL spectra for HDA-capped CdSe and CdSe/ZnS NPs. The NPs was dispersed in toluene and the concentration was fixed to 1×10^{-4} M. The optimal λ_{ex} of the HDA-capped CdSe and CdSe/ZnS NPs was found to be 375 nm, whereas the λ_{em} was observed to be 584 nm and 592 nm, respectively. The FWHM (full-width at half-maximum) of these colloidal NPs is about 30 nm. As compared to that of CdSe NPs, the PL emission of CdSe/ZnS NPs is red shifted by ~ 8 nm and the luminescence intensity is increased for about 1.5 times. As indicated in Fig. 2.7, the fluorescence decay of CdSe and CdSe/ZnS NPs was determined based on time-resolved luminescence measurements. According to the results of fluorescence decay of these NPs, the quantum efficiency can be easily calculated [14]. The PL quantum efficiency of CdSe/ZnS nanocrystals was increased to ~ 50%. It is well known that ZnS with the higher energy bandgap than CdSe can effectively improve the quantum efficiency of CdSe QDs, due to the quantum confinement effect of ZnS.

The composites of metal/semiconductor NPs have been reported to exhibit strongly enhanced nonlinear response by several orders of magnitude higher than their single-component [13]. A strong surface-enhanced Raman scattering (SERS) of semiconductors shell was observed in Au/semiconductor or Ag/semiconductor colloidal nanocomposites [13, 15]. The enhancement of the optoelelectronic properties is widely accepted from the surface plasma

excitation of Au or Ag NPs [13, 15]. It is interesting to explore the luminescent mechanism between metallic NPs and CdSe NPs. Here, we have reported the synthesis of Au/CdSe and Au-CdSe/ZnS nanocomposites, and explored the possibility of PL intensity enhancement of CdSe QDs in the presence of Au NPs.

Figure 2.8 shows the powder XRD patterns of Au, CdSe and Au-CdSe NPs. When the amounts of Au NPs in CdSe NPs were larger than 5%, the XRD peak of Au (2 θ = 38° and 44°) was observed clearly. The TEM images of HDA-capped Au-CdSe nanocomposites show that spherical dots have diameter of ~ 5 nm as indicated in Fig. 2.9. Due to the SERS effect of Au NPs, the PL quantum efficiency of Au-CdSe/ZnS nanocomposites was increased to ~ 70%. The SERS-activity of Au metal in Au-CdSe/ZnS NCs. will be detailed and discussed in Chapter 5.

2.4 Conclusions

By employing a modified synthetic route we have synthesized high-quality HDA-capped CdSe and Au-CdSe NPs by chemical colloid methods that exhibit decent PL intensity and photostability. The PL quantum efficiency of HDA-capped CdSe NPs is markedly higher than that of TOPO-capped CdSe NPs. The PL quantum efficiency of HDA-capped CdSe/ZnS NPs was ~ 50 %. The PL quantum efficiency of HDA-capped Au-CdSe/ZnS NPs was ~ 70 %. The increase in the PL intensity of Au-CdSe/ZnS NCs was attributable to the SERS-activity of Au metal in Au-CdSe/ZnS NCs.

2.5 Reference

[1] A. P. Alivisatos: Science **271** (1996) 933.

[2] X. G. Peng, L. Manna, W. D. Yang, J. Wickham, E. Scher, A. Kadavanich, A. P. Alivisatos: Nature **404** (2000) 59.

[3] W. Huynh, X. Peng, A. P. Alivisatos: Adv. Mater. **11** (1999) 923.

[4] H. Mattoussi, L. H. Radzilowski, B. O. Dabbousi, E. L. Thomas, M. G. Bawendi, M. F. Rubner: J. Appl. Phys. **83** (1998) 7965.

[5] S. Coe, W.K. Woo, M. Bawendi, M. & V. Bulovic´: Nature **420** (2002) 800.

[6] T. Tsutsui: Nature **420** (2002) 752.

[7] X. G. Peng, J. Wickham, A. P. Alivisatos: J. Am. Chem. Soc. **120** (1998) 5343.

[8] (a) A. R. Kortan, R. Hull, R. L. Opila, M. G. Bawendi, M. L. Steigerwald, P. J. Carroll, L. E. Brus: J. Am. Chem. Soc. **112** (1990) 1327. (b) M. A. Hines, P. Guyot-sionnest, J. Phys. Chem. **100** (1996) 468. (c) B. O. Dabbousi, J. Rodriguez-Viejo, F. V. Mikulec, J. R. Heine, H. Mattoussi, R. Ober, K. F. Jensen, M. G. Bawendi: J. Phys. Chem. **101** (1997) 9463.

[9] M. Bruchez, M. Moronne, P. Gin, S. Weiss, A. P. Alivisatos: Science **281** (1998) 2013.

[10] W. C. W. Chan, S. M. Nie: Science **281** (1998) 2016.

[11] C. B. Murray, D. J. Norris, M. G. Bawendi: J. Am. Chem. Soc. **115** (1993) 8706.

[12] Z. A. Peng, X. G. Peng: J. Am. Chem. Soc. **123** (2001) 183.

[13] I. Honma, T. Sano, H. Komiyama, J. Phys. Chem. **97** (1993) 6692.

[14] B. Valeur, Molecular fluorescence: principles and applications;

Wiley-VCH : New York; (2002) p. 42, 172.

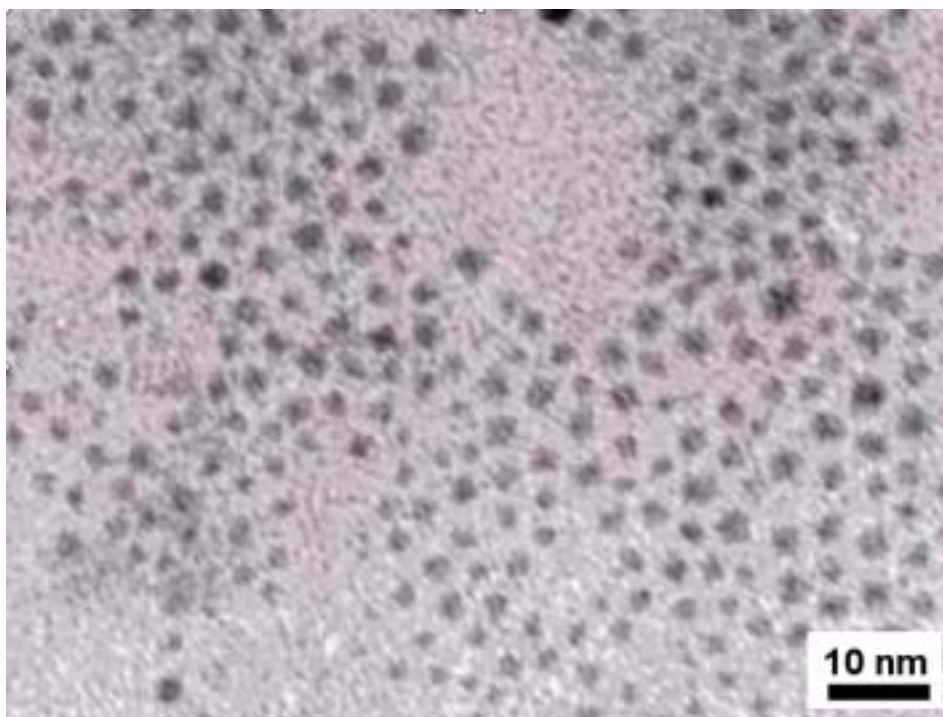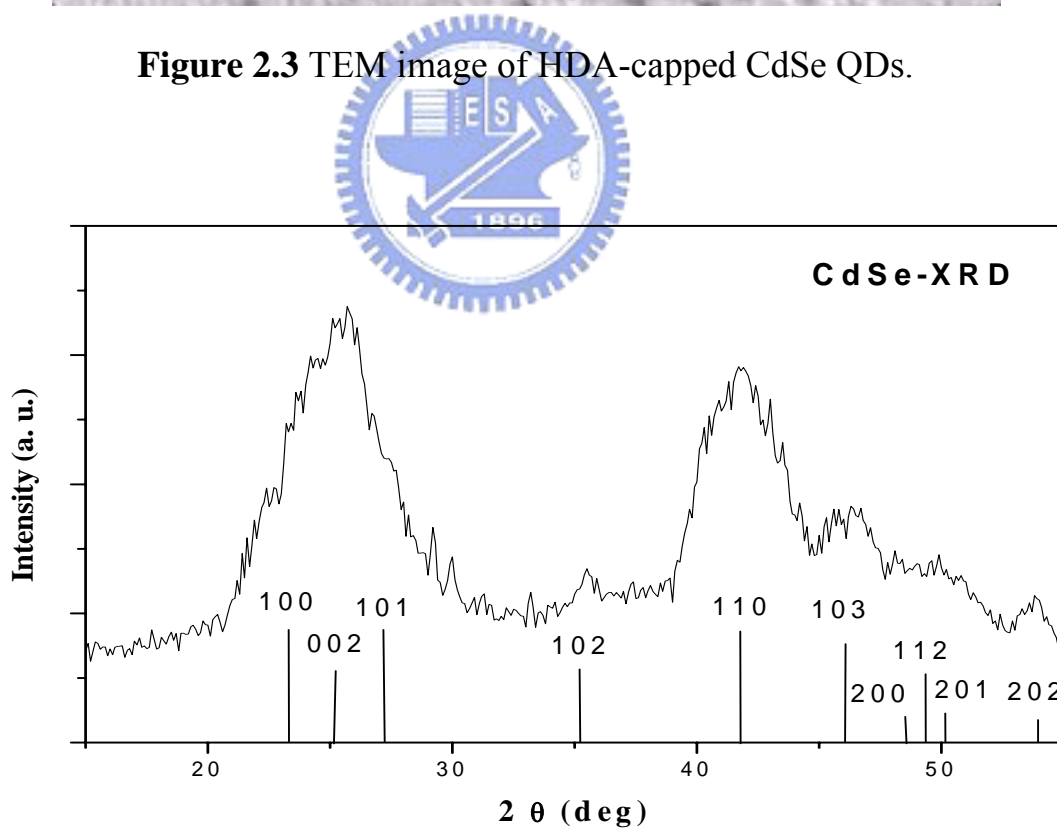[15] G. Oldfield, T. Ung, P. Mulvaney, Adv. Mater. **12** (2000) 1519.
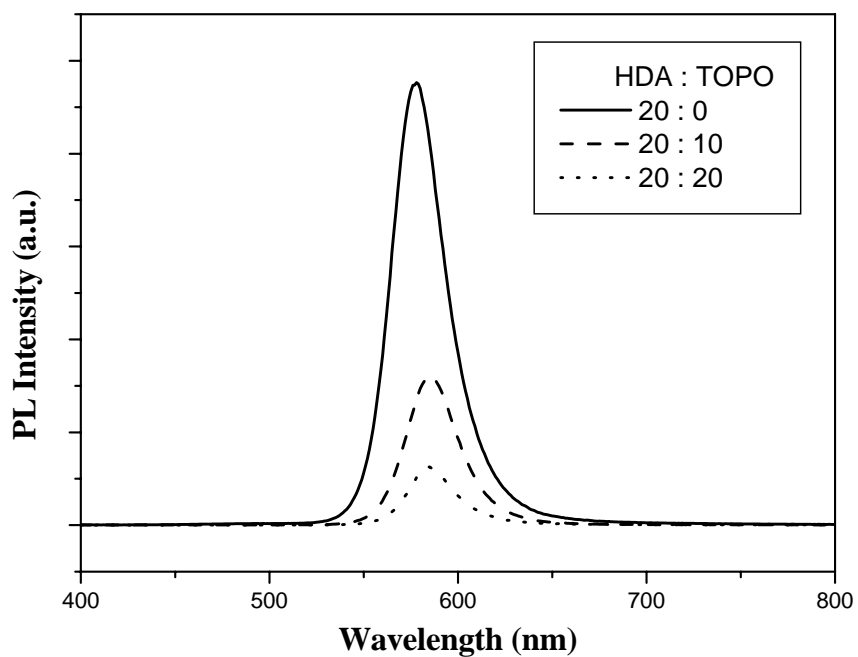
Figure 2.1 Comparison of solution PL spectra of CdSe QDs capped with different compositions of HDA/TOPO in chloroform.
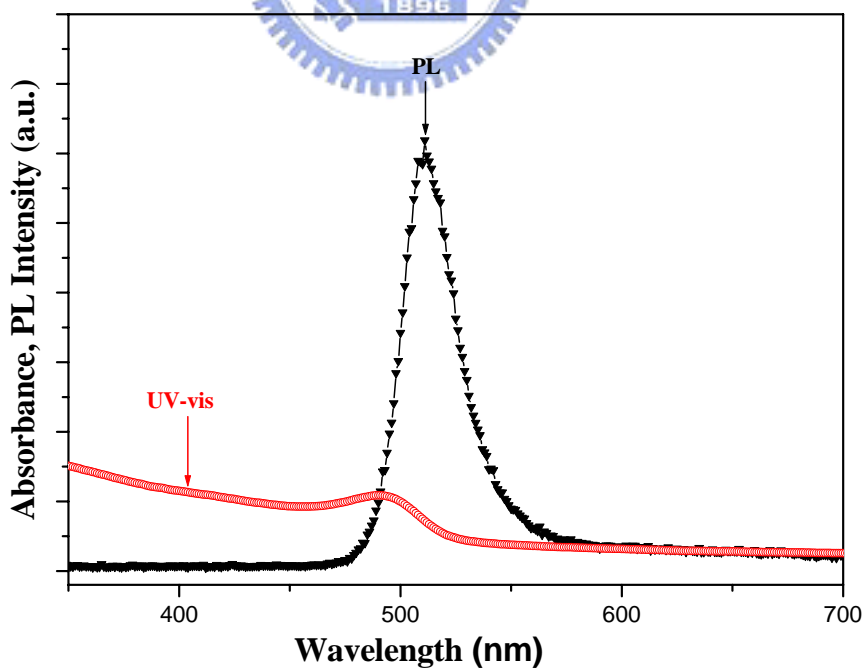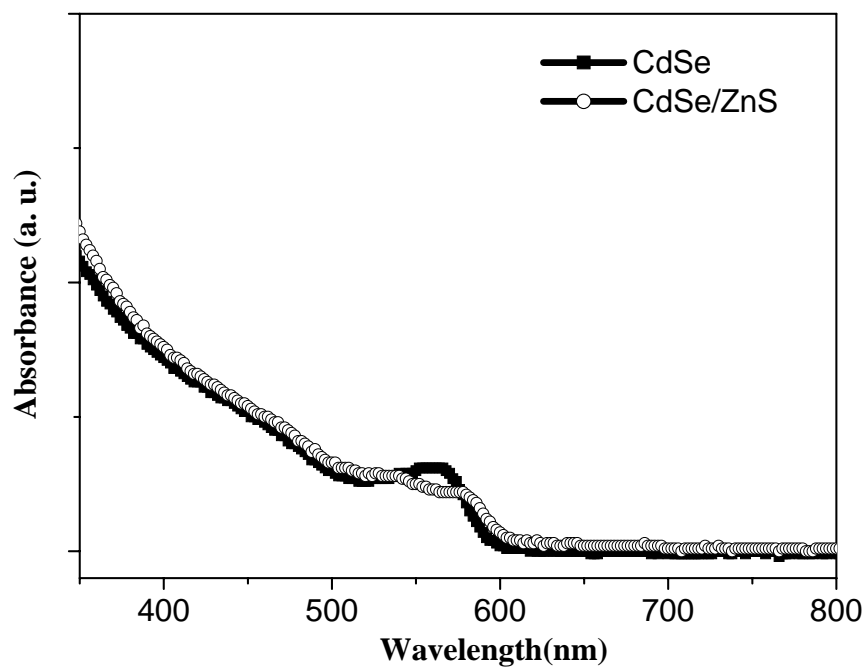

Figure 2.2 Comparison of PL and UV-Vis absorption spectra for HDA-capped CdSe QDs (size of ~2 nm) in chloroform.
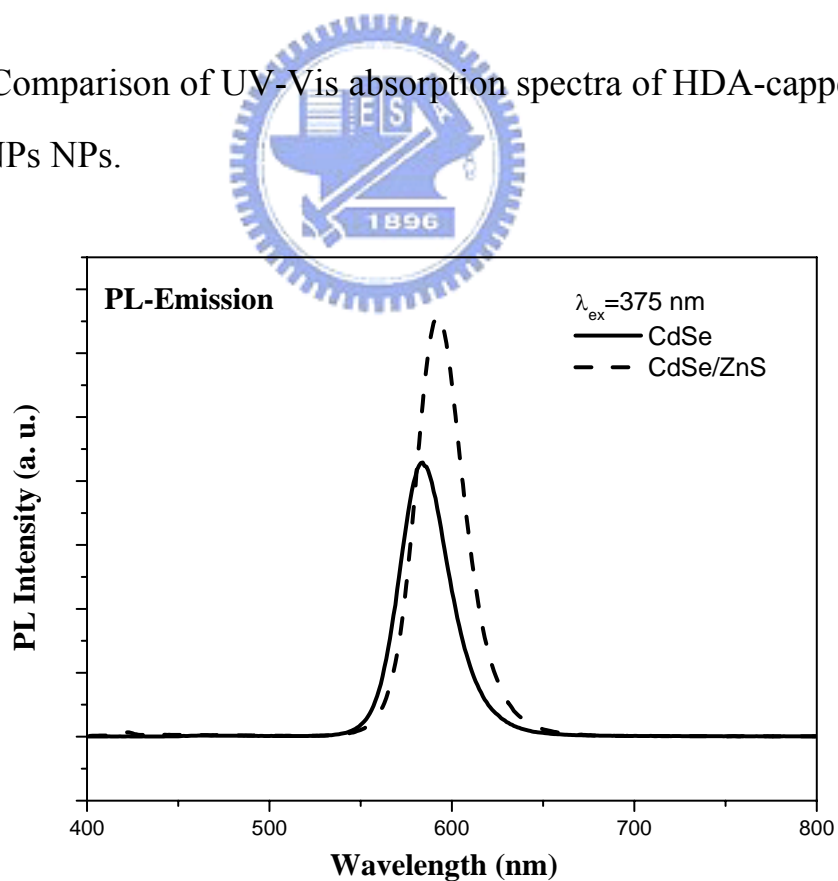
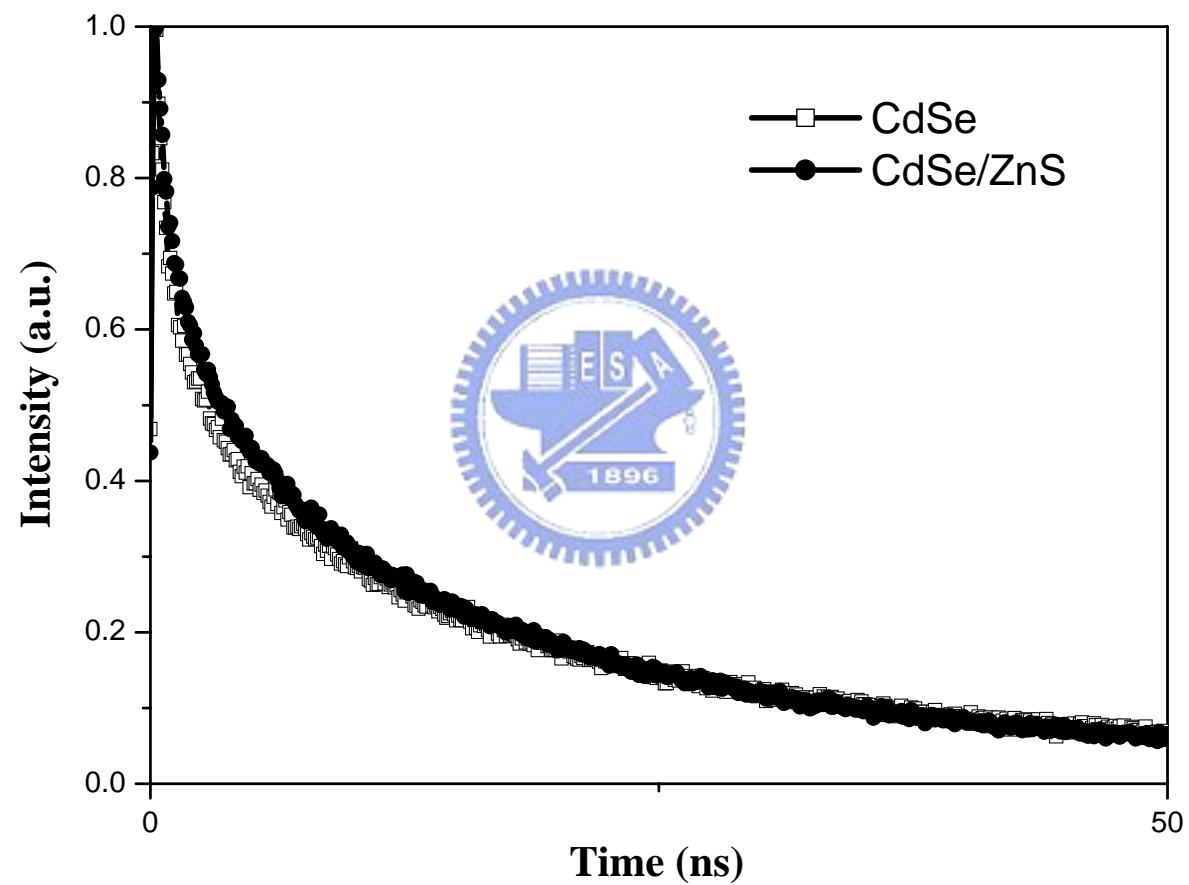**Figure 2.3** TEM image of HDA-capped CdSe QDs.

Figure 2.4 Powder X-ray diffractogram of CdSe nanocrystals. Vertical lines indicate bluk hexagonal CdSe reflections (wurtzite).

Figure 2.5 Comparison of UV-Vis absorption spectra of HDA-capped CdSe and CdSe/ZnS NPs NPs.

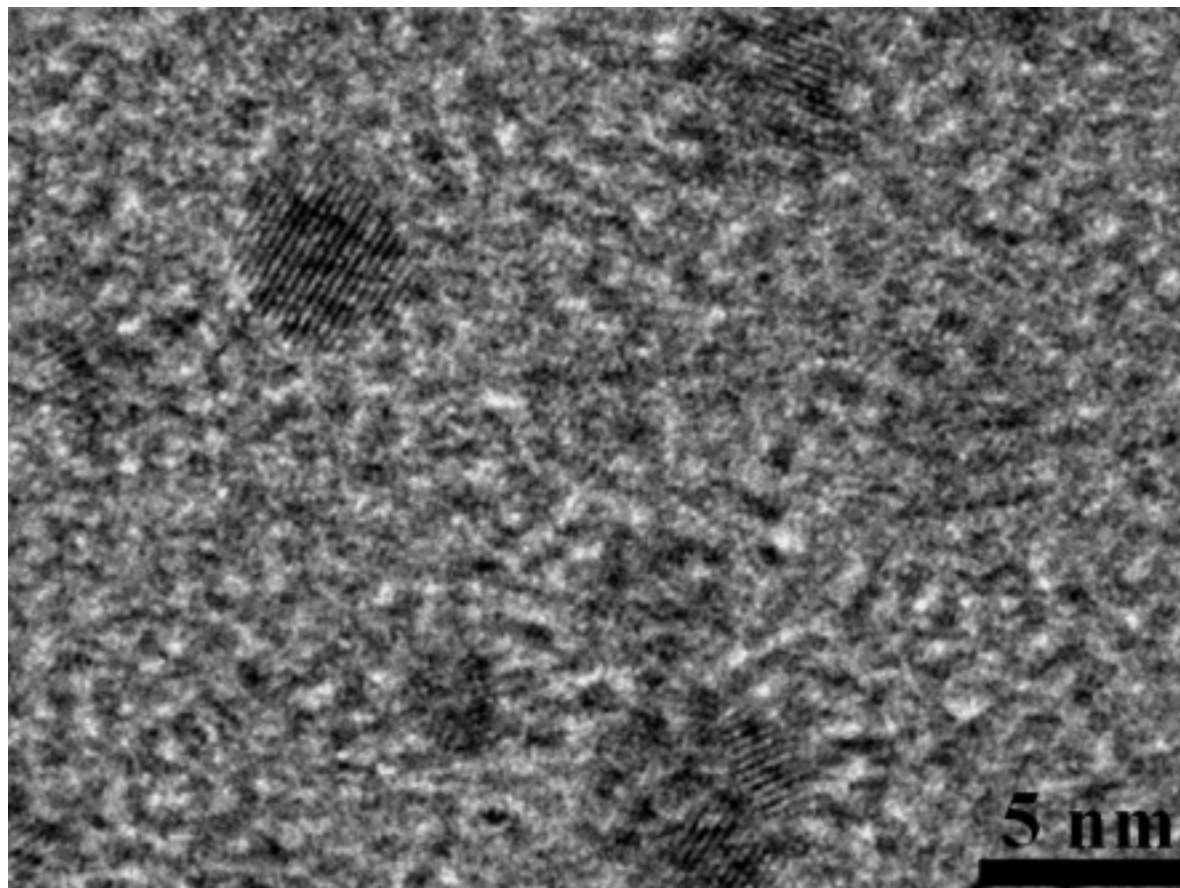**Figure 2.6** Comparison of PL spectra of HDA-capped CdSe and CdSe/NPs NPs.

Figure 2.7 Comparison of fluorescence decay of CdSe and CdSe/ZnS NPs.
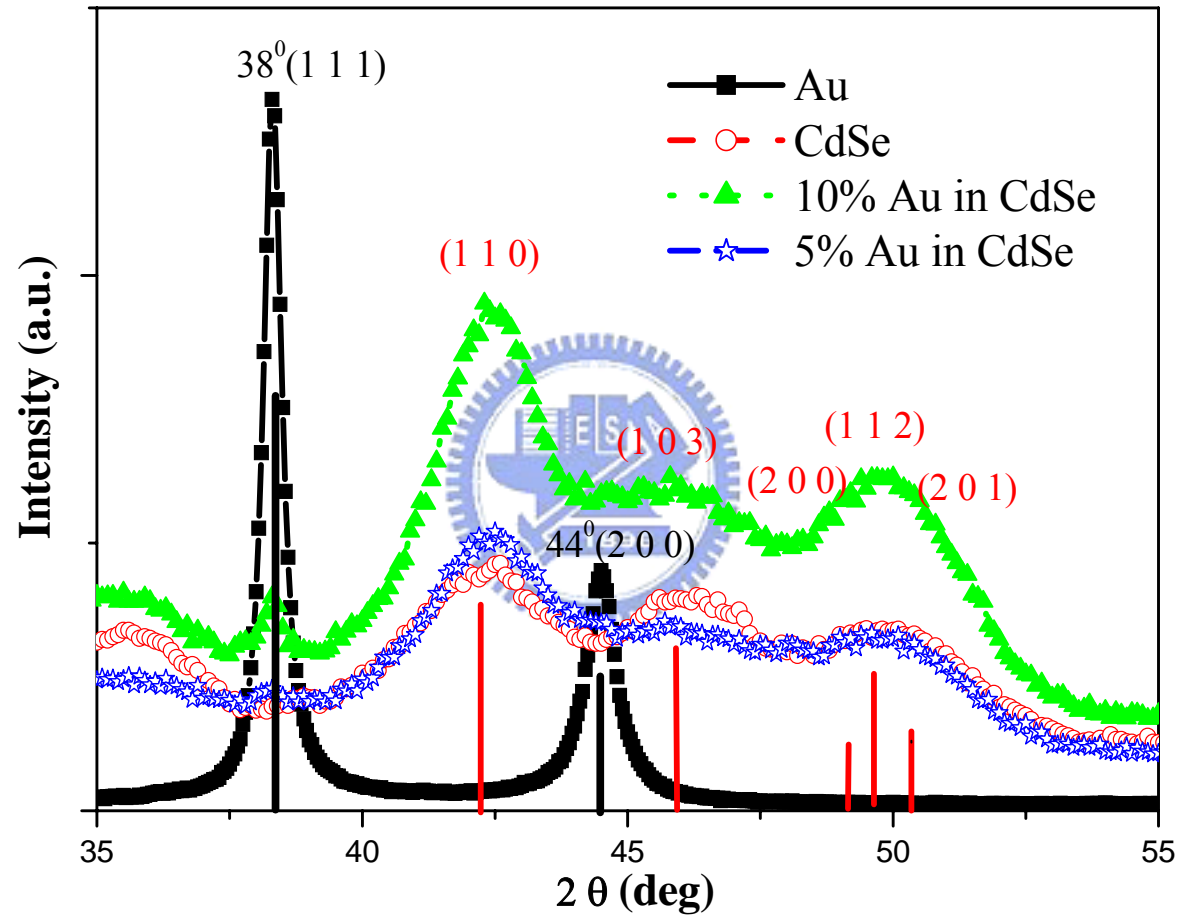
Figure 2.8 Comparison of powder X-ray diffractogram of Au, CdSe and Au-CdSe nanoparticles.

Figure 2.9 HR-TEM image of HDA-capped Au-CdSe NPs.

Chapter 3

Synthesis, Characterizations and Applications of Surface-Functionalized CdSe Quantum Dots in Immuno-assay

Abstract

High-quality hexadecylamine (HDA)-capped CdSe quantum dots (QDs) that exhibit excellent photoluminescence (PL) and photostability have been successfully synthesized with a modified synthetic route. The HDA-capped CdSe QDs can be further converted into -COOH functionalized water-soluble mercaptoacetic acid (MAA)-capped and mercaptosuccinic acid (MSA)-capped CdSe QDs that also exhibit decent PL intensity and photostability. The feasibility of water-soluble MAA-capped CdSe QDs used as fluorescent immuno-labeling agents in the detection of human antibody IgE have also been demonstrated and the results are reported.

3.1 Introduction

Conventional organic dyes used for diagnostics applications and in biological labeling reagents often exhibit characteristics that limit the effectiveness in these applications. Organic fluorophores have narrow excitation bands and broad emission spectra compared with CdSe QDs. High-quality CdSe QDs represent a new class of luminescent probes that overcome many inherent problems associated with organic fluorophores. Synthesis of high-quality water-soluble CdSe quantum dot have received much attention to bio-technical applications, due to the size-dependent tunable photoluminescence with broad

excitation spectra of CdSe QDs and narrow emission bandwidths (full width at half maximum of ~ 30 nm) that span the visible spectrum. Luminescence of CdSe QDs can be detected at concentrations comparable to organic dyes by using conventional fluorescence methods, and individual QDs and QD-bioconjugates are easily observed by confocal microscopy or bio-scanner [1-3]. In this research, we present the synthesis of water-soluble CdSe QDs and their applications for fluorescence bio-labeling.

3.2 Experimental Section

3.2.1 Chemicals

Cadmium oxide (99.5 %), selenium powder (99.5 %) and technical-grade (90 %) trioctylphosphine oxide (TOPO) were all purchased from Aldrich Chemicals (Saint Louis MO, USA). 1-Hexadecylamine (HDA) (98 %), stearic acid (99 %), mercaptoacetic acid (MAA) (98 %) and mercaptosuccinic acid (MSA) were purchased from Lancaster (Lancashire, UK). Tri-n-butylphosphine (TBP) was purchased from Showa. Anhydrous methanol, toluene, chloroform, ether, pyridine and tetrahydrofuran (THF) was purchased from TEDIA (Fairfield OH, USA). α-Human-IgE-biotin and bovine serum albumin (BSA) were purchased from Kirkegaard & Perry Laboratories (Gaithersburg MD, USA). Ethyl-3-(dimethylaminopropyl)-carbodiimide (EDC) and N-hydroxysulfo-succinimide (NHS) were purchased from Pierce Chemicals (Woburn MA, USA).

3.2.2 Instrumentations

Furthermore, a JEOL JEM-4000EX transmission electron microscope (TEM)

operated at 200 kV was used for morphology determination of QDs. Photoluminescence (PL) excitation and emission spectra were collected at room temperature using a monochromatized Xe light source (450W). The emission spectra of various QDs were obtained using an excitation wavelength (λ_{ex}) of 367 nm. Absorption spectra of QDs were measured with a UV-visible spectrophotometer (Hitachi, U-3010). The concentration of samples for PL and UV-visible measurements were 20 mg in chloroform or in phosphate buffer solution (pH = 7.4). A Gene Pix model 4000 microarray laser confocal scanner obtained from Axon Instruments, Inc. (Union City, CA) and a Jobin-Yvon Spex Fluolog-3 spectrophotometer were used to investigate the fluorescence characteristics of the samples. Nitrocellulose slides were supplied by Industrial Technology Research Institute, Taiwan.
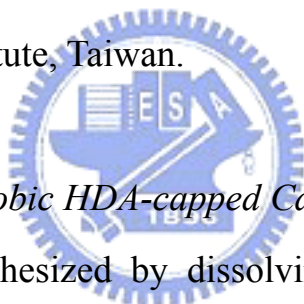
3.2.3 Synthesis of hydrophobic HDA-capped CdSe and CdSe/ZnS QDs

CdSe QDs were synthesized by dissolving CdO (0.6 mmol), HDA (10 mmol), TOPO (4 mmol) and stearic acid (1.5 mmol) in 20 ml TBP, which was then heated at 250 °C for 2 h under nitrogen atmosphere. The parent CdSe QDs were readily obtained by reacting with Se stock solution (0.12 mmol of Se powder was dissolved in 5 ml of TBP) with CdO and the reaction mixture was kept for 10 sec at desired temperature (160 ~ 220 °C). The reaction temperature was adjusted to 120 °C immediately after the injection. Purified nanocrystallites are dispersed in 20 ml of anhydrous 1-heptanol forming an optically clear solution. Then anhydrous methanol was added to precipitate the CdSe QDs and excess TBP, TOPO and HDA were removed. The resulting powder is readily dispersed in chloroform.

3.2.4 Synthesis of water-soluble MAA-capped CdSe QDs

To 20 mg of CdSe QDs in 5 ml of chloroform was added 7 ml pyridine, then it was stirred for 2 h at room temperature. 5 ml MAA / CHCl$_3$ (1M) was injected to the reaction vessel and the pH value was adjusted to basic condition (pH = 9 ~ 10) with pyridine. The vessel was placed under argon flow and the mixture was stirred at room temperature for few days (2 ~ 14 days). Then CdSe QDs were then precipitated with THF. The aliquots were centrifuged, and the supernatant was decanted. The final purified MAA-capped CdSe QDs were obtained by washing with THF to remove excess pyridine and capping agents. A stock solution of the soluble QDs was obtained by dissolving the MAA-capped QDs in a phosphate buffer solution (PBS) with pH = 7.4.

3.2.5 Synthesis of water-soluble MSA-capped CdSe QDs

To design water-soluble CdSe QDs, we have selected MSA was selected as the surface capping reagent to form water-soluble MAA-capped QDs. 30 mg of CdSe QDs were dissolved in 10 ml of methanol, which was transferred to a reaction vessel. Then, a separate 50 ml methanolic solution of containing 180 mg of MSA was added into the above QD-containing solution and the pH value was adjusted to 11 by adding tetramethylammonium hydroxide pentahydrate. The mixture was then heated at 70˚C for 3 hours with refluxing and the sample was stored in the dark. In addition, in order to remove the organic solvent, the QDs were precipitated with anhydrous ether, centrifuged at 6000 rpm, and the supernatant was then decanted to remove the organic solvent. Methanol was added to wash the precipitates mixture which was further centrifuged for at least over four more times. Finally, the precipitate was dissolved in a phosphate buffer solution (PBS, pH = 7.4), and stored in the dark [4, 5].

3.2.6 Preparation of fluorescent QDs-streptavidin bioconjugate

The fluorescent QDs-streptavidin (QDs-SA) complex can be used to detect the biotin that has been conjugated to human anti-IgE [1-3]. 4 µl of anti-IgE-biotin in coating buffer solution was first coated and immobilized on nitrocellulose slides, equilibrated at 37 °C for 2 h, and excess anti-IgE-biotin was then washed off by using PBS-T solution (containing 0.05 % Tween-20). A 200 µl of streptavidin (SA) solution was added into 100 µl of the above QDs stock solution. The CdSe QDs were allowed to bind to SA to form QDs-SA complexes with 200 µl of 1-ethyl-3-(3-dimethylaminopropyl) carbodiimide (EDAC) as a catalyst. QD-SA was further purified by carrying out centrifugation to remove the free EDC and SA. The QDs-SA complexes were then redissolved in a PBS buffer (pH = 7.4) and stored at 4 °C in dark, which were then added to a nitrocellulose slide (NC slide) pre-coated with α-IgE-biotin (5 mg / ml) for investigations of binding specificity. The modified substrate was then soaked in PBS solution that contained 2% BSA to eliminate the non-specific binding sites at 4℃ for overnight at 4℃. Then the slide was rinsed with PBS-T five times to wash off excess QDs-SA complexes and dried prior to scanning fluorescence imaging measurements.

3.2.7 Detection of fluorescence signal

The fluorescent QD-SA conjugates can be used to capture biotinated α-human-IgE by affinity binding between SA and biotin, so the α-human-IgE-biotin was used as the probe and QD-SA conjugate was spread onto the probe NC slide. A Gene Pix model 4000 laser confocal scanner with an excitation wavelength (λ_{ex}) of 532 nm was used for fluorescence imaging measurements.

3.3 Results and discussions

3.3.1 The optical properties of water-soluble MAA-coated CdSe QDs and QD-SA

In the meanwhile, we have synthesized the water-soluble QDs by modifying the hydrophobic surface of CdSe QDs into hydrophilic phase. As expected, the carboxy-modified NPs were highly hydrophilic and maintained their luminescence properties. The photoluminescence and photostability of the water-soluble CdSe QDs that initially capped with different molar ratios of HDA/TOPO was explored in chapter 2. The PL spectrum of CdSe QDs which was modified to hydrophilic phase (MAA-capped) has been shown in Fig. 3.1. As compared to Fig. 2.3, the trend of photoluminescence spectra was found to be similar to that the concentration of TOPO increased and the PL luminescent intensity decreased. The optical properties of the hydrophilic QDs were strongly influenced by the original quality of hydrophobic CdSe QDs and the synthetic conditions of thiol-coated, such as pH value (> 7), reaction temperature and ambience. With the CdSe QDs capped with only HDA as surfactants, the high-quality and high-photostability hydrophilic CdSe QDs can be prepared,successfully.

In Fig. 3.2(a), the only HDA coated CdSe QDs were modified into hydrophilic phase of MAA coated CdSe QDs. The optimal λ_{ex} of only HDA coated CdSe QDs was found to be 367 nm, whereas λ_{em} was observed to be 607 nm with FWHM of 30 nm for the red-emitting CdSe QDs. Compared to HDA coated CdSe, the MAA coated CdSe QDs were presented red-shift slightly. With the different capping time, the PL intensity of water-soluble QDs has an increasing trend with increasing capping days. As indicated in Fig. 3.2(b), when

the capping time was 14 days, the MAA coated CdSe QDs had the optimal photoluminescence with optimal λ_{ex} of 367 nm and the λ_{em} was observed to be 614 nm. The water-soluble CdSe QDs have board excitation band (365 ~ 560 nm) and narrow emission band (~ 610 nm, FWHM ~ 30 nm). We can apply the characteristic of water-soluble CdSe QDs in biological labeling reagents. The advantages of applying CdSe QDs for fluorescence signal detection in biochips lie in their intrinsic characters such as broad excitation range and narrow emission band width, as compared to conventional organic dyes.

3.3.2. Fluorescence imaging and intensity of MMA-coated QD-SA

As expected, the carboxylic-modified CdSe QDs were highly water-soluble with their luminescence intensity well retained. In our work, the -COOH functional group of MAA capped on QDs surface was allowed to react with the -NH₂ group of SA and form an amide linkage. The coupling mechanism involved in the conjugation of SA to MAA-capped QDs through EDAC is summarized and represented in Fig. 3.3 [3].

The slide contained fluorescent QDs-SA complexes can be used to detect the biotin biomaterials and it can replace the organic dye for biochip signal. We used the 532 nm laser line as excitation power of the confocal scanner to scan the chips. The fluorescent image shown in Fig. 3.4 reveals that QDs-SA complex has the highly sensitivity; the fluorescent intensity of the image was found to increase with the concentration of QDs-SA. It is known that the human's allergenic factor is stepped up with increasing concentration of IgE [6] in serum. Since SA has been known to exhibit a binding specificity toward biotin, we use it to do signal of biochip containing QDs-SA and anti-IgE-Biotin to do signal of biochip, it can be used in allergen detection. More concentrated

QDs-SA bind more anti-IgE-Biotin, so that the detected intensity of the fluorescence signal depends on the concentration of QDs-SA.

If the serum contains α-IgE, it will immediately react with QDs-SA which forms Qds-SA-α-IgE-biontin. It can be traced simply by observing the difference of absorbance of QDs-SA and QDs-SA-link-α-IgE-biontin. The broad excitation, sharp and high intensity emission light of water soluble QDs make it highly demanding in fluorescence biosensor. The method is versatile and can be further applied to biosensors using surface-functionalized fluorescent CdSe QDs as a labeling agent.

3.3.3 The optical properties of water-soluble MSA-coated CdSe QDs and QD-SA

Compared to MMA-coated CdSe QDs, MSA-coated CdSe QDs have better reactivity with $-NH_2$ group of SA. It was rational that one MSA molecule can provide two carboxyl groups which increase the binding equivalence of SA on each QD [7], so the surface of CdSe QDs was functionalized with MSA to become water-soluble. Figure 3.5 shows IR spectra for the powder sample of CdSe QD capped with only HDA and water-soluble CdSe/ZnS QDs capped with MAA and MSA in MeOH.

For the MSA-capped QDs synthesized herein, the optimal emission was found to be centered at 608 nm with an FWHM of 30 nm when excited by a wavelength of 467 nm. The PL spectra of the MSA-capped QDs have broad peaks, as presented in Fig. 3.6 These peaks help to select the suitable excitation wavelength of a scanner. With successful surface functionalization by carboxylic group (-COOH), MSA-capped QDs can be used to conjugate the SA to generate QD-SA complexes. The spectra shown in Fig. 3.7 reveal that the emission wavelength of QDs remained unchanged following conjugation with SA and coupling to the antibody-biotin complex. For steric reasons, only two to

five molecules of protein with a molecular weight of 100 kD are expected to be able to be attached to QDs with a size of 5 nm. This number is similar to that of protein molecules that can be attached to a colloidal gold nanoparticle with a size of 5 nm, as reported elsewhere [7, 8]. Given these spectral characteristics, a laser line with a λ_{ex} of 532 nm was used as the excitation source to investigate the fluorescence characteristics of the binding affinity between the QD-SA complex and biotin in the biotinated α-human-IgE-biotin complex.

3.3.4. Fluorescence imaging and intensity of MSA coated CdSe QD-SA

Figure 3.8 presents the fluorescence images of micro-array spots with various concentrations of QD-SA (0.8mg/ml~2.5 μg/ml) on the NC slides, as obtained using scanners with a λ_{ex} of 532 nm. The results demonstrate that the intensity of the fluorescence image increases with increasing QD concentration in the QD-SA complex. Figure 3.9 plots the calibration curve of fluorescence intensity versus QD-SA concentration; the fluorescent intensity of QD-SA was found to reach saturation at a QD concentration above 0.4 mg/ml. As depicted in Fig. 3.9, the plot of fluorescence intensity versus QD-SA concentration is linear at concentrations between 0.0026 mg/ml and 0.08 mg/ml. This range was considered to be inappropriate for bioassay because the fluorescence intensity detected by conventional immuno-assay was too low. A 0.1mg/ml concentration of QDs was used in QD-SA to generate a fluorescence signal with a similar intensity on a plate-base biochemical assay and to reduce the experimental costs. However, the detection characteristics are more linear and the range of detection limit was found to be 3.33 μg/ml in α-human-IgE-biotin.

3.3.5. Coupling between MSA-capped CdSe QDs and SA

The MSA-capped CdSe QDs contain the surface functional group –COOH, which can be conjugated with the amine group of SA. During conjugation, EDC, acting as a catalyst, and NHS as the stabilizer were used to facilitate the

coupling of SA onto the surface of QDs, whose structure and related coupling are presented in Fig. 3.10. Furthermore, gel electrophoresis with 10% tris-glycine SDS-page was used to determine the molecular weight of the formed QD-SA complexes and thus elucidate the coupling efficiency of QD-COOH and SA. The analytical results represented in Fig. 3.11 reveal that the molar weight of the QD-SA complex was between 75 kD and 100 kD and that of SA was 55 kD; no free streptavidin was present in the solution that contained QD-SA. Based on the QD-PG-anti-RDX model proposed by Mattoussi *et al.* [9], the immuno-assay based on the binding of the QD-SA complex with biotin is described and illustrated in Fig. 3.12. Therefore, in principle, no free SA is present to compete with QD-SA.

3.3.6 Affinity binding of MSA capped QD-SA to biotinlated α-human-IgE complex

When QD-SA was added to α-human-IgE-biotin immobilized on the nitrocellulose slide, the high affinity of SA for biotin resulted in the strong and specific conjugation of QD-SA with biotinated α-human-IgE on the NC slide. The unconjugated QD-SA can be removed from the NC slides by using a washing buffer. First, samples of α-human-IgE-biotin in various concentrations (100 μg/ml – 0 g/ml) were coated on the NC slide and the volume of each spot was 5 μl. The fluorescence images shown in Fig. 3.13 reveal that at a concentration of 100 μg/ml in QD-SA, the biotinated complex has the greatest affinity; the fluorescence intensity of the images was found to increase with the concentration of α-human-IgE-biotin. More concentrated α-human-IgE-biotin contains more biotin, so the detected intensity of the fluorescence signal depends on the concentration of α-human-IgE-biotin. Fluorescent MSA-capped QD-SA and a plate-based device were used to test the feasibility of biochemical assay under the testing conditions of constant humidity and suitable temperature and to investigate the possibility of using the proposed biochemical assay as a

potential biosensor. Immediately after a prototype plate-based biochip is fabricated and the affinity binding between QD-SA and α-human-IgE-biotin complex is completed, a confocal laser scanner was used to scan and collect the fluorescence signal of QDs in QD-SA conjugates captured by biotin immobilized as α-human-IgE-biotin in the micro-array of the testing NC glass plate. As depicted in Fig. 3.14, the measured fluorescence intensity increased monotonically with the concentration of α-human-IgE-biotin, and the sensitivity was found to be quite high. Table 3.1 summarizes the optimal testing conditions and performance of the biochemical assay described herein. The data reported in Table 3.1 reveals that the detection limit for QD-SA was 3.3 μg/ml of α-human-IgE-biotin in and the fluorescence intensity increases linearly with the concentration of α-human-IgE-biotin. Therefore, the observed characteristics can be extended to detect the biomolecules other than biotinlatyed antibody or protein, using a plated-base chemical assay. The method is thus versatile and can be further applied as the basis of calibration in the future fabrication of biosensors using surface-functionalized fluorescent QDs as a labeling agent. Further investigations are being undertaken to accelerate the realization of the plate-based biochemical assay as a biosensor.

3.4 Conclusions

By employing a modified synthetic route we have synthesized high-quality HDA-and MAA-capped CdSe QDs, respectively, that exhibit decent PL intensity and photostability. We have also demonstrated the potential application using water-soluble MAA-capped and MSA-capped CdSe QDs as a fluorescent immuno-labeling agent in the detection of human antibody IgE based on fluorescence imaging analysis with laser confocal scanning. Our results obtained

from the miniaturized nitrocellulose glass slide indicated that the readout method developed with CdSe QD labeled SA-biotin-anti-IgE biomolecules were suitable for applications in biochips in principle.

3.5 References

[1] D. Gerion, F. Pinard, S. C. William, W. J. Parak, D. Zanchet, S. Weiss, A. P. Alivisatos: J. Phys. Chem. B **105** (2001) 8861.

[2] J. Aldana, Y. A. Wang, X. Peng: J. Am. Chem. Soc. **123** (2001) 8844.

[3] W. Desheng, H. Jibao, R. Nista, R. Zeev: Nano lett. **4** (2004) 409.

[4] W. C. W. Chan, D. J. Maxwell, X. Gao, R. E. Bailey, M. Han, S. Nie, Biotechnology **13** (2002) 40.

[5] M. Bruchez Jr., M. Moronne, P. Gin, S. Weiss, A.P. Alivisatos, Science **281** (1998) 2013-2016.

[6] F. Lecaille, J. Kaleta, D. Bromme: Chem. Rev. **102** (2002) 4459.

[7] B. Sun, W. Xie, G. Yi, D. Chen, Y. Zhou, J. Cheng, J. Immunological. Methods **249** (2001) 85.

[8] W. C. W. Chan, S. Nie, Science **281** (1998) 2016.

[9] H. Mattoussi, I. L. Medintz, A. R. Clapp, E. R. Goldman, J. K. Jaiswal, S. M. Simon, J. M. Mauro, J. Association Lab. Automation **9** (2004) 28.
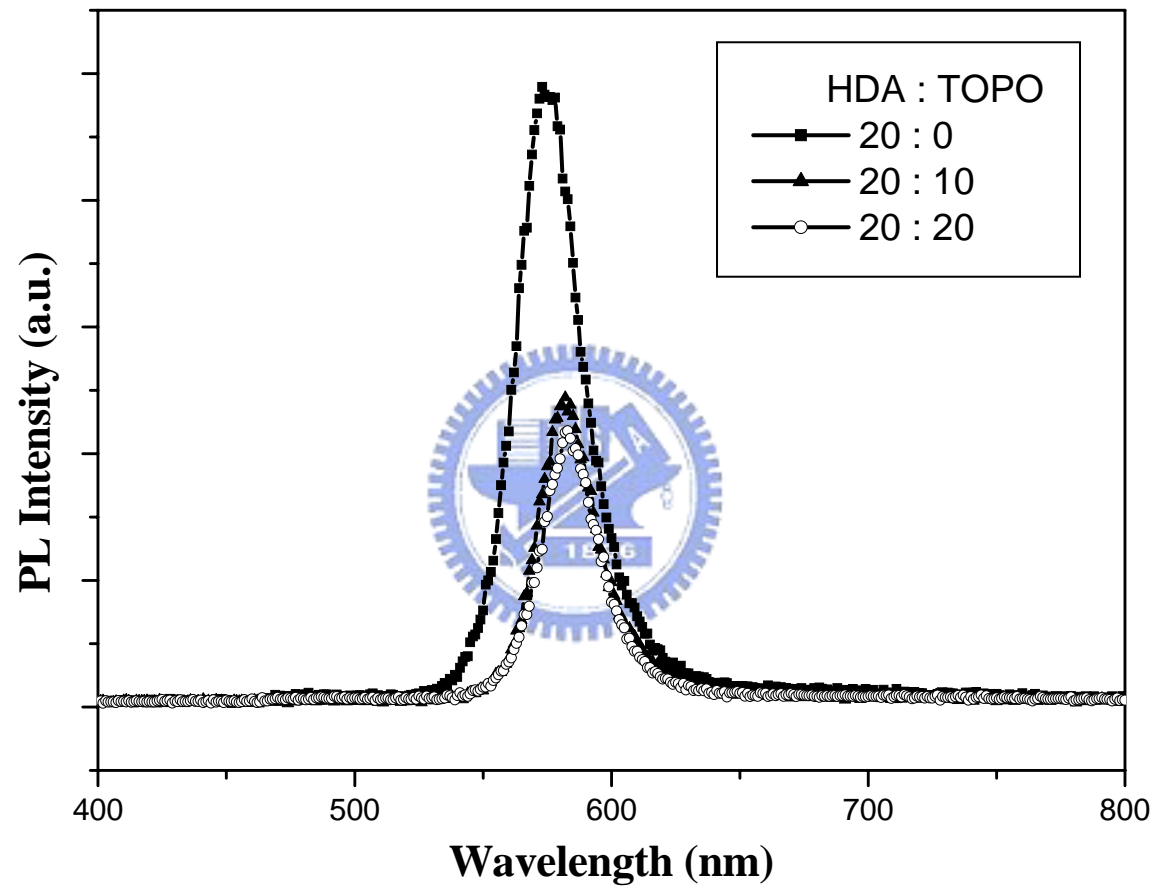
Figure 3.1 Comparison of PL spectra of water-soluble MAA-capped CdSe QDs with various HDA/TOPO in PBS solution.
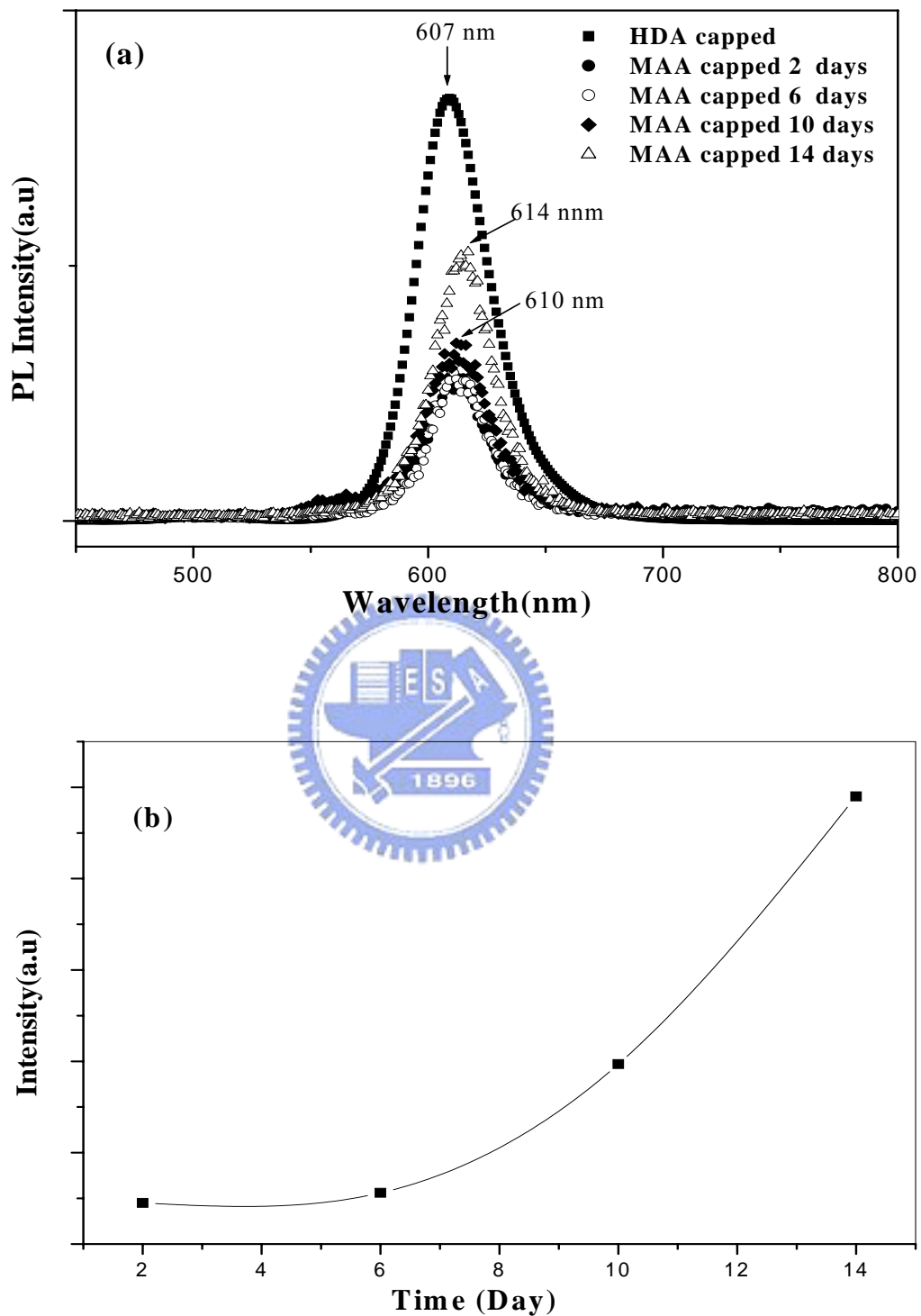
Figure 3.2 (a) Effect of capping reaction time on the solution PL spectra of MAA-capped CdSe QDs in PBS. (b) PL intensity as the function of capping time.
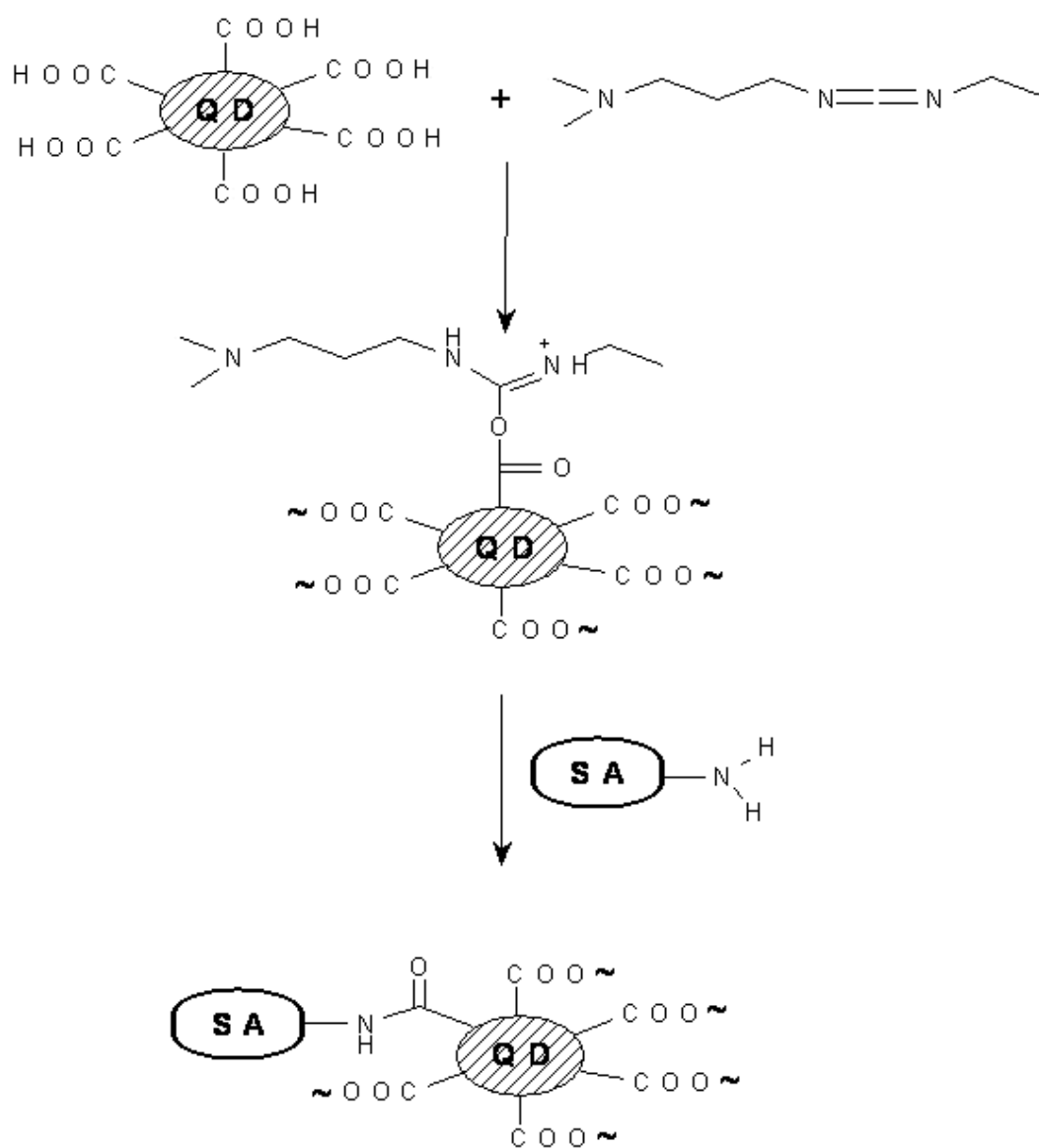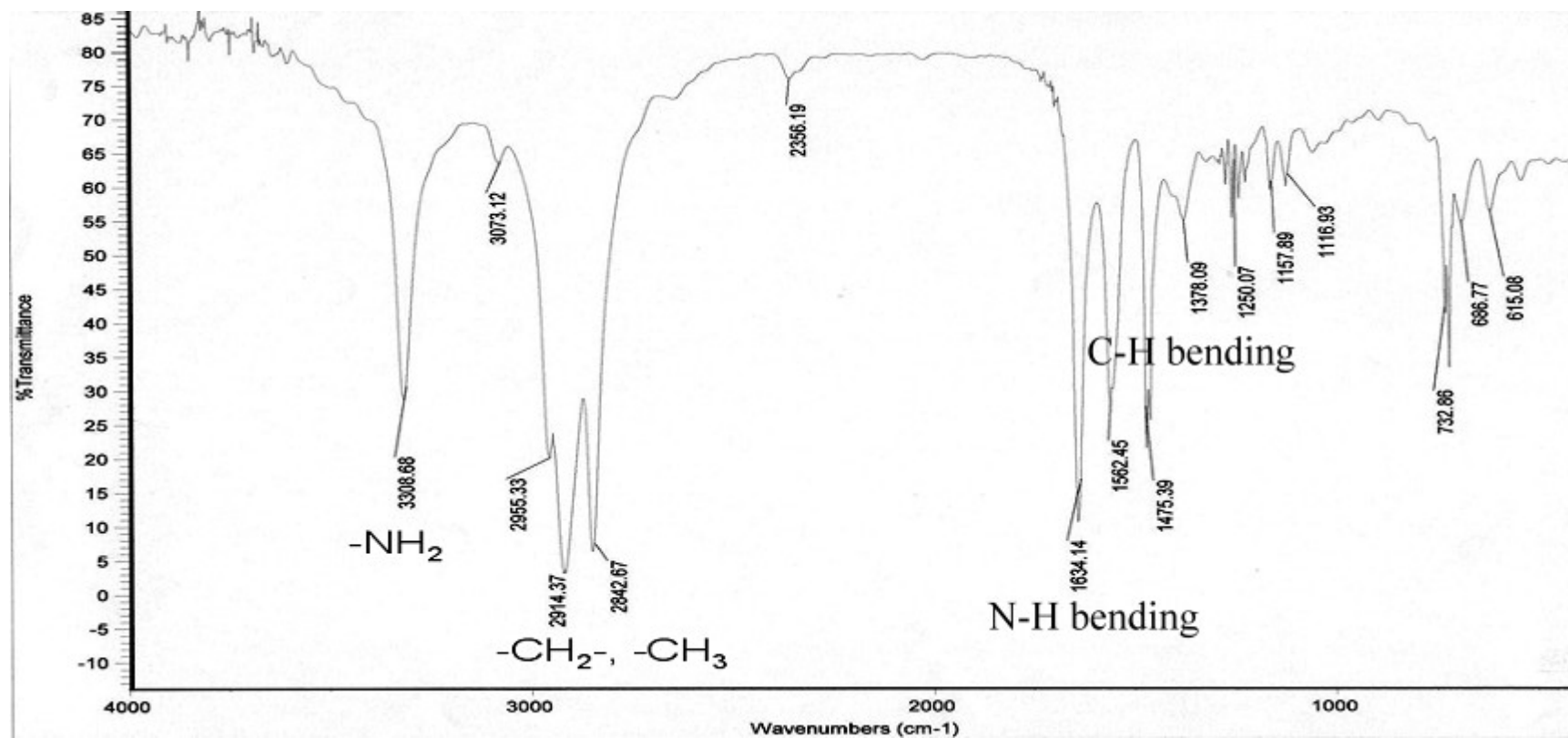
Figure 3.3 The principle for SA binding to MAA-capped CdSe QDs using EDAC as a coupling agent.
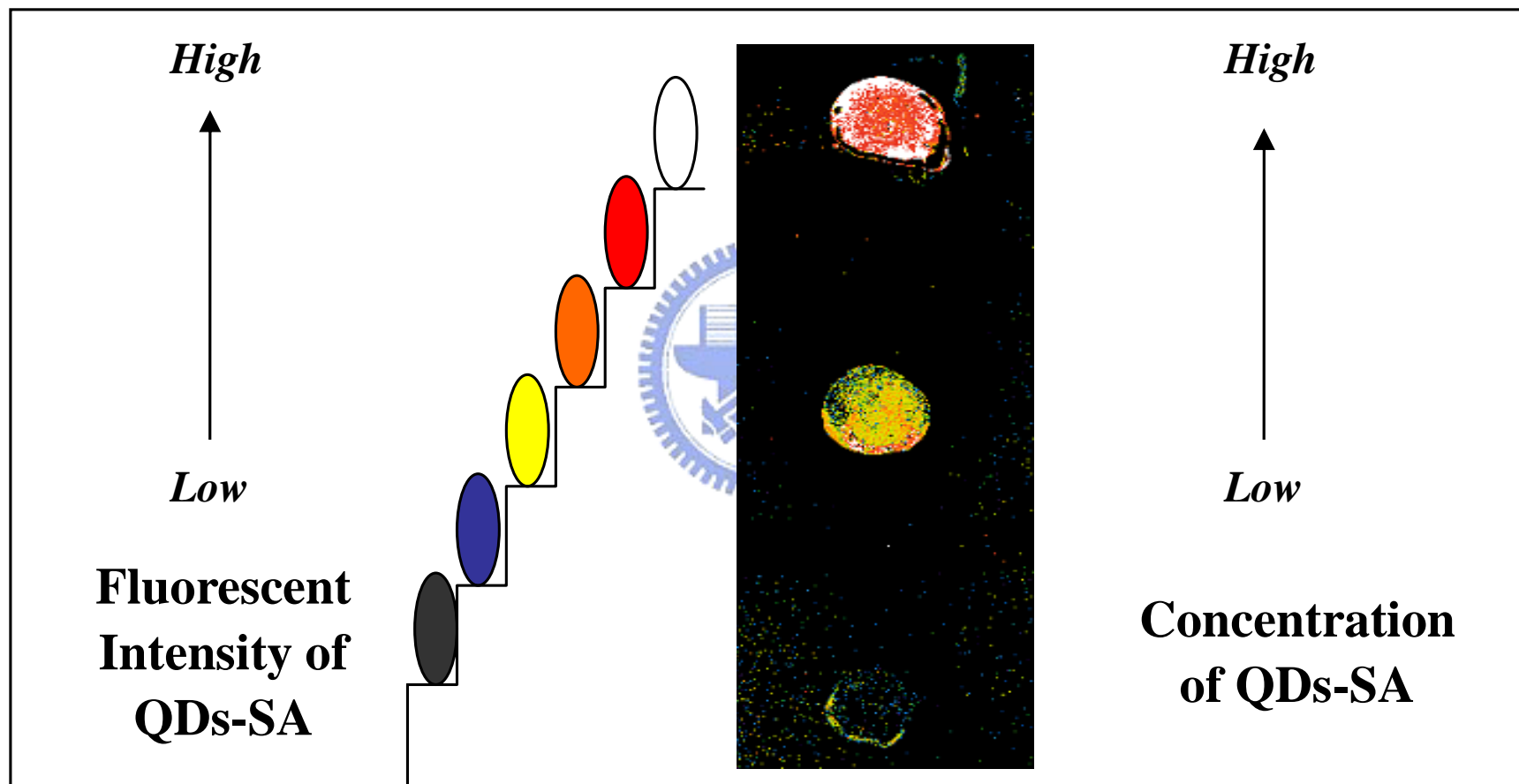
Figure 3.4 Laser confocal images of 0.0133, 0.13 and 1.33 mg/mL QDs-SA (from bottom to top) on NC slide.
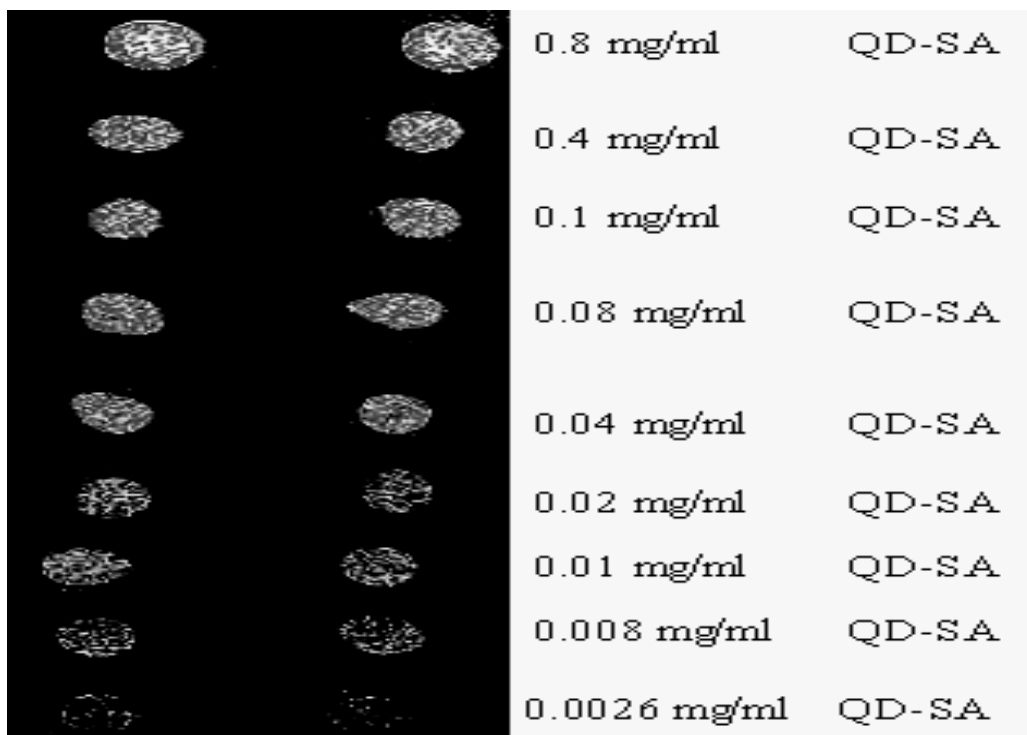
Figure 3.5 (a) IR spectra of water-insoluble HDA-capped CdSe/ZnS QDs.
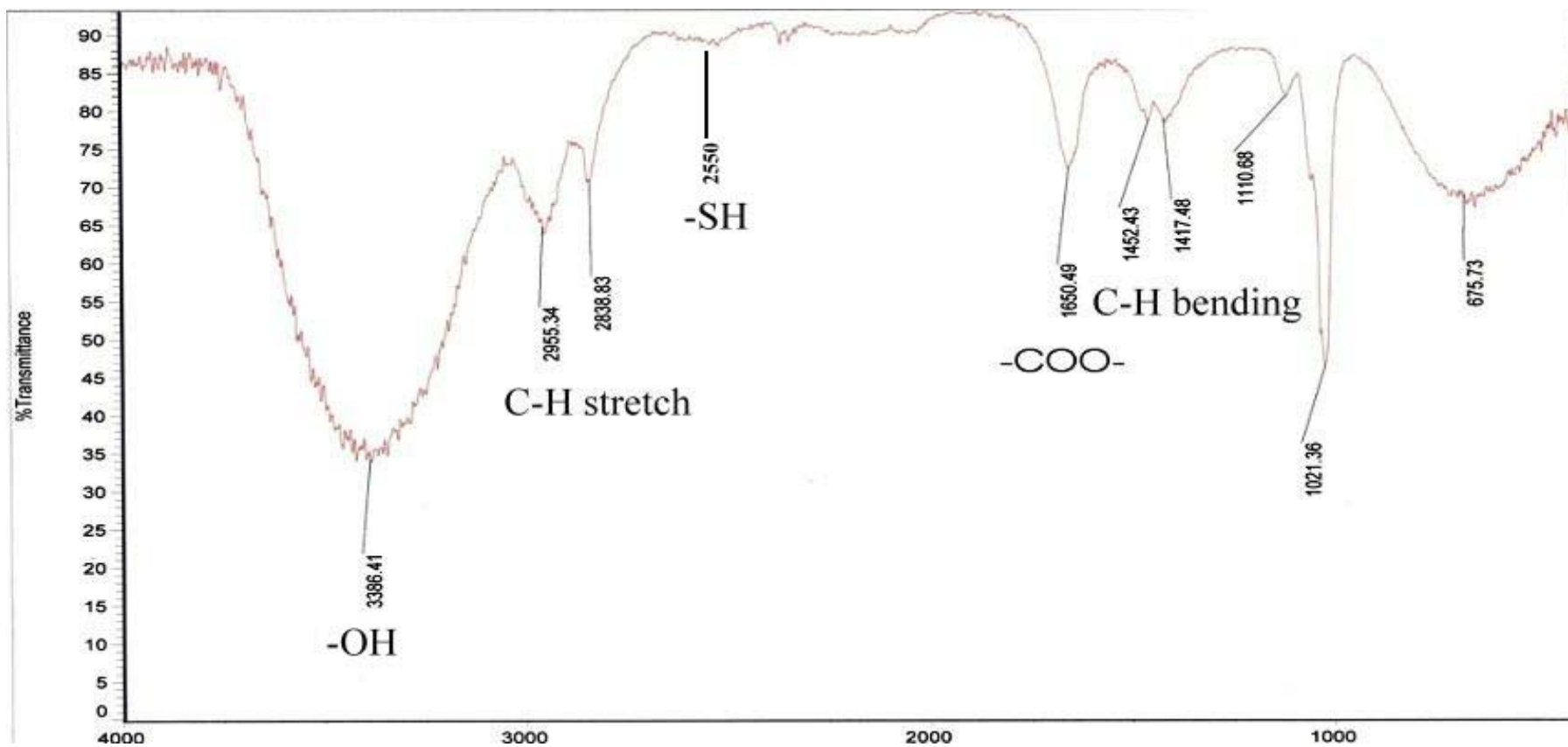
Figure 3.5 (b) IR spectra of water-soluble MAA-capped CdSe/ZnS QDs.
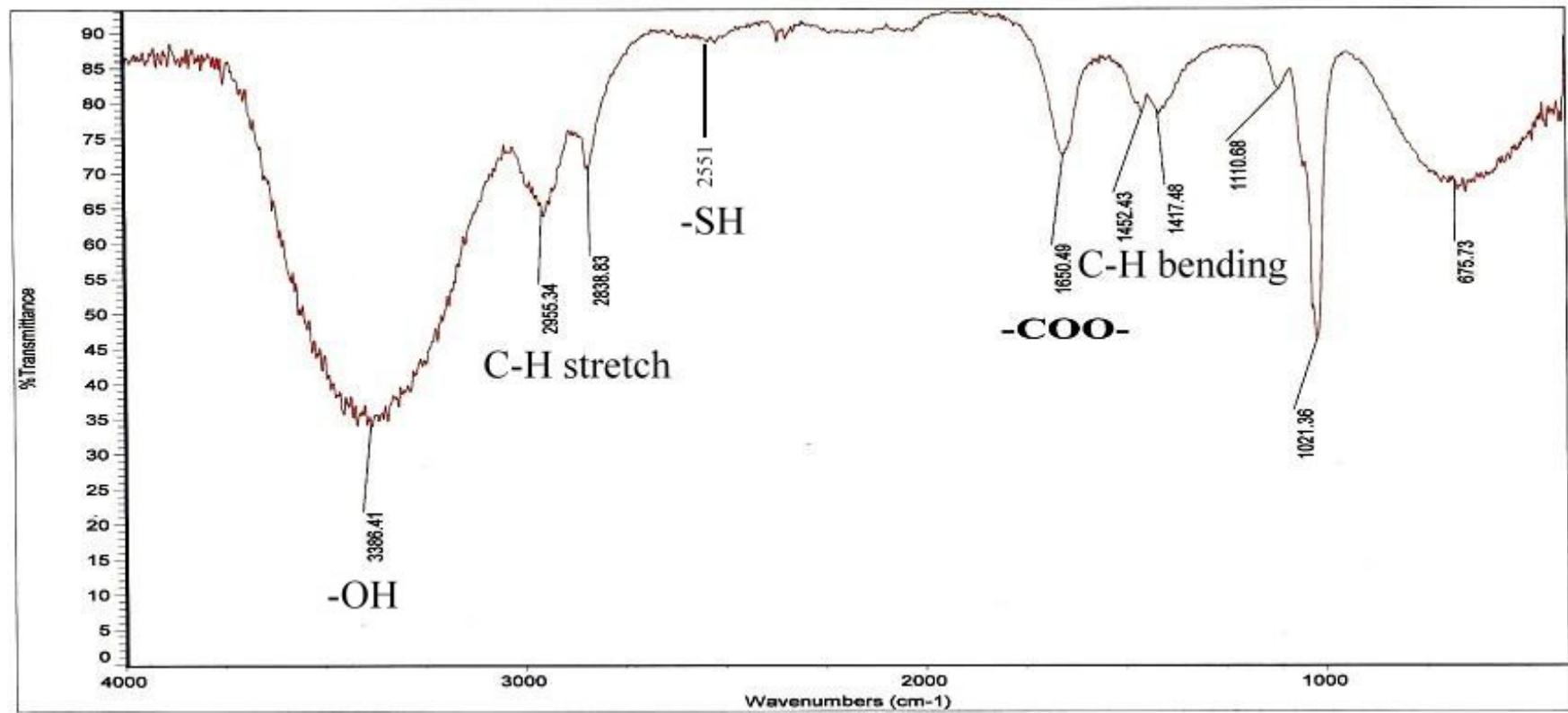
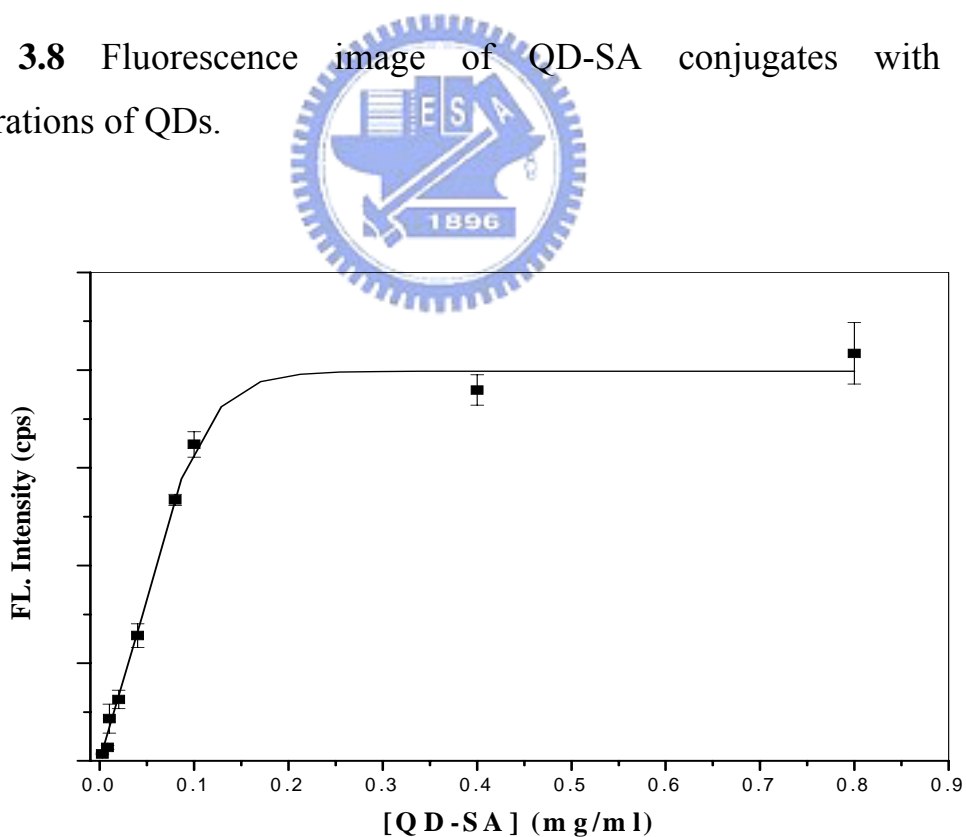**Figure 3.5 (c)** IR spectra of water-soluble MSA-capped CdSe/ZnS QDs.
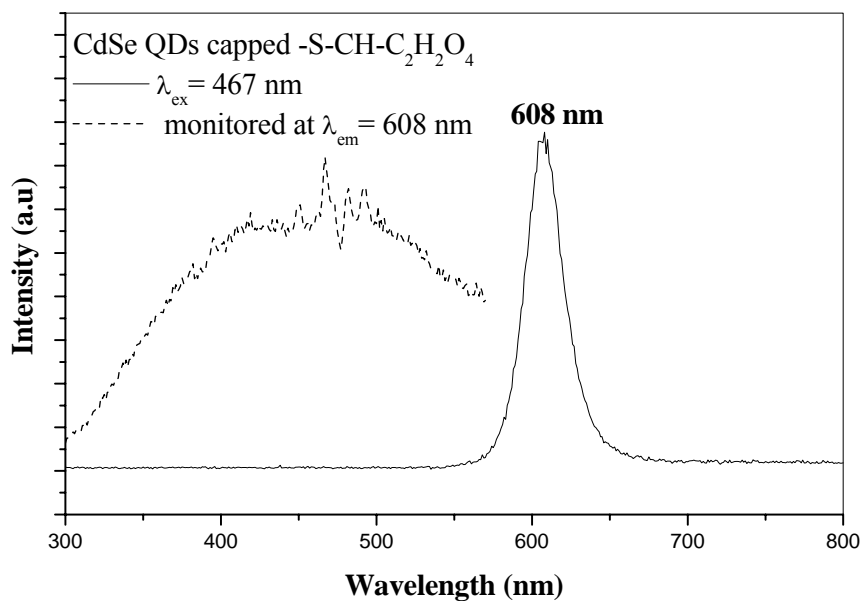
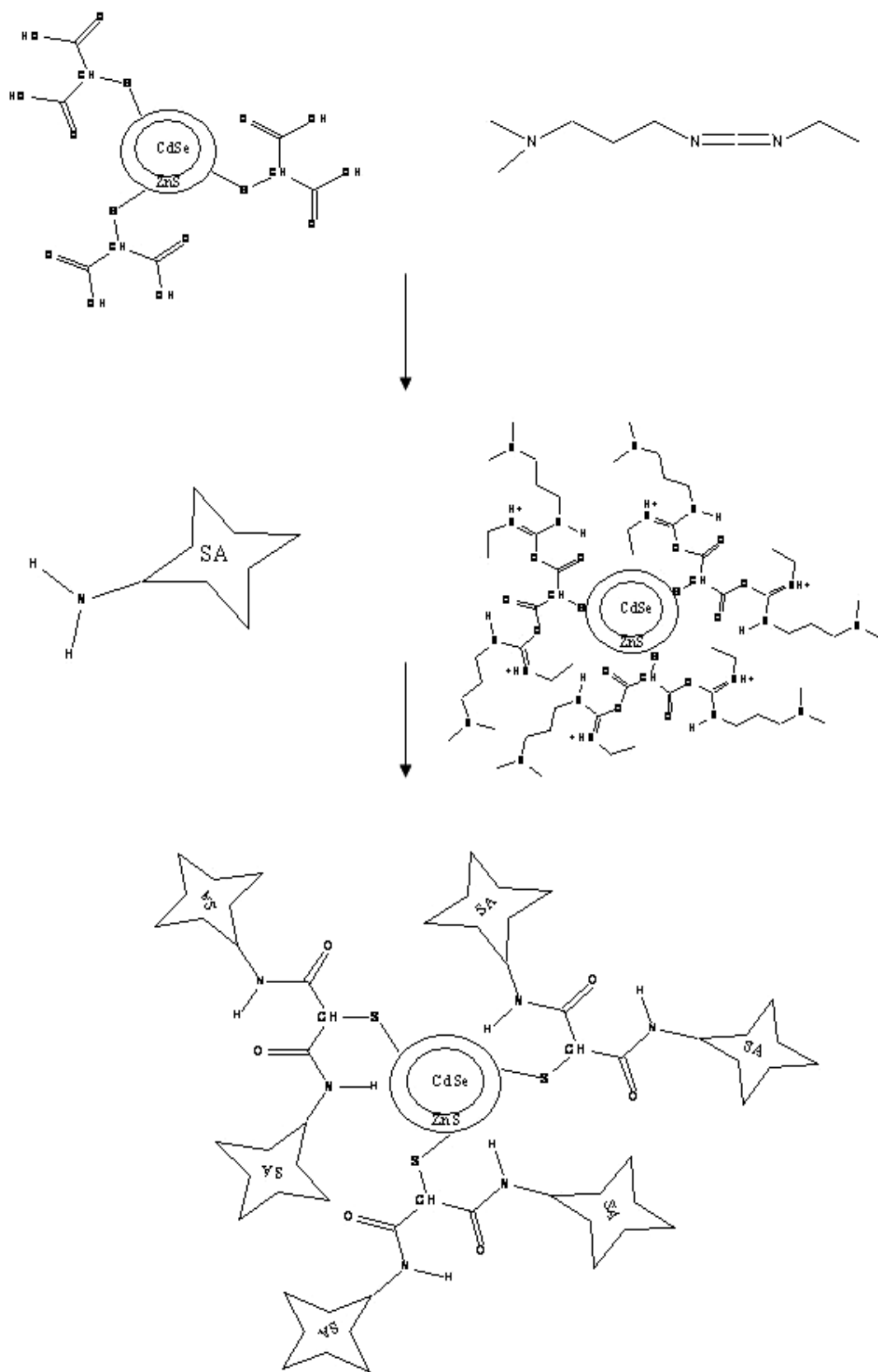**Figure 3.6** PL spectra of water-soluble red-emitting MSA-capped CdSe/ZnS QDs.
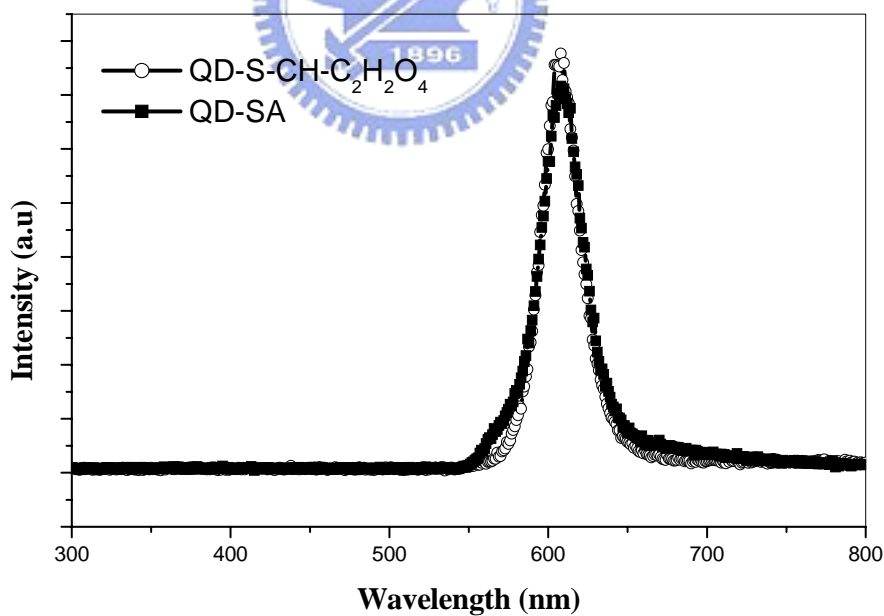
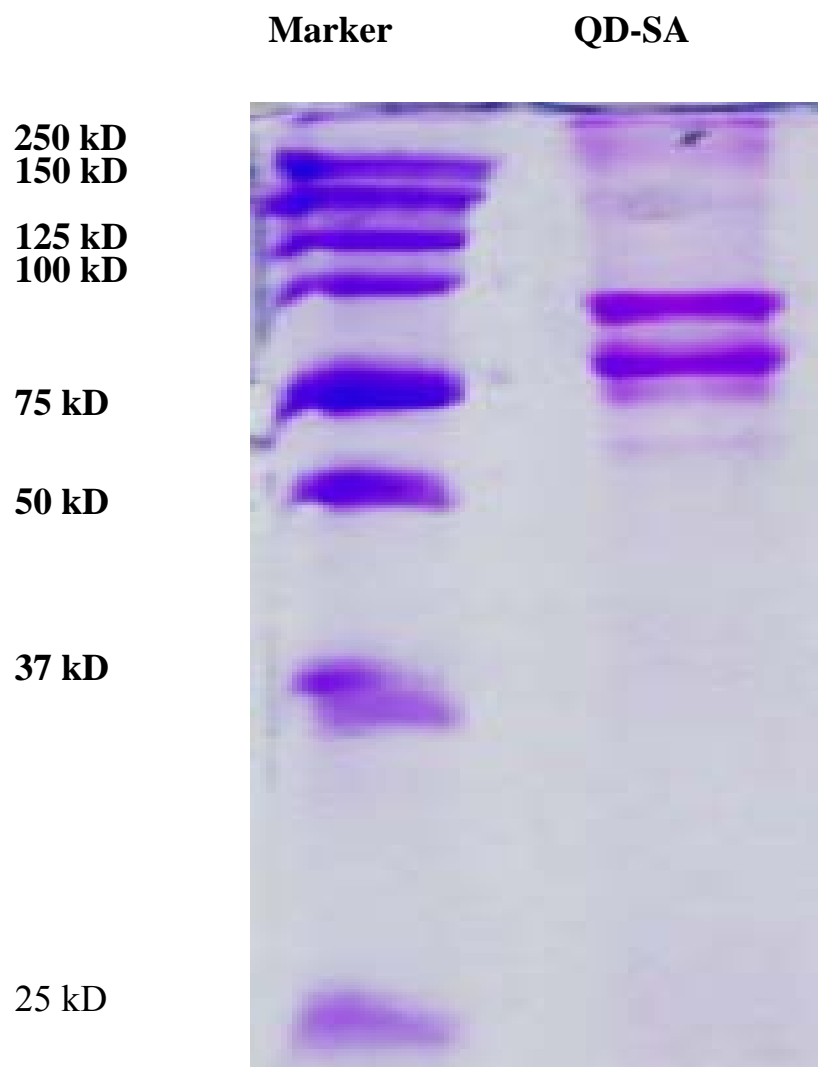**Figure 3.7** PL spectra of CdSe/ZnS QDs free and conjugated to SA**.**

Figure 3.8 Fluorescence image of QD-SA conjugates with various concentrations of QDs.

Figure 3.9 Calibration curve of fluorescence intensity versus QD-SA concentration.
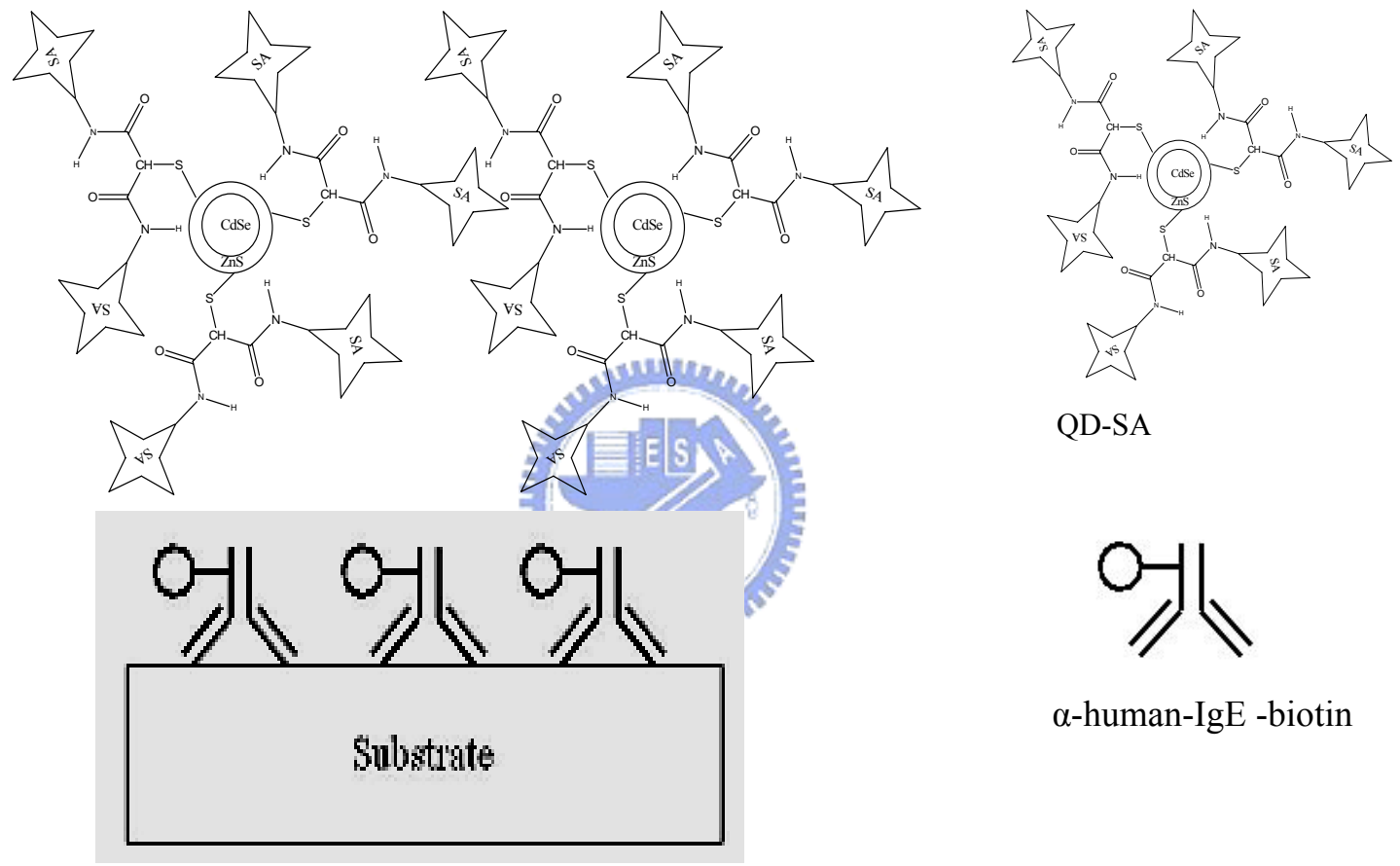
Figure 3.10 Covalent attachment of SA to QDs using coupling chemistry of EDC and NHS [3].
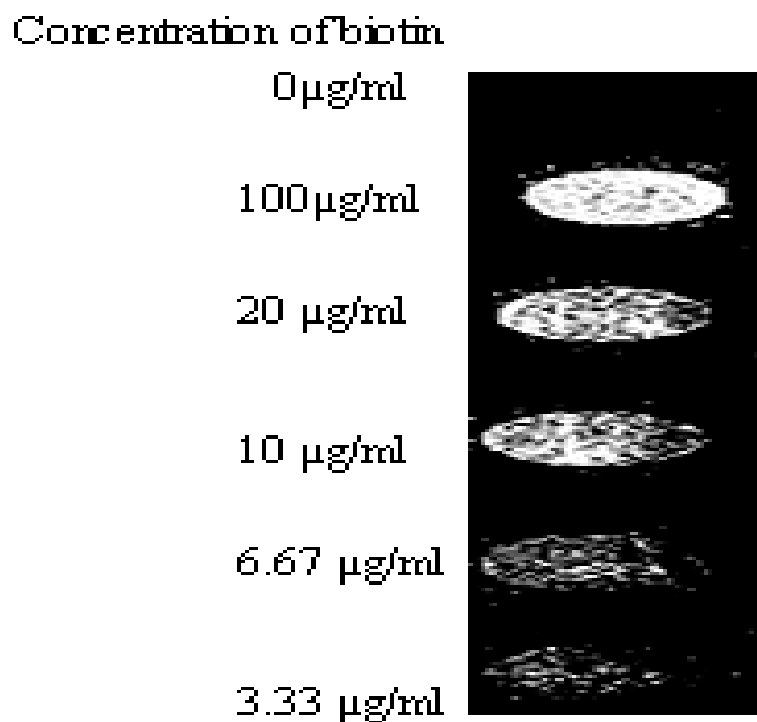
Figure 3.11 Molecule weight analysis of QD-SA by gel-electrophoresis using SDS-page gel with 10% tris-glycine.
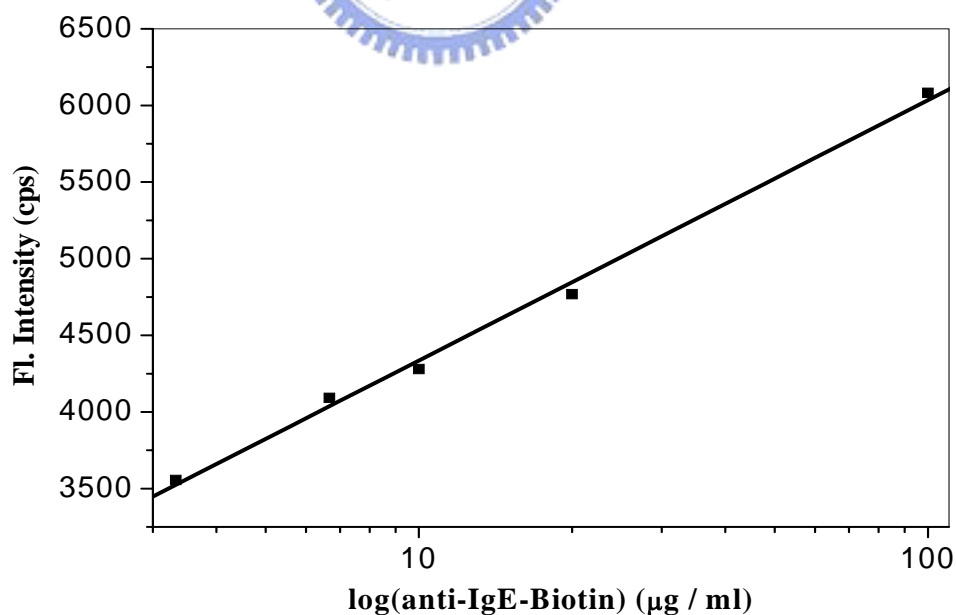
QD-SA

α-human-IgE -biotin

Figure 3.12 Schematic representation of QD-SA bound with biotinlated α-human-IgE [9].

Concentration of biotin

0 μg/ml

100 μg/ml

20 μg/ml

10 μg/ml

6.67 μg/ml

3.33 μg/ml

Figure 3.13 Confocal images of QD-SA conjugated α-human-IgE-biotin as a function of biotin concentration.

Figure 3.14 Fluorescence intensity of QD-SA versus concentration of α-human-IgE-biotin immobilized on the NC slide.

Table 3.1 Optimal conditions and performance of the plate-based biochemical assay using affinity binding of QD-SA and α-human- IgE-biotin complex.

Parameter	Condition
Immobilization environment	0.1 (M) sodium carbonate buffer solution (pH ~ 9.4)
Target	Anti-Human-IgE-Biotin 0 ~100 (μg/ml)
QD-SA concentration	0.1mg/ml
QD-SA fluorescence	3500 ~ 6200 (cps)
Linear range of [α-human-IgE-biotin]	3.33 ~100 (μg/ml)

Chapter 4

Observing Enhanced Phosphorescence and Electroluminescence from Triplet Emitter by Quantum Dot Doping

Abstract

Luminescent core-shell type CdSe/ZnS quantum dots (QDs) were synthesized by chemical colloidal methods. The photoluminescence (PL) intensity of triplet emitters iridium (III) complex 1 (Ir-complex 1) and Ir-complex 2 was dramatically enhanced when bluish-green emitting CdSe/ZnS QDs were incorporated into these compounds. Experimental results indicate that the emissive region of QDs substantially overlaps with the low-energy absorption bands of Ir-complexes, indicating that the photons were absorbed by both the QDs and the Ir-complexes and that the energy absorbed by the QDs was transferred efficiently to the Ir-complex triplet emitter, resulting in the observed enhancement of PL intensity. In the fabricated double-layer electroluminescent (EL) devices, the emitting layer contained either only Ir-complex or a mixture of Ir-complex and CdSe/ZnS QDs at a specific molar ratio (Ir-complex/QDs = 1/0 (D-I); 1/0.5 (D-II)…1/10 (D-V)). The EL intensity and the luminance efficiency for D-II were higher (luminescence yield = 19.3 cdA^{-1}) than those of the other devices. The PL and EL enhancement of the triplet emitter were also strongly supported by using ZnSe QDs rather than CdSe/ZnS QDs.

4.1 Introduction

Investigating nanometer sized crystallites provide an opportunity to observe

the evolution of material characteristics as dimensions are varied. The spatial confinement of electronic and vibrational excitations dominates the physical properties of semiconductor nanocrystallites. Quantum confinement and its implications for the electronic structure and photophysics of the nanocrystallites have attracted much attention [1]. This class of materials exhibits quantum efficiencies of over 50 % according to solution photoluminescence (PL) spectra. These materials also have high electron affinity, spectrally narrow band-width (FWHM < 30 nm) and a peak wavelength that can be systematically varied in the visible range, simply by controlling the dimensions [1, 2]. Additionally, the nature of the surface can be manipulated by attaching various organic capping groups, which allows the passivation of surface electronic states, thus improving the spectroscopic characteristics of the material. These desirable emissive properties, unmatched by any class of organic chromophores, motivated the formation of hybrid organic-inorganic light emitting diodes (LED) that contain QDs [3].

Much work on PL and EL properties has been performed on hetero-structures, mainly on polymers and inorganic CdSe nanocrystals [5]. A literature review on this class of hybrid device structures indicated that when QDs were incorporated into organic light emitting devices (OLEDs), QDs themselves were the light emitting centers [3-5]. No observation has been made of the QDs' enhancement of the PL intensity and quantum efficiency of the fluorescent or phosphorescent materials. In conventional OLEDs devices, singlet fluorescent materials exhibit fluorescence associated with singlet excitons, so the energy contained in the triplet excitons is wasted. However, if the triplet excited state is perturbed, for instance, by spin-orbit coupling (typically introduced by the presence of heavy metal atoms), then efficient phosphorescence is more likely. In such a situation, triplet excitons adopt some singlet character and are more likely to undergo radiative decay to the ground state. Indeed, phosphorescent materials with such properties exhibit high

quantum efficiency. This work is the first to report the sharp uplifting of PL intensity of a phosphorescent material when core-shell CdSe/ZnS QDs [2c-6] were incorporated into a matrix of yellowish-orange emitting Ir-complex triplet emitter and a film-forming poly(methylmethacrylate) (PMMA) polymer.

4. 2 Experimental Section

4.2.1 Chemicals and reagents

Cadmium oxide (~1 μm, 99.5 %), selenium (Se) powder (~100 mesh, 99.5%), zinc acetate dehydrate (> 98 %), polyvinylcarazole (PVK), poly(methylmethacrylate) (PMMA) and sulfur powder (99.8 %) were all purchased from Aldrich Chemicals (Saint Louis MO, USA). 1-hexdecylamine (HDA, 98+ %), lithium fluoride (LiF), aluminum (Al) was obtained from Lancaster (Lancashire, UK). Tri-*n*-butylphosphine (TBP) was obtained from Showa Chemicals Company (Tokyo, Japan). Anhydrous toluene and chloroform were purchased from TEDIA (Fairfield OH, USA). Bis(4-trifluoro-methyl)-2-phenyl-benzothiazolatoacetyl-acetonate-iridium(III) (Ir-complex 1) and bis(4-methyl)-2-phenylbenzothiazolatoacetylacetonate-iridium (III) (Ir-complex **2**) was synthesized following the method reported in the literature [7].

4.2.2 Preparation of CdSe/ZnS QDs

CdSe/ZnS QDs was prepared as followings. CdO (0.6 mmol) and HDA (9 mmol) were dissolved in 20 ml of tributlyphosphine (TBP). The reaction mixture was then heated at 260   for 2 h under nitrogen atmosphere. The prepared Se solution (0.7 mmol of Se in 5ml TBP solution) was immediately injected into the reaction mixture, where the temperature was kept at 180   for

1 min. Then, zinc acetate (0.1 mmol) and sulfur (0.12 mmol) were dissolved in 5 ml of TBP, and injected into the reaction mixture. The temperature of the reaction mixture was maintained at 120   for 0.5 h. Toluene was injected into the reaction vessel.

4.2.3 Instrumentations

A Jeol JEM-4000EX TEM operated at 200 kV was used to determine the microstructure of QDs. Photoluminescence (PL) excitation and ambient temperature emission spectra were measured using a Jobin-Yvon Spex Fluorolog 3 spectrofluorometer with a monochromatized Xe light source (450 W). The emission spectra of various QDs were obtained at an excitation wavelength (λ_{ex}) of 367 nm. ultraviolet-visible (UV-Vis) absorption spectra of QDs were measured using a Hitachi U-3010 UV-visible spectrophotometer. The concentration of the samples used for PL and UV-visible measurements was maintained at the concentration of 1×10^{-4} M in toluene.

4.2.4 Fabrication of thin films and EL devices

By spinning from concentrated dispersions in chloroform (3 ml) on flat quartz substrate of mixture containing Ir-complex 1 : CdSe/ZnS of 1 : 0; 1 : 0.5,…,.1 : 10, we have fabricated several uniform thin films comprising a fixed number of moles of Ir-complex with various molar concentrations of CdSe/ZnS QDs in a fixed amount of CdSe/ZnS PMMA matrix. The 1: 1 mixture of Ir-complex and CdSe/ZnS QDs were prepared as followings. 1 ml of Ir-complex (1.6×10^{-6} M) was mixed with 0.016 ml of CdSe/ZnS (1×10^{-4} M) in chloroform. Similarly, we have prepared other Ir-complex and CdSe/ZnS QDs mixture solutions proportionately. Then, 30 mg of PMMA was added to each of the mixtures and the total volume was kept constant to 3 ml by adding chloroform. The thicknesses of the thin films were measured by the alpha-stepper method at various arbitrary points (8 ± 0.5 nm).

A series of double-layered EL devices with structure represented in Fig. 4.1 were designed and fabricated. These devices mainly contain green-emitting CdSe/ZnS QDs doped with the orange-emitting iridium (III) triplet emitter (Ir-complex 1 & Ir-complex 2) in different proportions in the emitting layer. The emitting layer contains Ir-complex and CdSe/ZnS QDs in PVK matrix with the molar ratios of Ir complex 1 : CdSe/ZnS compositions of 1:0 (blank; D-I), 1:0.5 (D-II); 1:2 (D-III); 1:7 (D-IV) and 1:10 (D-V), respectively. The emitting components were spin-cast from chloroform onto the poly(3,4-ethylenedioxythiophene) (PEDOT)/ poly(4-styrenesulfonate) (PSS)-coated indium tin oxides (ITO) glass substrates. Tris(8-hydroxyquinolinato)aluminum(III) (Alq$_3$) was subsequently spin-cast onto the emitting layers and LiF/Al cathode was vacuum-deposited on top of the emitting layers at 1.3×10^{-4} Pa. The layer sequences and the thicknesses of each layer were the same across the three fabricated devices. The current-voltage profiles and EL intensity characteristics of the above fabricated devices were measured in a vacuum chamber at 1.3×10^{-4} Pa at ambient temperature using a Keithley 2400 source meter-2000 multimeter, coupled to a PR 650 optical meter.

4.3 Results and discussions

As depicted in Fig. 4.2, the PL intensity increases considerably with the doping concentration of CdSe/ZnS QDs. The sample with an Ir-complex 1 : CdSe/ZnS molar ratio of 1/3 exhibits the highest PL intensity and that for the sample with the next highest concentration of QDs was found to be lower. The observed fall in the PL intensity (as shown in Fig. 4.2) for the sample with higher QDs concentrations (i.e., Ir-complex:QDs > 1:3) may be caused by the self-quenching effect, resulting from the aggregation of QDs at higher concentration. Similar experiments were conducted using another triplet emitter

(Ir-complex 2) and similar PL enhancement was also observed in Fig. 4.3, supporting the above results. A more informative experiment was carried out to keep the QDs concentration in the PMMA matrix constant and slowly increased the Ir-complex 1 concentration. As indicted in Fig. 4.4, the mixture of QDs : Ir-complex = 0.4 : 0.05 was prepared as follows: 50 μl of Ir complex (5.9 X 10^{-4} M) was mixed with 0.4 ml of QDs (4.7 X 10^{-2} M) in chloroform with 12 mg of PMMA and the total volume was maintained to 1.1 ml. Similarly the other mixtures were prepared by maintaining the proportions mentioned. PL spectra were taken on several positions of each thin film and the presented PL spectra were the average of those. It was observed that the slow quenching of QDs emission, as shown in Fig. 4.4, with increasing concentration of Ir-complex 1 which strongly supports the energy transfers from the QDs to the Ir-complex. Similar quenching effect of QDs emission was found on conducting the experiment in solution phase with chloroform, as displayed in Fig. 4.5, where the mixture of QDs : Ir-complex = 0.2 : 0.1 was prepared as follows: 100 μl of Ir complex (5.9 x 10^{-4} M) was mixed with 2 ml 4.7 X 10^{-2} M of QDs in chloroform and the total volume was maintained to 5 ml. The other mixtures were prepared by following the similar method keeping the proportions as mentioned at the inset in the figure. The maximum of the excitation wavelength (λ_{ex}^{max}) for bare CdSe/ZnSe QDs and that of the mixture of Ir-complex and CdSe/ZnS shows almost the same value (i.e., 365 nm), as indicated in Fig. 4.7. The λ_{ex} for each exciting thin film sample was chosen as 365 nm. Figure 4.6 presents the UV-Vis absorption spectra of Ir-complexes in the thin film with PMMA as a matrix. Several broad peaks (^{1}MLCT and ^{3}MLCT) in the range of 375 nm to 575 nm were observed and the emission spectra of QDs excited with 365 nm ultraviolet was also shown. The emissive region (360-600 nm) of CdSe/ZnS QDs was found to overlap with the absorptive part of the complexes 1 and 2, suggesting that the photons were absorbed by both QDs and the Ir-complexes 1 and 2, and the absorbed energy of QDs was transferred efficiently to the Ir-complex triplet

emitter, resulting in the enhancement of the PL intensity.

Figure 4.8 presents the EL spectra of all devices described above; the shape of these spectra were almost the same as that of the PL spectrum of Ir complex 1 (as shown in Fig. 2), except for a very weak emission peak at around 520 nm that was attributed to from the electron transport layer Alq_3. This observation indicates that the main origin of emission in the devices was complex 1 in the emitting layer. Figure 4.8 reveals that the EL intensity observed for device D-I was lower than that of the D-II and D-III devices, but higher than that of the D-IV and D-V. An exceptionally high luminance yield was observed for D-II (19.3 cdA^{-1}), whereas that of D-III (7.1 cdA^{-1}) was lower than that of D-II but higher than that of the blank one (D-I; 3.3 cdA^{-1}). The other two devices, D-IV and D-V, exhibited lower EL luminance yields than that of the blank (D-I). A high concentration of QDs can thus be considered normally to cause aggregation which results in low luminance yield for D-IV and D-V, respectively. Accordingly an optimal concentration of QDs (Ir-complex : QDs = 1/0.5), at which the EL luminance yield was maximal was obtained as shown in Fig. 4.8.

Table 4.1 compares the EL performance of all of the devices of interest. The organic layers in the EL device transport charge carriers to the vicinity of the monolayer that contains QDs and Ir-complex in the PVK matrix. PVK has been identified as both a host [8] and a hole transporting material [9], but it has no electron transporting ability [10]. Again, the CdSe semiconductor is also a weak charge transporter [2b]. The role of the electron transporting layer (Alq_3) that was sandwiched between the emitting layer and the cathode (LiF/Al), was to transport electrons injected from the cathode and the blocked holes from the PVK matrix in the emitting layer. Therefore, most of the excitons were confined in the emitting layer or near the interface of the emitting layer and Alq_3. Consequently, weak emission was observed from Alq_3, because the electron transporting ability of PVK and CdSe QDs was both weak, along with the strong emission from Ir-complex 1, as shown in Fig. 4.8 (also in Fig. 4.10 for ZnSe

QDs; see later). The excitons on the Ir-complex 1 in emitting layer are suggested to be generated by two parallel processes - exciton energy transfer from QDs to complex 1 and direct charge trapping by the complex 1. Electrons can be trapped at the QDs owing to the relative energy alignment of the lowest unoccupied molecular orbital (LUMO) levels of PEDOT-PSS, Alq_3 and QDs, as shown in Fig. 4.9. For these charged QDs the barrier to hole injection from the PEDOT-PSS is reduced which also facilitates QDs in trapping holes efficiently [2b]. Upon acceptance of holes from PEDOT-PSS, excitons form on the QDs and then transfer these to the Ir complex 1. Some portion of exciton formation on PVK and subsequent transfer these to the Ir complex has not been excluded [11]. Small proportions of electrons were also likely to be trapped directly by the complex 1 molecule; to be recombined with holes, and then to decay radiatively.

The emission spectrum of blue-emitting, zinc selenides (ZnSe) nanocrystals [12] is depicted in Fig. 4.7. ZeSe nanoparticles were synthesized to support the claim that doped CdSe/ZnS QDs enhance PL and EL of the triplet emitter through energy transfer. Several uniform thin films were fabricated by mixing Ir-complex 1 and ZnSe QDs in a PMMA matrix with proportion for complex 1 / ZnSe = 1:0; 1:0.05,…, 1:1, as described above. The PL intensity enhancement was maximal for the sample with the lowest concentration of ZnSe QDs, which was that with a given complex 1/QDs composition of 1:0.05 (as indicated in Fig. 4.11). These facts reveal an energy transfer from ZnSe QDs to the Ir-complex. Three EL devices [Ir-complex-1/ZnSe = 1: 0 (D-VI; blank); 1:0.025 (D-VII); 1:0.05 (D-VIII)] were fabricated using Ir-complex 1 and ZnSe QDs embedded in the PVK matrix in the emitting layer, as described above. Figure 10 reveals that incorporation of ZnSe QDs into the emitting layer increases the intensity of EL emission from Ir-complex 1, indicating that the energy transfer from QDs to Ir-complex 1 and the corresponding luminance and luminance yields were obtained as followings: 40, 45, 76 cdm^{-2} and 0.54, 4.4 and 6.6 cdA^{-1} at 1 $mAcm^{-2}$ for D-VI, D-VII and D-VIII, respectively. As shown in Fig. 4, the

sample doped with ZnSe QDs exhibited a larger overlap, but the EL devices with ZnSe QDs exhibited worse luminance and luminance efficiency than the devices that contained CdSe/ZnS QDs. The EL performance of CdSe/ZnS was optimal in the sample with an Ir-complex: CdSe/ZnS composition of 1/0.5. When the highest concentration of ZnSe QDs used was much lower (i.e., Ir-complex 1 : ZnSe =1/0.05), the optimal EL performance was not determined. Inorganic shell materials with a larger band gap may be adopted to improve the EL performances of ZnSe QDs to a level observed for CdSe/ZnS QDs.

4.4 Conclusion

Triplet emitting materials harvest both singlet and triplet excitons, allowing OLEDs to be fabricated with external quantum efficiencies (photon/electron) of about 20% [7c-13]. Our experimental results reveal that the EL quantum efficiency can be further improved by incorporating QDs into the phosphorescent materials. This work focused on optimizing the devices described above, by changing either the materials or the thicknesses of the layers, or by adding a hole-blocking layer in the OLEDs.

4.5 Reference

[1] (a) G. K. Ujjal, M. Rajamathi, F. Meldrum, P. Morgan and R. Seshadri: Chem. Commun. (2001) 629. (b) Y. Jun, J. Koo and J. Cheon: Chem. Commun. (2000) 1243.

[2] (a) T. Tsutsui: Nature **420** (2002) 752. (b) S. Coe, W. Woo, M. Bawendi and V. Bulovic: Nature **420** (2002) 800. (c) C. B. Murray, D. J. Norris, M. J. Bawendi, J. Am. Chem. Soc. **115** (1993) 8706.

[3] (a) H. Mattoussi, L. H. Radzilowski, B. O. Dabbousi, E. L. Thomas, M. G. Bawendi and M. F. Rubner: J. Appl. Phys. **83** (1998) 7965. (b) M. C.

Schlamp, X. Peng and A. P. Alivisatos: J. Appl. Phys. **82** (1997) 5837.

[4] (a) C. R. Kagan, D. B. Mitzi and C. D. Dimitrakopoulos: Science **286** (1999) 945. (b) Y. Yang, J. Huang, S. Liu and J. C. Shen: J. Mater. Chem. **7** (1997) 131. (c) V. L. Colvin, M. C. Schlamp and A. P. Alivisatos: Nature (London) **370** (1994) 354.

[5] (a) B. O. Dabbousi, M. G. Bawendi, O. Onitsuka and M. F. Rubner: Appl. Phys. Lett. **66** (1995) 1316. (b) W. U. Huynh, J. J. Dittmer and A. P. Alivisatos: Science **295** (2002) 2425.

[6] Z. A. Peng and X. G. Peng: J. Am. Chem. Soc. **123** (2001) 183.

[7] (a) A. Brembilla, D. Roizard and P. Lochon: Syn. Commun. **20** (1990) 3379. (b) S. Lamansky, P. Djurovich, D. Murphy, F. Abdel-Razaq, H. Lee, C. Adachi, P. E. Burrows, S. R. Forrest and M. E. Thompson: J. Am. Chem. Soc. **123** (2001) 4304. (c) I. R. Laskar, T. M. Chen, Chem. Mater. **16** (2004) 111.

[8] (a) X. Chow, M. Liu, Z. Xu, Y. Hou, F. Teng and X. Xu, J. Phys. D : Appl. Phys. **37** (2004) 1007. (b) T. J. Chow, R. Lin, C.-W. Ko and Y. T. Tao, J. Mater. Chem. **12** (2002) 42.

[9] (a) G. E. Jabbour, J. F. Wang and N. Peyghambarian, Appl. Phys. Lett. **80** (2002) 2026. (b) U. Mitschke and P. Bauerle, J. Materials Chemistry **10** (2000) 1471. (c) A. Patra, M. Pan, C. S. Friend, T. C. Lin, A. N. Cartwright, P. N. Prasad, Chem. Mater. **14** (2002) 4044.

[10] J. Kido, K. Hongawa, K. Okuyama, K. Nagai: Appl. Phys. Lett. **63** (1993) 2628.

[11] F. Chen, S. Chang, G. He, S. Pyo, Y. Yang, M. Kurotaki, J. Kido, J. Poly. Sc: Part B: Poly. Phys. **41** (2003) 2681.

[12] M. A. Hines, P. Guyot-Sionnest: J. Phys. Chem. B **102** (1998) 3656.

[13] M. E. Thompson, P. Djurovich, S. Lamansky, D. Murphy, R. Kwong, F. Abdel-Razzaq, S. R. Forrest, M. A. Baldo and P. E. Burrows, US Patent 2002/0034656 A1.

[14] R. H. Friend, Pure Appl. Chem, **75** (2001) 425.
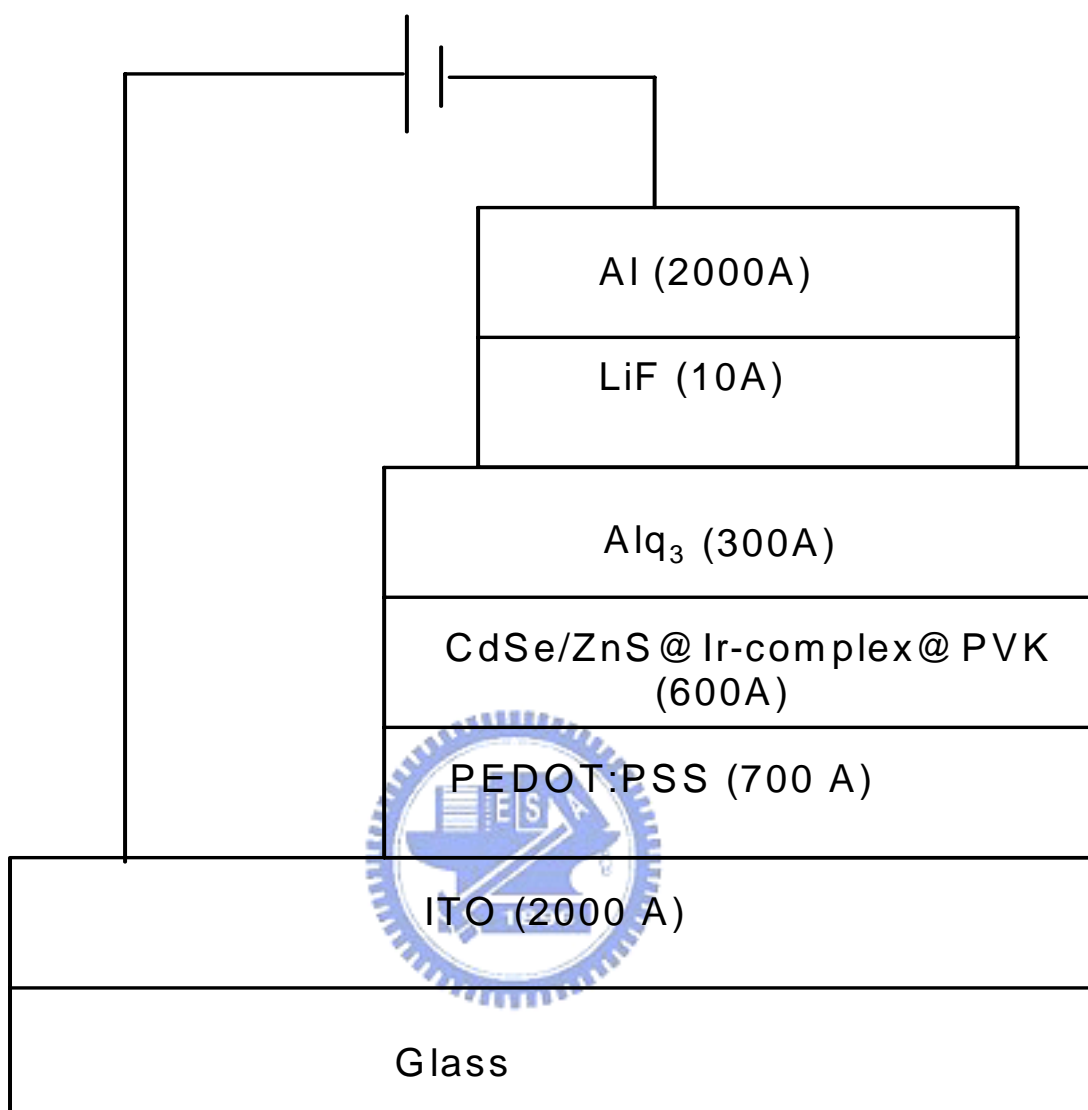
Figure 4.1 The EL device structure with CdSe/ZnS NCs and Ir-complex in PVK matrix as emitting materials. EL device layer sequences and their thicknesses are displayed.
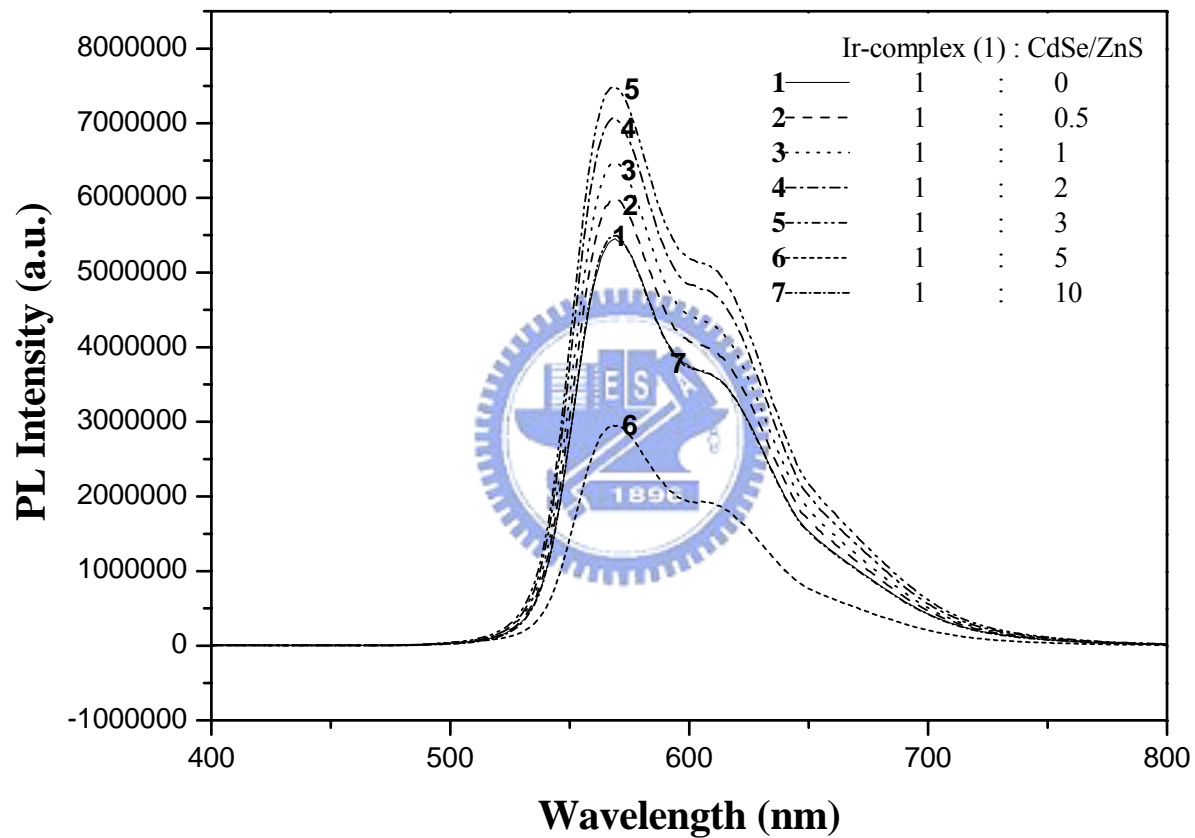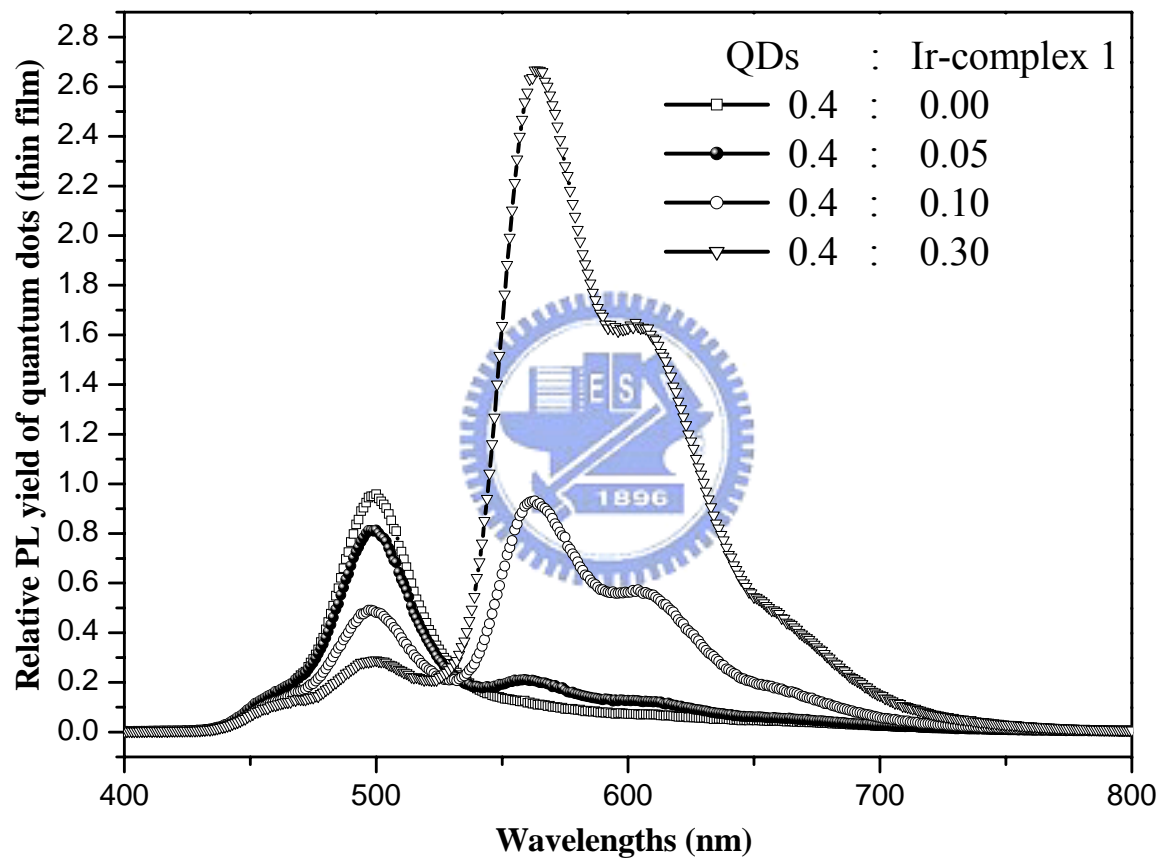
Figure 4.2 Comparison of PL spectra for the mixture of Ir-complex 1 and QDs dispersed in PMMA matrix in thin film sample with a fixed molar concentration of Ir-complex with increasing order of molar proportion of QDs.
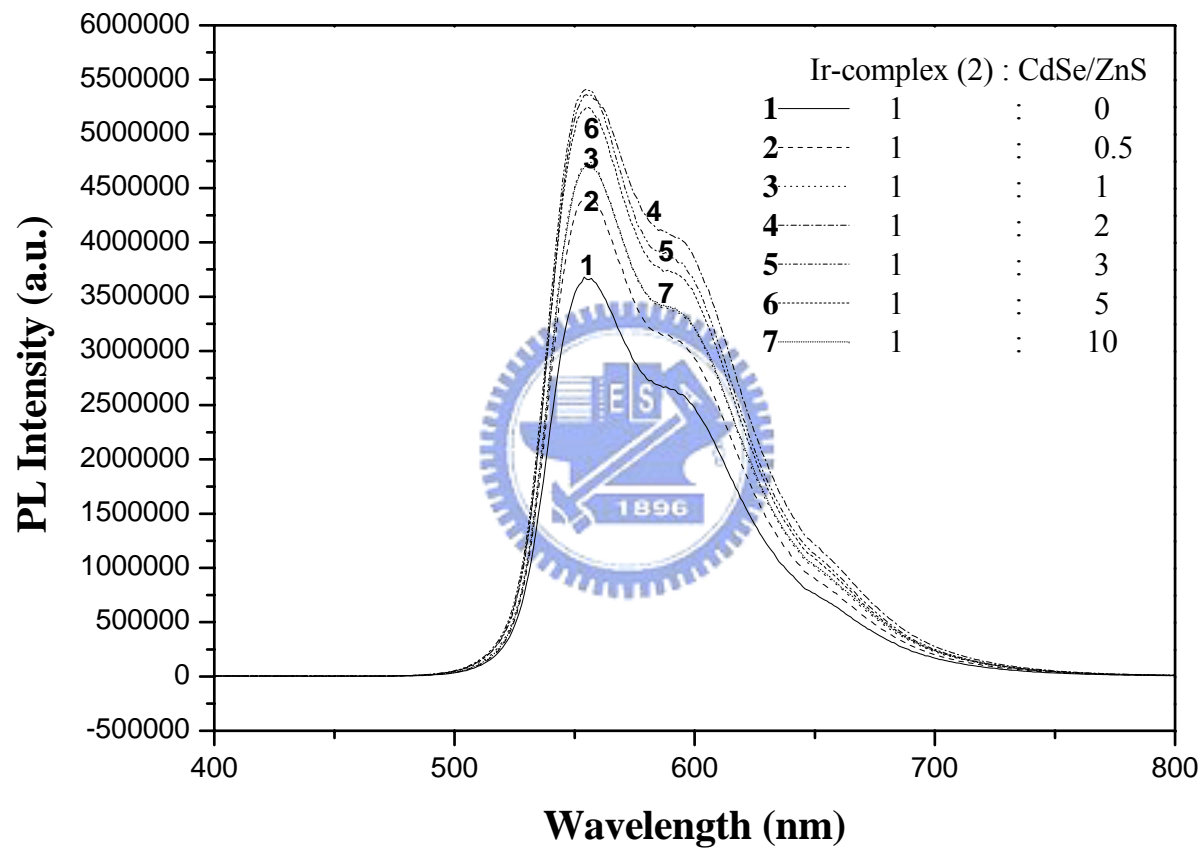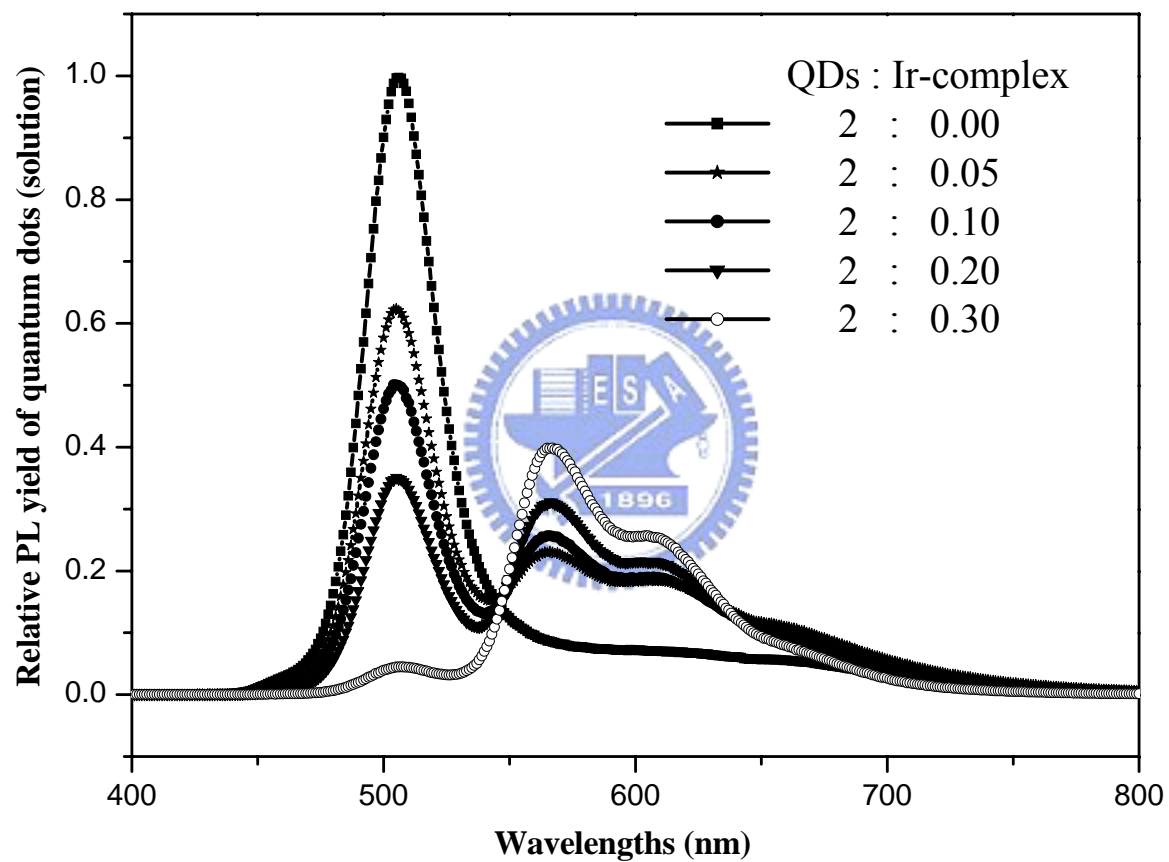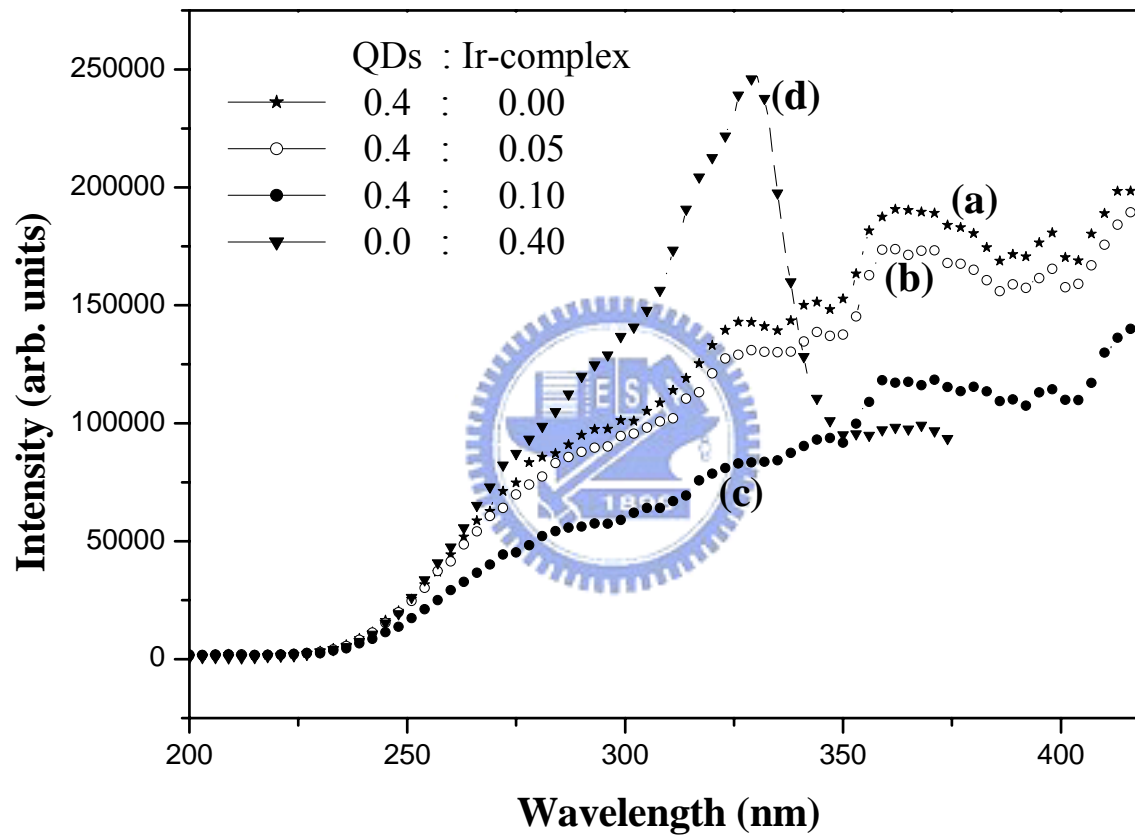
Figure 4.3 Comparison of PL emission spectra for thin films of Ir-complex 2 incorporated with CdSe/ZnS quantum dots in systematic varied proportions.

Figure 4.4 Comparison of PL spectra for the mixture of Ir-complex 1 and QDs dispersed in PMMA matrix in thin film sample with a fixed molar concentration of QDs with increasing order of molar proportion of Ir complex 1.

Figure 4.5 PL spectra for the mixture of Ir-complex 1 and QDs in chloroform with a fixed molar concentration of QDs with increasing order of molar proportion of Ir complex 1.

Figure 4.6 Comparison of excitation spectra for thin film samples of bare CdSe/ZnS QDs (a)**,** mixture of Ir-complex 1 and CdSe/ZnS QDs (b) and (c), bare Ir-complex 1 (d).
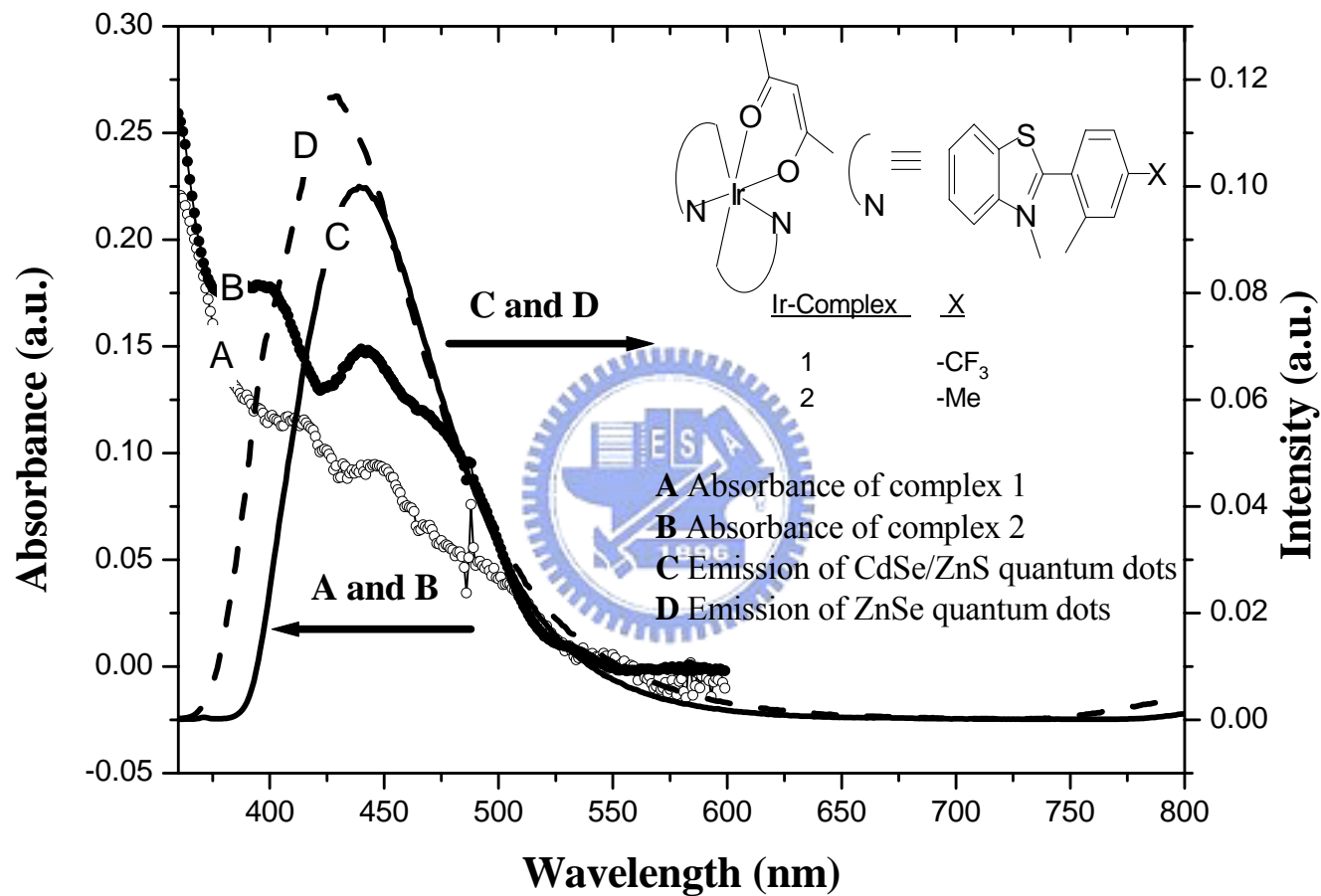
Figure 4.7 Comparison of the absorption spectra of the Ir-complexes 1 and 2 and the emission spectra of CdSe/ZnS and ZnSe QDs showed the extent of overlapping area; molecular structures of ligands and the Ir-complexes appear in inset.
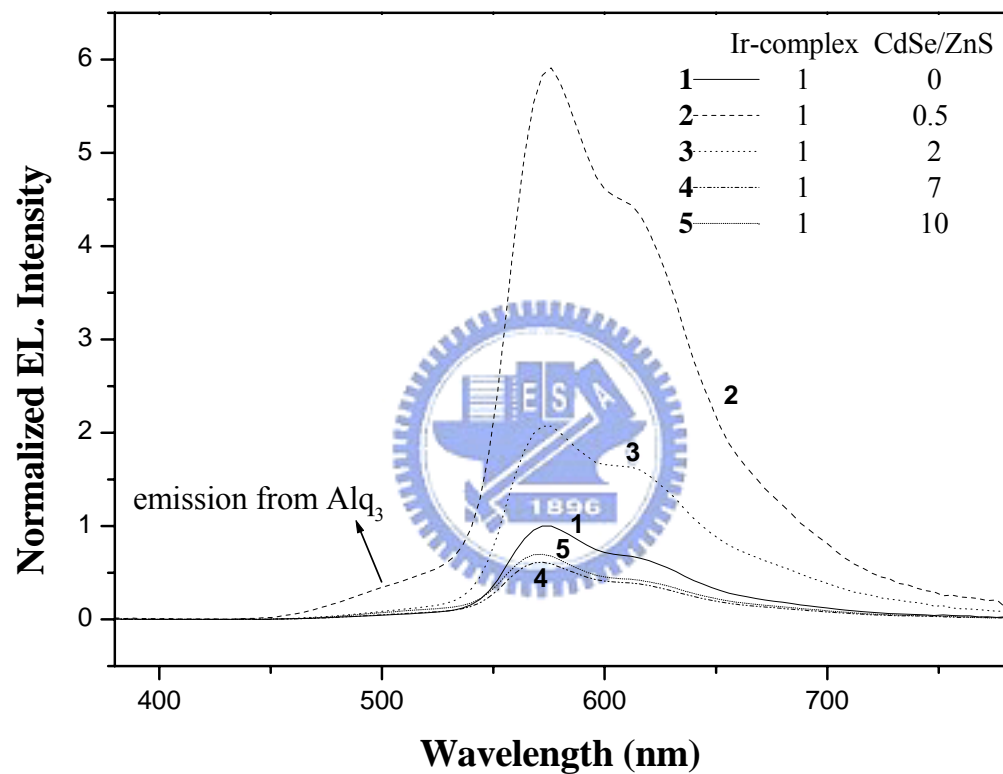
Figure 4.8 Comparison of EL spectra of the fabricated devices with emitting layer of Ir-complex 1 and the CdSe/ZnS QDs dispersed in PVK polymer matrix with fixed molar proportions. EL device layer sequences and their thicknesses are displayed in the inset.
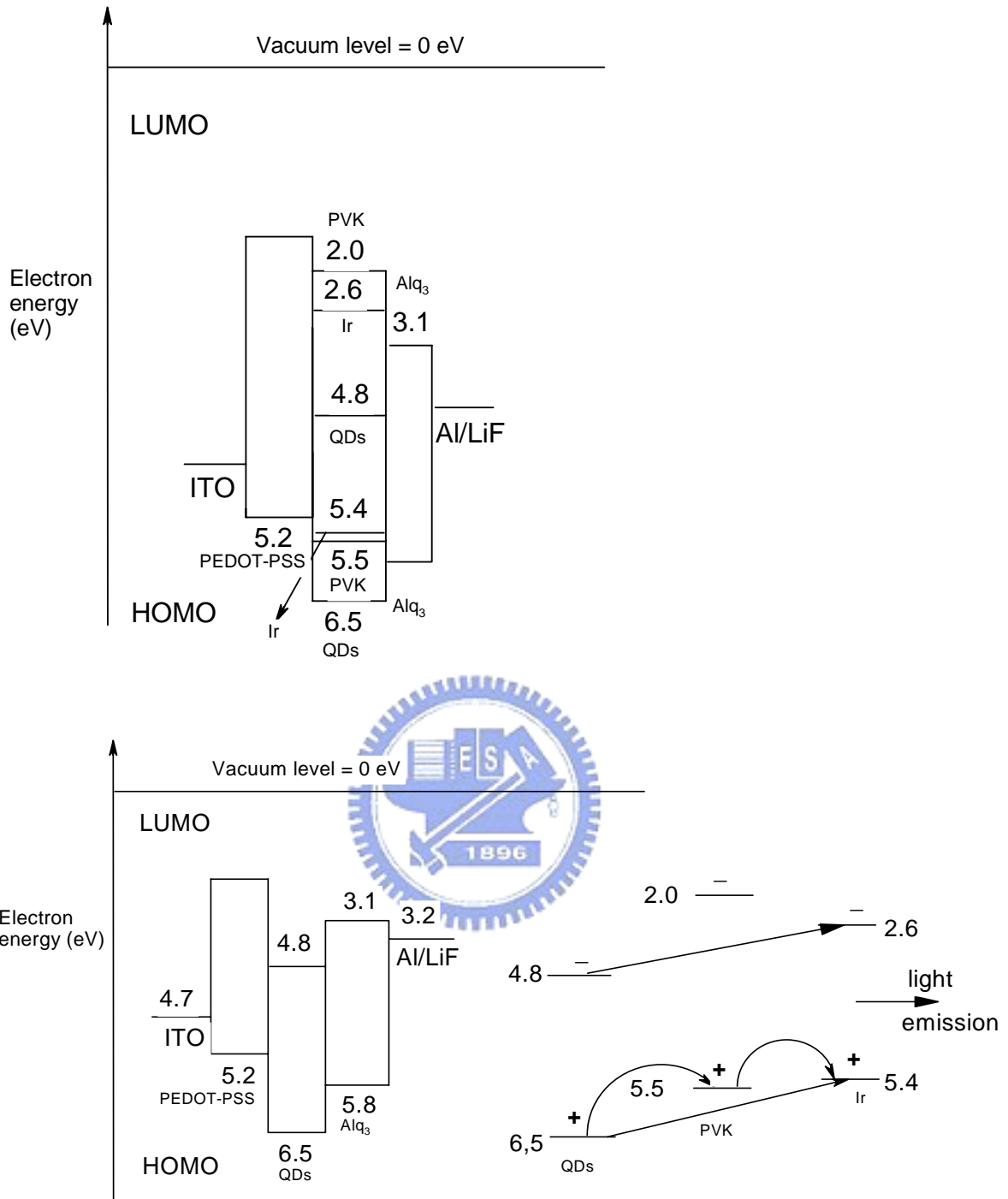
Figure 4.9 Proposed energy level diagram of the EL device; the ionization energy and the electron affinity values of QDs represent the bulk materials, Ir complex measured from cyclic voltametric analysis and the absorption data [7c] and for the remaining materials were collected from the literatures [2b, 13-14].
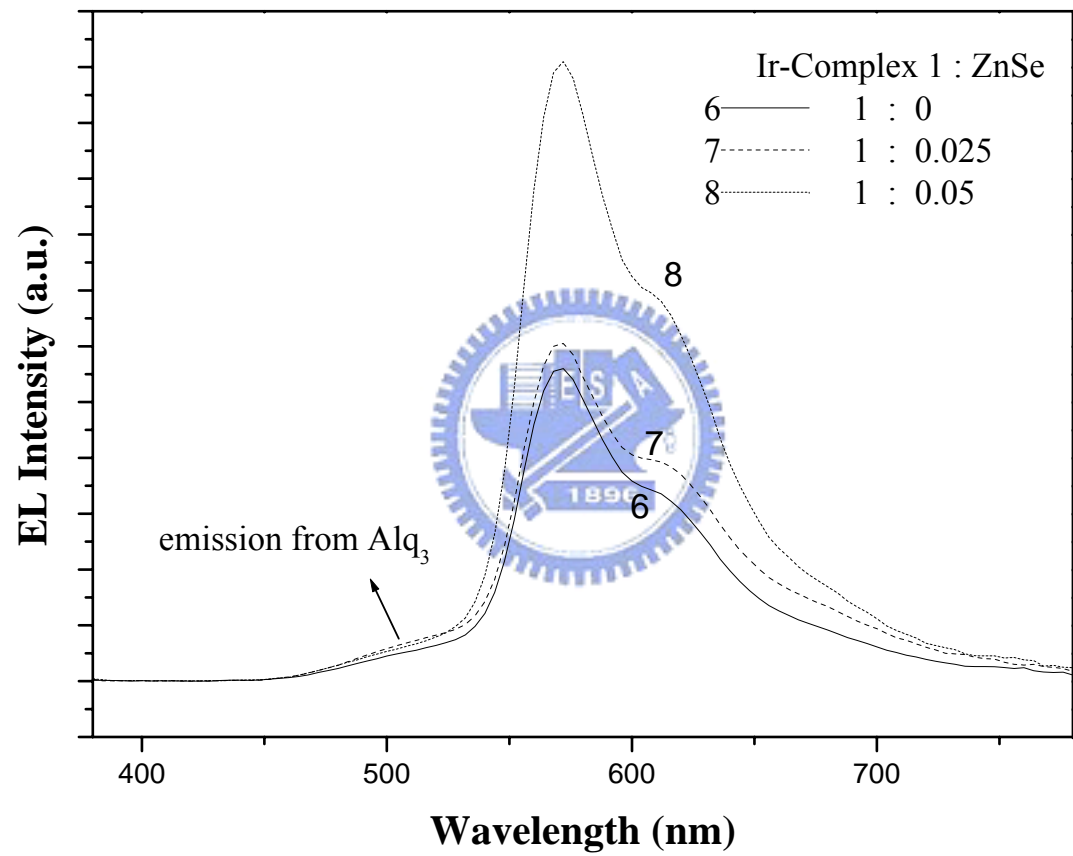
Figure 4.10 Comparison of EL spectra of the fabricated devices with emitting layer of Ir-complex 1 and the ZnSe QDs dispersed in PVK polymer matrix with fixed molar proportions.
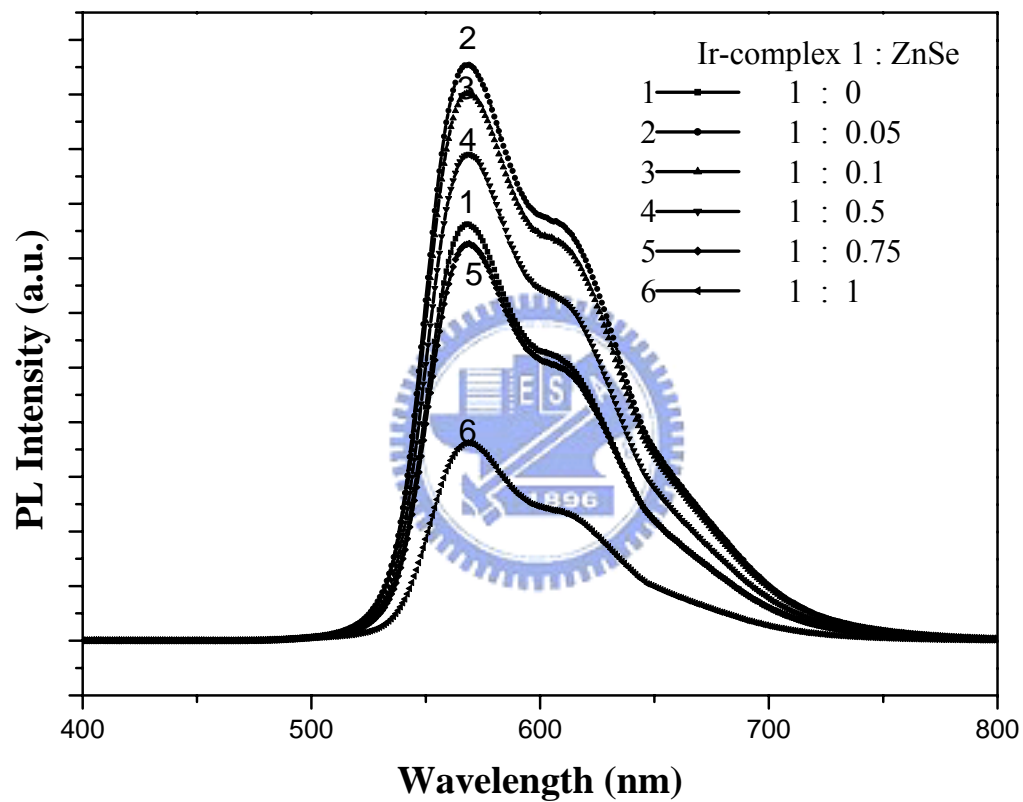
Figure 4.11 Comparison of PL spectra of the mixture of Ir-complex 1 and ZnSe QDs dispersed in PMMA matrix in thin film sample with a definite molar ratio. On increasing molar concentrations of QDs with a fixed molar concentrations of Ir-complex **1**, the PL intensity of the Ir-complex were enhanced until it reached to optimum value.

Table 4.1 Comparative electroluminescent characteristics of all fabricated devices at a fixed current density (4.5 mAcm^{-2}) using Ir-complex 1 and CdSe/ZnS QDs in the emitting layer.

| EL characteristics (Ir-complex 1 : CdSe/ZnS)	D-I (blank)	D-II (1:0.5)	D-III (1:2)	D-VI (1:7)	D-V (1:10)
External quantum yield (CdA^{-1})	3.3	19.3	7.1	2.0	2.3
Luminance (cdm^{-2})	145	858	301	83	95
Turn-on voltage (V)	17.9	21.5	19.4	16.2	14.0
CIE value (x, y)	(0.53, 0.46)	(0.53, 0.46)	(0.54, 0.46)	(0.51, 0.48)	(0.50, 0.48)
Maximum peak wavelength (nm)	576	576	576	572	572

Chapter 5

Enhanced Phosphorescence and Electroluminescence in Triplet Emitters by Doping Gold into Cadmium Selenide/Zinc Sulfide Nanoparticles

Abstract

Gold-cadmium selenide/zinc sulfide (Au-CdSe/ZnS) nanocomposites (NCs) were synthesized and characterized by transmission electron microscopy (TEM), energy dispersive X-ray analysis (EDX), ultraviolet-visible (UV-Vis) absorption and photoluminescence (PL) emission spectroscopy.
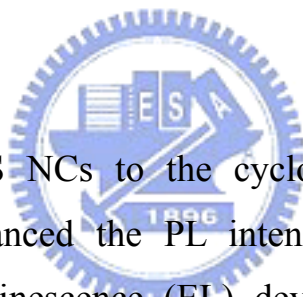
Adding Au-CdSe/ZnS NCs to the cyclometalated iridium(III) complex (Ir-complex) greatly enhanced the PL intensity of a triplet emitter. Three double-layered electroluminescence (EL) devices were fabricated where the emitting zone contains the definite mixture of Ir-complex and the NCs [molar concentration of Ir-complex / NCs = 1 : 0 (Blank, D-**1**), 1 : 1 (D-**2**) and 1 : 3 (D-**3**)] and the device, D-2 exhibited optimal EL performances.

5.1 Introduction

CdSe quantum dots (QDs) exhibit size-dependent tunable PL with broad excitation spectra and narrow emission bandwidths that span the visible spectrum. Therefore, they are potentially useful in a wide range of applications [1-3]. These characteristics of semiconductor CdSe QDs have inspired scientific communities to fabricate hybrid organic light emitting diodes (OLEDs), which combine the diversity of organic materials with the excellent electronic and

optical properties of inorganic materials. Coe *et al.* reported [4] the fabrication of a hybrid OLED, where QDs function exclusively as lumophores. Recently, Chaudhary *et al.* [5] demonstrated a trilayer polymer-quantum dot OLED which was fabricated by sandwiching a CdSe/ZnS QDs layer between films of polyvinylcarbazole (PVK) and butyl-oxadiazole derivative. The benefit of such a QD-based OLED is that each recombination of a hole and an electron generates a photon, resulting in a possible 100 % quantum efficiency at any visible wavelength, since the tuning property of the emission wavelengths depends on the variability of the QDs' size. In most hybrid OLED devices, the ODs themselves act as light emitting centers [4-6]. For the first time, we reported elsewhere [7] that the enhancement of quantum efficiency of a triplet iridium(III) complex (Ir-complex) emitter in presence of CdSe/ZnS QDs in the emitting layer of OLED.

The nonlinear response of composites of nanoparticles (NPs) with a metal and semiconductor suspended in a nonlinear medium exhibited was several orders of magnitude stronger than that of each of their components [8-11]. A strong surface-enhanced Raman scattering (SERS) effect was observed in Au/semiconductor or Ag/semiconductor colloidal nanocomposites (NCs) [8-12]. Nayak *et al.* generated Au-CdSe NCs [13], although a large fraction of the particles was a mixture of individual gold and CdSe NPs, as indicated by transmission electron microscopy (TEM) micrographs. Enhanced optoelelectronic properties have been extensively reported and have been determined from the SERS activity of Au and Ag metallic NPs [14, 15]. These facts motivated the exploration herein of the optical and electronic properties of metallic NPs and CdSe NPs and observations of the effect of these NPs on the PL and electroluminescence (EL) of a triplet emitter. This work reports the syntheses and characterizations of Au-CdSe/ZnS NCs and their applications in enhancing the thin-film PL and EL efficiencies of a triplet iridium (III) emitter when the NCs incorporated into the triplet emitter in the emitting layer of a

hybrid OLED.

5.2 Experimental Section

5.2.1 Chemicals and reagents

Hydrogen tetrachloroaurate (III) and tetraoctylammonium bromide were purchased from Acros Chemicals Company. Cadmium oxide (~1 μm, 99.5 %), selenium (Se) powder (~100 mesh, 99.5+ %), zinc acetate dehydrate (> 98 %), polyvinylcarazole (PVK) and sulfur powder (99.8 %) were all purchased from Aldrich Chemicals (Saint Louis MO, USA). 1-hexdecylamine (HDA, 98+ %), lithium fluoride (LiF), aluminum (Al) was obtained from Lancaster (Lancashire, UK). Tri-*n*-butylphosphine (TBP) was obtained from Showa Chemicals Company (Tokyo, Japan). Anhydrous toluene and chloroform were purchased from TEDIA (Fairfield OH, USA). Bis(4-trifluoro-methyl)-2-phenyl-benzothiazolatoacetyl-acetonate-iridium(III) (Ir-complex) was synthesized following the method reported in the literature [16].

5.2.2 Preparation of Au NPs

The Au NPs were synthesized according to the method reported in the literature [17]. A 25 ml aqueous solution of $HAuCl_4$ (0.3 mmol) was added to an 80 ml toluene solution of tetraoctylammonium bromide (1.8 mmol). The transfer of the Au metal salt to the toluene phase was clearly visualized within a few seconds. 25 ml of 0.25 M $NaBH_4$ solution was then added to the stirred mixture, resulting immediately reduction. The toluene phase was then saved and the water phase was removed.

5.2.3 Preparation of Au-CdSe/ZnS NCs

A mixture of Au and CdSe/ZnS NPs with 0.02 : 1 in molar ratio was prepared as followings. CdO (0.6 mmol) and HDA (9 mmol) were dissolved in 20 ml of tributlyphosphine (TBP). The reaction mixture was then heated at 260 for 2 h under nitrogen atmosphere. 4 ml of Au NPs (3×10^{-3} M) was injected

into the reaction mixture. The prepared Se solution (0.7 mmol of Se in 5ml TBP solution) was immediately injected into the reaction mixture, which was kept at the desired temperature (160 ~ 260   ) for 1 min. Then, zinc acetate (0.1 mmol) and sulfur (0.12 mmol) were dissolved in 5 ml of TBP, and injected into the reaction mixture. The temperature of the reaction mixture was maintained at 120

for 0.5 h. Toluene was injected into the reaction vessel. Other nanocomposites of Au and CdSe/ZnS NPs with different stoichiometries have been prepared following the method described above and all of the samples were dispersed and stored in toluene.

5.2.4 Instrumentations

Raman scattering spectra were obtained using a Jobin Yvon HR 800 spectrometer and a He-Ne laser as a light source. A Jeol JEM-4000EX TEM operated at 200 kV was used to determine the microstructure of QDs and their composition was analyzed using energy dispersive X-ray (EDX) analysis. PL excitation and ambient temperature emission spectra were measured using a Jobin-Yvon Spex Fluorolog 3 spectrofluorometer with a monochromatized Xe light source (450 W). The emission spectra of various NCs were obtained at an excitation wavelength (λ_{ex}) of 367 nm. ultraviolet-visible (UV-Vis) absorption spectra of NCs were measured using a Hitachi U-3010 UV-Vis spectrophotometer. The concentration of the samples for PL and UV-Vis measurements was maintained at the concentration of 1 x 10^{-4} M in toluene. The fluorescence decay lifetimes were obtained by time-correlated single photon counting (TCSPC; Fluo Time 200, Pico-Quant) and the samples were excited by using a short pulse diode laser (LDH-P-C 375, Pico-Quant) at 375 nm.

5.2.5 Fabrication of thin films and EL devices

By spinning from concentrated dispersions in chloroform (3 ml) on flat

quartz substrate of mixture with Ir-Complex : Au-CdSe/ZnS = 1 : 0 to 1 : 5, we have fabricated several uniform thin films comprising a fixed amount of Ir-complex with various molar concentrations of Au-CdSe/ZnS NCs in a fixed amount of Au-CdSe/ZnS PVK matrix. The 1:1 mixture of Ir-complex and Au-CdSe/ZnS NCs (Au : CdSe/ZnS = 0.001 : 1) was prepared as followings. 1 ml of Ir-complex (1.6×10^{-6} M) was mixed with 0.016 ml of Au-CdSe/ZnS (1×10^{-4} M) in chloroform. Similarly, we have prepared other Ir-complex and Au-CdSe/ZnS NCs mixture solutions proportionately. Then, 30 mg of PVK was added to each of the mixtures and the total volume was kept constant at 3 ml by adding chloroform. The thicknesses of the thin films were measured by the alpha-stepper method at various arbitrary points (8 ± 0.5 nm).

A series of double-layered EL device with structure represented in Fig. 5.1 were designed and fabricated. These devices mainly contain green-emitting Au-CdSe/ZnS NCs doped with the orange-emitting iridium (III) triplet emitter in different proportions in the emitting layer. The emitting layer contains Ir-complex and Au-CdSe/ZnS NCs in PVK matrix with the molar ratios of 1 : 0 (Blank, D-**1**), 1 : 1 (D-**2**) and 1 : 3 (D-**3**), respectively. The emitting components were spin-cast from chloroform onto the poly(3,4-ethylenedioxythiophene) (PEDOT)/ poly(4-styrenesulfonate) (PSS)-precoated indium tin oxides (ITO) glass substrates. Tris(8-hydroxyquinolinato)aluminum(III) (Alq$_3$) was subsequently spin-cast onto the emitting layers and LiF/Al cathode was vacuum-deposited on top of the emitting layers at 1.3×10^{-4} Pa. The layer sequences and the thicknesses of each layer were the same across the three fabricated devices. The current-voltage profiles and EL intensity characteristics of the above fabricated devices were measured in a vacuum chamber at 1.3×10^{-4} Pa at ambient temperature using a Keithley 2400 source meter-2000 multimeter, coupled to a PR 650 optical meter.

5.3 Results and discussions

Au-CdSe/ZnS NCs, stabilized in toluene, were successfully synthesized. Figure 5.2 presents the UV-Vis spectra of the CdSe/ZnS NPs and Au-CdSe/ZnS NCs. The sample of CdSe/ZnS NPs alone was found to absorb at 490 nm. At an Au NPs concentration of 0.0025 moles per mole of CdSe/ZnS NPs, the absorption wavelength was found to be blue-shifted with respect to CdSe/ZnS NPs by approximately 20 nm. In general, the Au colloids exhibit absorption with a maximum at 530 nm identified as a surface plasmon band, which was similar to that suggested by Gitlins *et al.* [17]. However, as presented by Fig. 5.2, no surface plasmon band was observed, indicating that the concentration of Au NPs is not sufficiently high enough to reveal the band. The Au NPs are probably covered by CdSe/ZnS NPs, such as Au/CdS NCs [18]. Surfactants tend to make Au-CdSe/ZnS NCs less responsive to UV-Vis. However, possible electron transfer from CdSe/ZnS NPs to Au was assumed to be responsible for the bleaching of the surface plasmon band and to occur within few picoseconds [18]. Therefore, the absorption actually was observed from the CdSe/ZnS NPs.

Figure 5.3 displays a series of solution PL spectra for samples of Au-CdSe/ZnS NCs with various molar proportions of Au to CdSe/ZnS in toluene. The emission of Au-CdSe/ZnS was slightly blue-shifted from that of pure CdSe/ZnS NPs. Surprisingly, the PL intensity of Au-CdSe/ZnS NCs was found to exceed that of CdSe/ZnS NPs. The highest PL intensity was found for the sample with the molar ratio Au:CdSe/ZnS = 0.001 : 1 and the PL intensity was found to be 1.5 times higher than that of CdSe/ZnS. The observed dramatic increase in the PL intensity of Au-CdSe/ZnS NCs was probably attributable to the SERS-activity of Au metal in Au-CdSe/ZnS NCs [14, 19]. When more Au NPs were incorporated into CdSe/ZnS NPs, the concentration quenching of PL intensity of Au-CdSe/ZnS NCs is expected.

The diameter of Au NPs was found to be around 5 nm and that of green-emitting CdSe/ZnS NPs was ~1 nm as determined by TEM. As shown in

Fig. 5.4(a), the TEM image of Au-CdSe/ZnS NCs where the amount of CdSe/ZnS NPs used to prepare Au-CdSe/ZnS NCs was 50 times larger than that of the Au-precursor. This large quantity of CdSe/ZnS NPs used with respect to the Au NPs suggests that almost all the Au particles have been covered by the CdSe/ZnS NPs. It has been supported by the observed diameters of the particles shown in the TEM image (Fig. 5.4(a)) which falls in the range of 6 ~ 8 nm. A similar observation has also been reported earlier by Kamat and co-workers [18] in their study of Au/CdS composite nanoclusters. The characteristic EDX elemental analytical data represented in Fig. 5.4(b) demonstrate the presence of Au, Cd, Se, Zn and S, supporting the formation of Au-CdSe/ZnS NCs.

Figure 5.5 represents the Raman spectra of Au NPs, CdSe/ZnS NPs and Au-CdSe/ZnS NCs (with Au: CdSe/ZnS = 1 / 50), respectively. It was suggested that the SERS activity of the gold NPs was supported by the observed strong enhancement in the Raman signal [20, 21] in Au-CdSe/ZnS NCs. In the given spectral range, three Raman peaks at 731 cm^{-1}, 801 cm^{-1} and 978 cm^{-1} were observed in the sample of Au-CdSe/ZnS with a high proportion of Au in CdSe/ZnS (with Au : CdSe/ZnS = 1 / 50) (as shown in Fig. 5.5), whereas no discernible Raman features were observed from the bare Au and CdSe/ZnS NPs. It is proposed that the increased PL intensity (as shown in Fig. 5.3) is attributed to the presence of the SERS-active Au NPs.

The Strickler-Berg relation [22] was used to determine the radiative lifetime (τ_R) of CdSe/ZnS and Au-CdSe/ZnS NCs. The fluorescence decay was examined by TCSPC techniques and the average lifetime (τ_S) was obtained [22]. The number of photons emission per electron absorption (quantum yield) of Au-CdSe/ZnS NCs was calculated from Eq. (1).

$$\text{Quantum yield} = \frac{\tau_S}{\tau_R} \qquad (1)$$

As depicted in Table 1, optimal fluorescence quantum yield was obtained for the NCs with Au : CdSe/ZnS = 0.001 : 1 and at the same concentration the maximum quantum yield was found to be almost 1.5 times higher than that of CdSe/ZnS NPs (without Au doping).

Many optical and physical properties of colloidal CdSe NPs, including their energy transfer mechanism and excited-state lifetime, are not yet well understood. The Ir-complex is a good phosphorescent material for use in OLEDs and CdSe NPs is a fluorescence material with excellent optical characteristics. It is curious to observe the effect on PL-intensity/quantum efficiency of an Ir-based triplet emitter on gradual increasing of molar concentration of Au-CdSe/ZnS NCs into the Ir-complex. A series of thin films were fabricated, in which the amount of Au-CdSe/ZnS NCs was varied by increasing the molar proportions of Au-CdSe/ZnS NCs, while the molar concentration of Ir-complex was held constant (see experimental section). Fig. 5.6(a) indicates that the PL intensity dramatically increased with the doping concentrations of Au-CdSe/ZnS NCs at an exciting wavelength, 330 nm. Fig. 5.6(a) reveals that the PL emission intensity was maximum for the composition Ir-complex : Au-CdSe/ZnS = 1 : 3 and was approximately ten times greater than that of the blank Ir-complex.

Figure 5.6(b) presents the UV-Vis absorption spectra of the Ir-complex doped in the thin-film with PVK as a matrix. Several broad absorption bands of metal to ligand charge transfer transitions (^{1}MLCT and ^{3}MLCT) [16] from 375 nm to 575 nm, and the emission spectrum of CdSe NPs excited by light with a wavelength of 330 nm. were observed. The emissive region (360-600 nm) of Au-CdSe/ZnS NCs was clearly found to overlap with the absorptive part of the Ir-complex, suggesting that the photons were effectively absorbed by both NCs and the Ir-complex, and that the energy absorbed by the NCs was transferred efficiently to the Ir-complex triplet emitter, increasing the PL intensity, as observed [23]. The Ir-complex was a phosphorescent material with strong emission around 575 nm. The aggregation of NCs in the solid film was such that

the PL emission of NCs was too weak to be observed clearly in Fig. 5.6(a).

It has been attempted to explore the energy transfer mechanism involved in the Ir-complex / NCs thin films. In this case, the fluorescence decay of NCs was determined based on time-resolved luminescence measurements, as shown in Fig. 5.7. It is observed that the fluorescence decay lifetime for mixtures of Au-CdSe/ZnS NCs and Ir-complex is much shorter than that of bare NCs. When each of the decay kinetics was treated as a two-exponent curve [24, 25], it was deconvoluted and resolved as slow and fast components of decay, respectively. Due to the pulse limitation of TCSPC, it was only possible to resolve the component of the slow decay compontent. As shown in Fig. 5.7, the PL lifetime for the mixtures containing Au-CdSe/ZnS NCs and Ir-complex is much shorter than that of Ir-complex free NCs alone, which also supports the energy transfer from NCs to the triplet emitter [26]. Hence, it can be proposed that the enhanced luminescence of Ir-complex can probably be attributed to non-radiative energy transfer from the NCs to Ir-complex. The decay lifetime decreases from 4.0 ns (for sample of Au-CdSe/ZnS NCs alone) to 2.6 ns (for sample with Ir-complex : NCs = 1 : 1) and 2.0 ns (for that with Ir-complex : NCs = 1 : 3), respectively. If the observed slow decay of the donor (NCs) following pulse excitation is a single exponential, then the measurement of the decay lifetime in the presence (τ_D) and absence (τ_0) of energy transfer is a straightforward method of determining the transfer rate constant, in that case the efficiency of the energy transfer can be determined by using time-resolved method [22]. The efficiency of energy transfer can be described by the equation (2):

$$\text{Efficiency of energy transfer} = \frac{\tau_0 - \tau_D}{\tau_0} \tag{2}$$

The efficiency of energy transfer calculated from the above equation was found to be 35% and 51 % for the samples of Ir-complex and Au-CdSe/ZnS NCs having molar ratios of 1 : 1 and 1 : 3, respectively.

The EL devices were designed and fabricated with the structure depicted in Fig. 5.1. EL luminance was found to be maximal in the device D-2, but that for D-3 was found to be lower than that of D-1, as presented in Fig. 5.8. Luminescence decay in D-3 was attributed to quenching in the device with a higher concentration of Au-CdSe/ZnS NCs. As revealed by the PL spectra represented in Fig. 5.6(a), the main EL emission of the three devices originated from the Ir-complex, while the electron transport material Alq$_3$ was associated with the weaker emission around 520 nm. Table 5.2 presents the comparative EL characteristics of all fabricated devices. At a fixed current density (44.5 mA/cm^2), D-2 performed best among the three devices and the corresponding EL luminance was found to be 521 cd/m^2. All three devices exhibited similar commission internationale del'Eclairage 1931 (CIE 1931) coordinates and maximal emission wavelength. Excitons are suggested to be generated in the Ir-complex *via* two parallel processes. Firstly, excitons are generated on NCs and then Förster-type energy transfer undergoes efficiently to the Ir-complex and secondly, direct charge trapping by the Ir-complex occurs. The excitons on the Ir-complex subsequently decay radiatively.

The quantum efficiency of the present device was not found as we expected for the previous devices fabricated based on only CdSe/ZnS NPs [7]. As presented in Fig. 5.8, the broad emission of the three devices observed near 520 nm was associated primarily with the electron transport material Alq$_3$. This observation suggests that the recombination of holes and electrons in the emitting zone was ineffective, leading to low quantum efficiency. A hole-blocking layer between the emitting and electron transport layers can be assumed to be required to confine the holes and electrons in the emitting zone. More attempts will be made to improve the efficiency of this device in the future.

5.4 Conclusion

A series of Au-CdSe/ZnS NCs with significantly higher quantum efficiencies than prestine CdSe/ZnS NPs, was synthesized and characterized. The observed enhancement of PL and EL intensity and the quantum efficiencies of fabricated EL devices supported the observed efficient energy transfer from the Au-CdSe/ZnS NCs to the triplet iridium (III) emitter. The energy transfer has also been evidenced by the time-resolved PL measurement. The enhancement in the PL intensity of the Ir-complex observed in the thin-film sample was found to increase with increasing doping concentration of Au-CdSe/ZnS NCs in the emissive layer, but the EL performance was not as expected. This investigation demonstrated that the novel energy transfer from the NCs to the Ir-complex is of great interest and reveals the feasibility of applying NCs in hybrid OLEDs. The authors are now focusing on improving device performance by either optimizing the thicknesses of the layers or incorporating a hole-blocking layer between the emitting and electron transport layers.
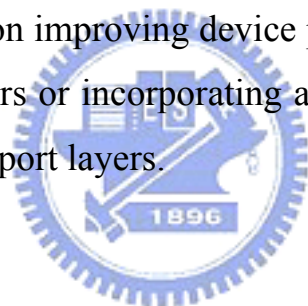
5.5 References

[1] M. Bruchez, M. Moronne, P. Gin, S. Weiss, A. P. Alivisatos, Science **281** (1998) 2013.

[2] W. C. W. Chan, S. M. Nie, Science **281** (1998) 2016.

[3] H. Mattoussi, L. Radzilowski, B. Dabbousi, E. Thomas, M. Bawendi, M. Rubner, J. Appl Phys. **83** (1998) 7965.

[4] S. Coe, W.-K. Woo, M. Bawendi, V. Bulovic, Nature **420** (2002) 800.

[5] S. Chaudhary, M. Ozkan, W. C. W. Chan, Appl. Phys. Lett. **84** (2004) 2925.

[6] T. Tsutsui, Nature **420** (2002) 752.

[7] I. R. Laskar, H. W. Liu, C. P. Huang, J. A. Cheng, T. M. Chen, Jpn. J. Appl. Phys. Lett., **44** (2005) 727.

[8] I. Honma, T. Sano, H. Komiyama, J. Phys. Chem. **97** (1993) 6692.

[9] M. Kerker, C. G. Blatchford, Phys. Rev. B **26** (1982) 4052.

[10] T. M. Cotton, R. A. Uphaus, D. Mobius, J. Phys. Chem. **90** (1986) 6071.

[11] M. Kerker, O. Siiman, D. S. Wang, J. Phys. Chem. **88** (1984) 3168.

[12] G. Oldfield, T. Ung, P. Mulvaney, Adv. Mater. **12** (2000) 1519.

[13] R. Nayak, J. Galsworthy, P. Dobson, J. Hutchinson, J. Mater. Res. **13** (1998) 905.

[14] J. H. Park, Y. T. Lim, O. O. Park, Y. C. Kim, Macromol. Rapid Commun. **24** (2003) 331.

[15] J. W. Hu, G. B. Han, B. Ren, S. G. Sun, Z. Q Tian, Langmuir **20** (2004) 8831.

[16] I. R. Laskar and T-M. Chen, Chem. Mater. **16** (2004) 111.

[17] D. I. Gittins, F. Caruso, Angew. Chem. Int. Ed. **40** (2001) 3001.

[18] P. V. Kamat, B. Shanghavi, J. Phys. Chem. B. **101** (1997) 7675.

[19] J. H. Park, Y. T. Lim, O. O. Park, J. K. Kim, J.-W. Yu, Y. C. Kim, Chem. Mater. **16** (2004) 688.

[20] T. Zhu, X. Zhang, J. Wang, X. Fu, Z. Liu, Thin Solid Films **327-329** (1998) 595.

[21] S. Sanchez-Cortes, C. Domingo, J. V. Garcia-Ramos, J. A. Aznarez, Langmuir **17** (2001) 1157.

[22] B. Valeur, Molecular fluorescence: principles and applications; Wiley-VCH : New York; (2002) p. 42, 172.

[23] A. R. Clapp, I. L. Medintz, J. M. Mauro, B. R. Fisher, M. G. Bawendi, H. Mattoussi, J. Am. Chem. Soc. **126** (2004) 301.

[24] X. Y. Wang, J. Y. Zhang, A. Nazzal, M. Darragh, M. Xiao, Appl. Phys. Lett. **81** (2002) 4829.

[25] B. R. Fisher, H. J. Eisler, N. E. Stott, M. G. Bawendi, J. Phys. Chem. B. **108** (2004) 143.

[26] Z. Tang, B. Ozturk, Y. Wang, N. A. Kotov, J. Phys. Chem. B. **108** (2004) 6927.

Table 5.1 Room-temperature luminescence and decay parameters for Au-CdSe/ZnS NCs samples with various ratios of CdSe/ZnS and Au NPs in toluene.

Au : CdSe/ZnS (molar ratio)	PL (λ_{max})	τ_R [a] (ns)	τ_S [b] (ns)	Quantum yield [c]
0 : 1	507	31.8	14.1	0.44
0.0005 : 1	502	31.9	20.7	0.65
0.001 : 1	498	29.8	20.7	0.69
0.0025 : 1	501	27.2	16.5	0.61

[a] Radiative lifetime was calculated by using Strickler-Berg relation

[b] Average decay time at room temperature

[c] Quantum yield = τ_S / τ_R

Table 5.2 Comparative EL characteristics of all fabricated devices (D-**1**, D-**2** and D-**3**) at a fixed current density of 44.5 mA/cm^2.

EL characteristics	D-1	D-2	D-3
External quantum yield (cd/A)	0.8	1.2	0.7
Luminance (cd/m^2)	353	521	267
Drive voltage (V)	5.5	5.9	7.2
CIE 1931 value (x, y)	(0.45, 0.49)	(0.46, 0.49)	(0.46, 0.49)
λ_{max} of EL (nm)	568	568	568

Al/LiF (200 nm)

Alq$_3$ (30 nm)

Ir-complex & Au-CdSe/ZnS NCs in PVK (60 nm)

PEDOT : PSS (70 nm)

ITO
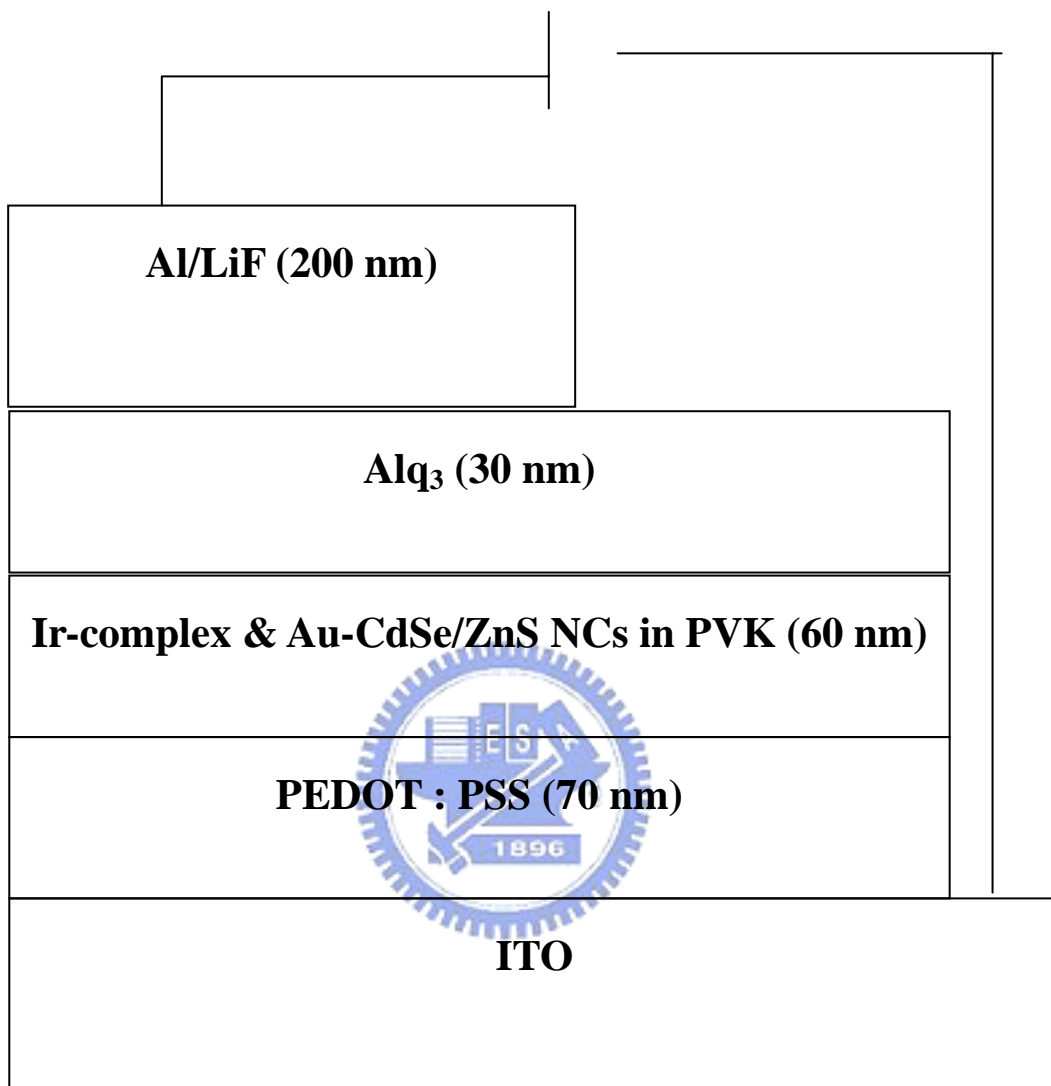
Figure 5.1 The EL device structure with Au-CdSe/ZnS NCs and Ir-complex in PVK matrix as emitting materials.
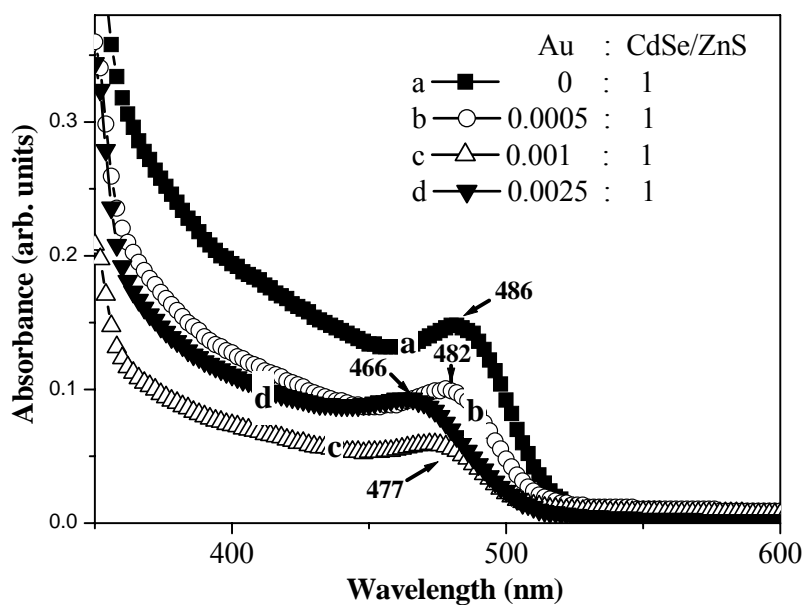
Figure 5.2 UV-Vis absorption spectra of CdSe/ZnS NPs and Au-CdSe/ZnS NCs in toluene (concentration =1 x 10^{-4} mol/L); Au-CdSe/ZnS NCs show blue-shifted absorbance as compared to CdSe/ZnS NPs.
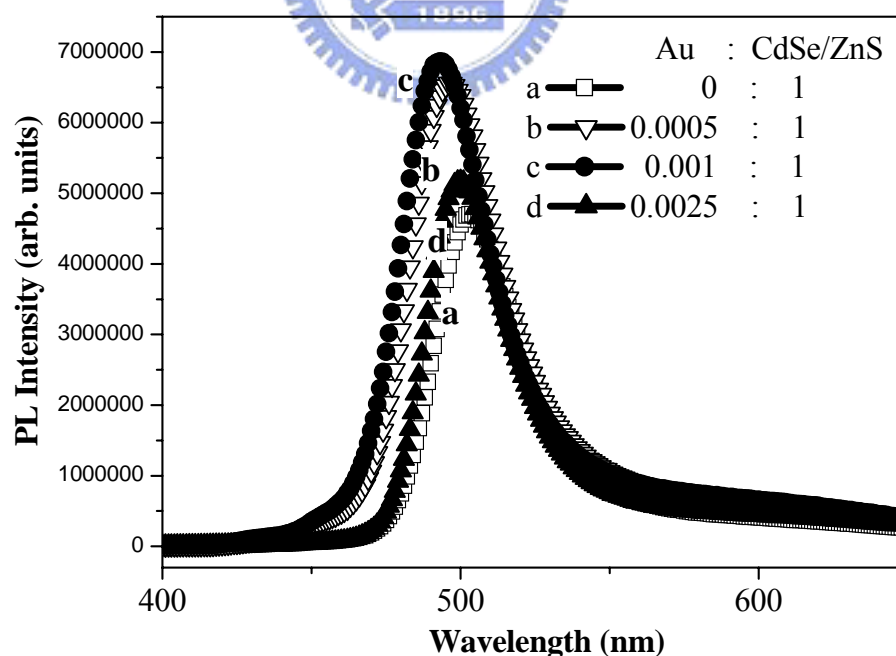
Figure 5.3 Comparison of PL spectra for of CdSe/ZnS NPs and Au-CdSe/ZnS NCs in toluene (concentration =1 x 10^{-4} mol/L).
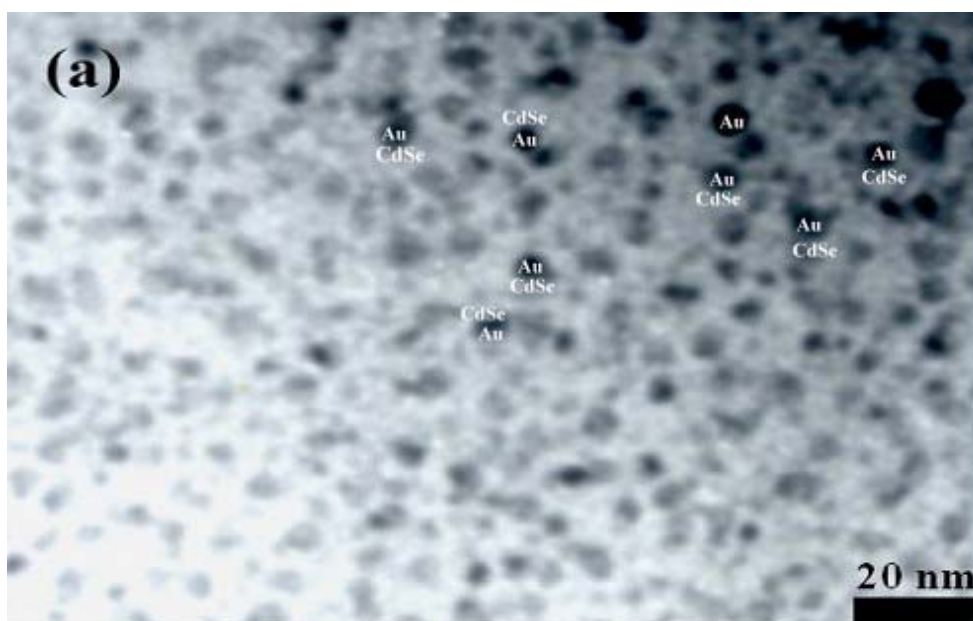
Figure 5.4(a) TEM micrograph of Au-CdSe/ZnS NCs.
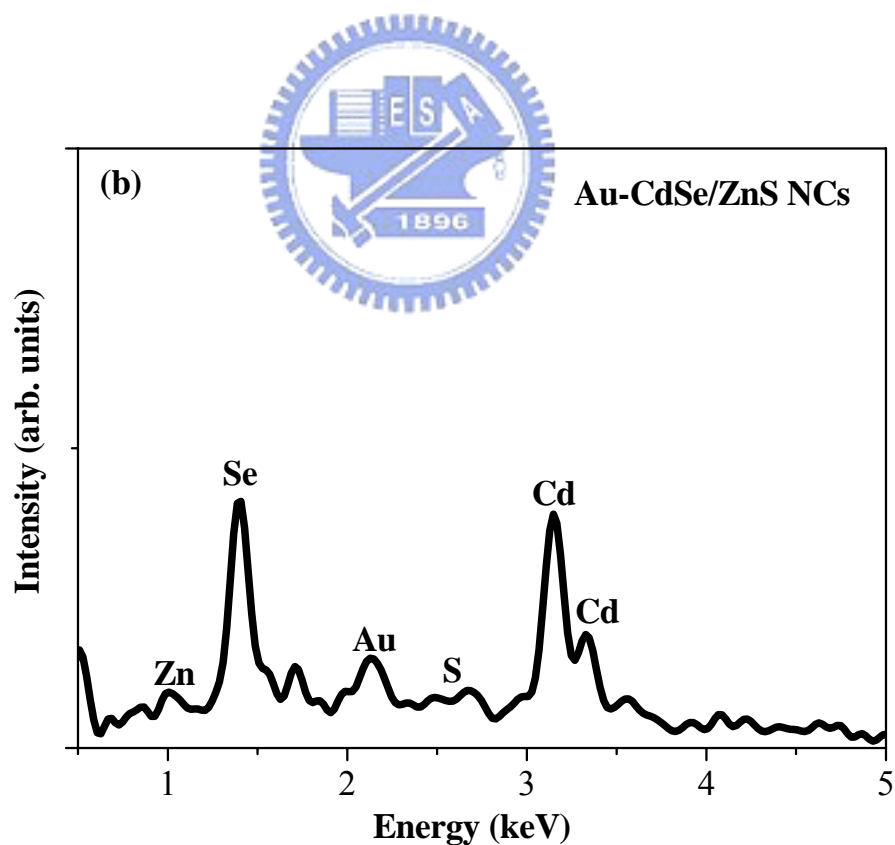
Figure 5.4(b) EDX elemental analysis for Au-CdSe/ZnS NCs.
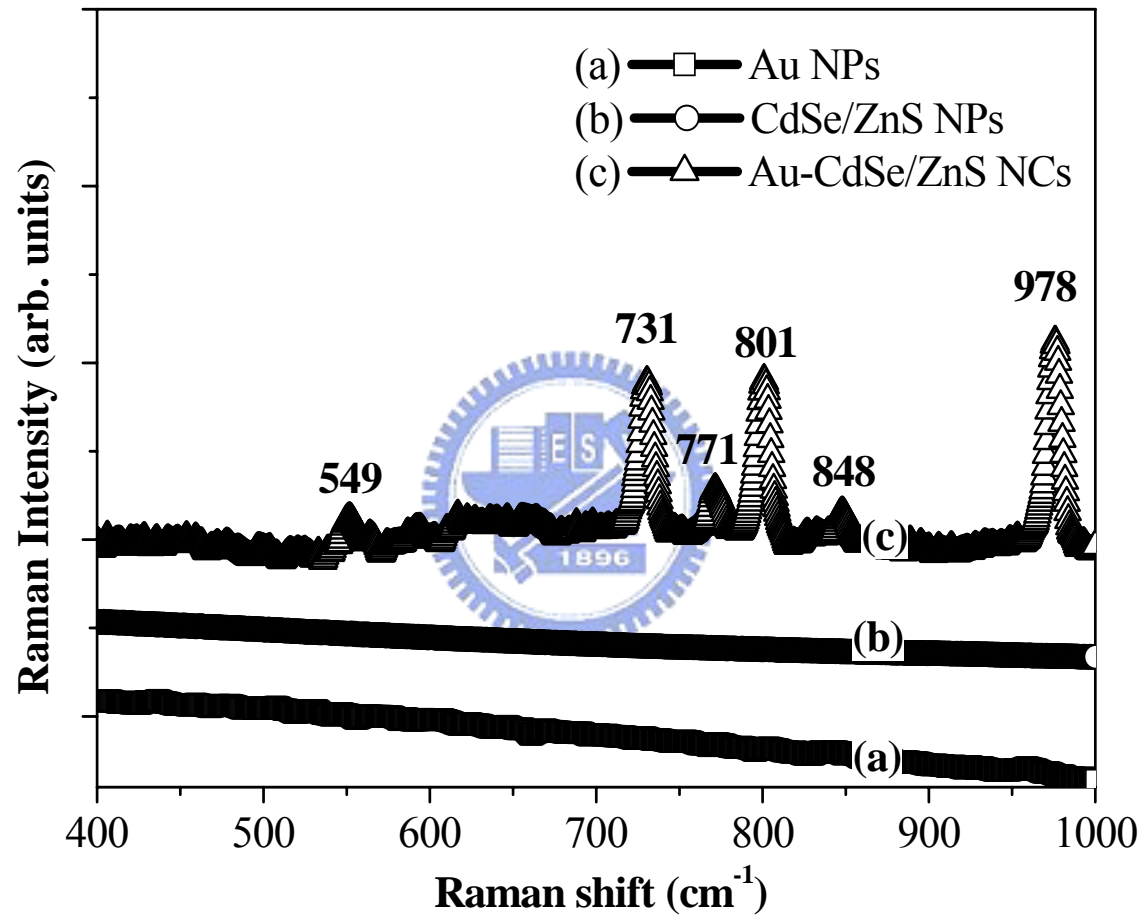
Figure 5.5 Raman scattering spectra for the (a) Au NPs, (b) CdSe/ZnS NPs and (c) Au-CdSe/ZnS NCs (Au : CdSe/ZnS = 1 : 50). Raman signals are clearly observed in Au-CdSe/ZnS hybrid NPs. [20, 21]
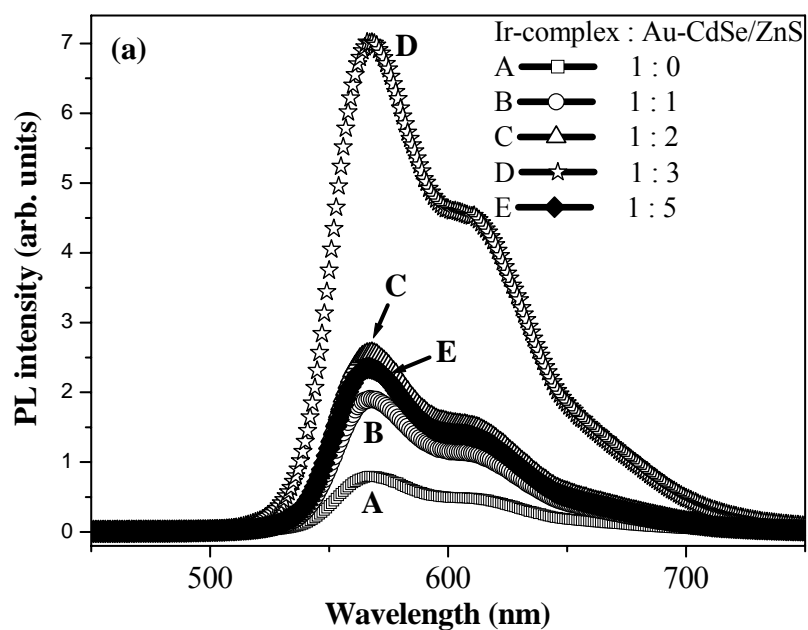
Figure 5.6(a) Solid-state thin-film PL spectra of fixed molar concentration of Ir-complex incorporated by various concentration of Au-CdSe/ZnS NCs in PVK matrix.
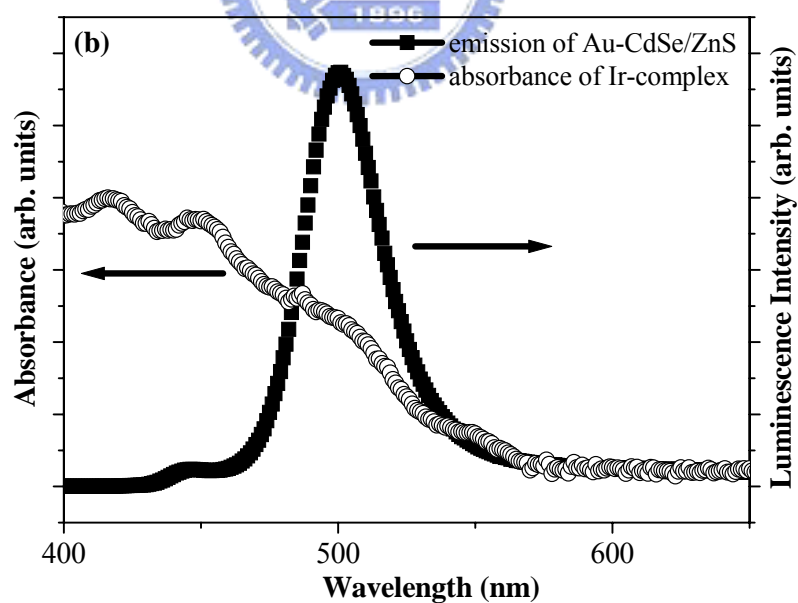
Figure 5.6(b) UV-Vis absorption spectrum of Ir-complex in PVK matrix and PL spectrum of Au-CdSe/ZnS NCs in the PVK matrix, showing the overlapping region.
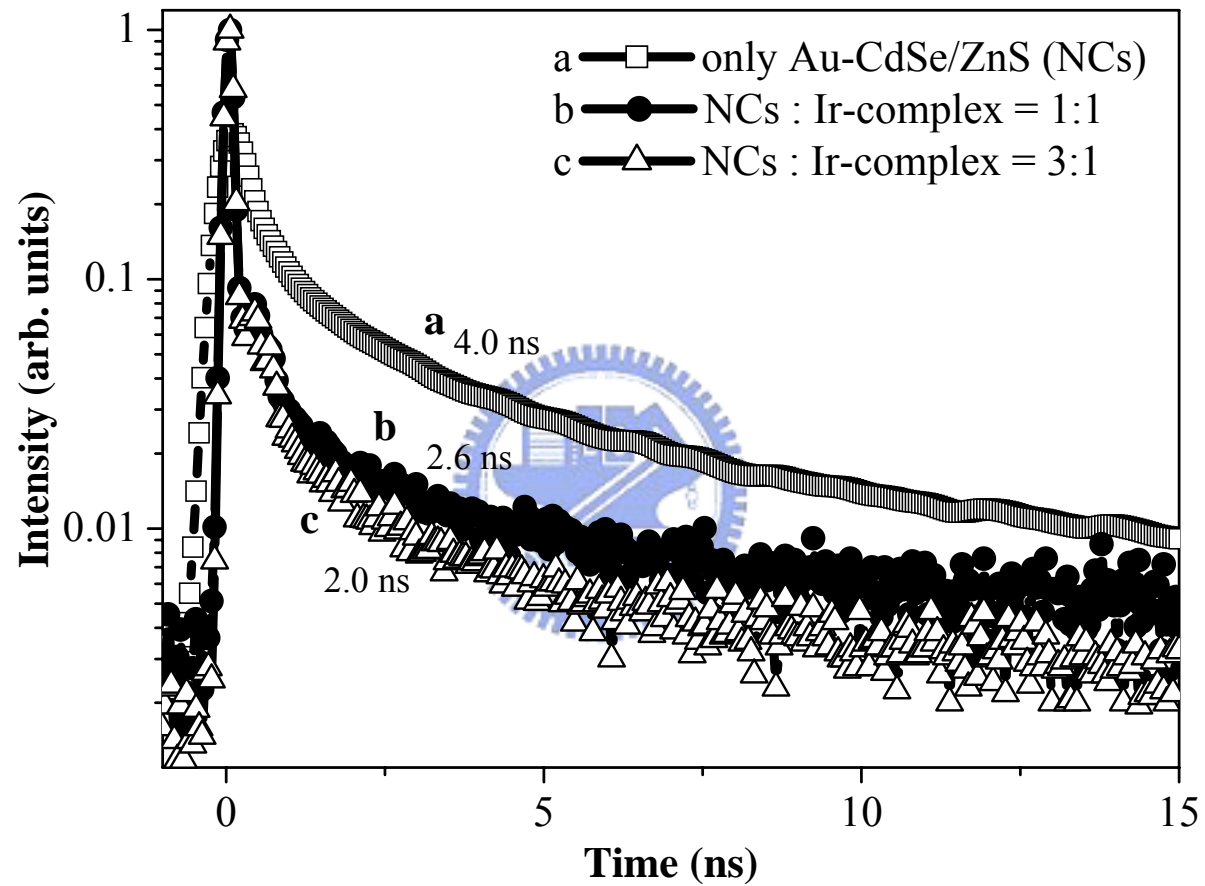
Figure 5.7 Time-resolved photoluminescence decay curves for Au-CdSe/ZnS NCs films doped with the Ir-complex.
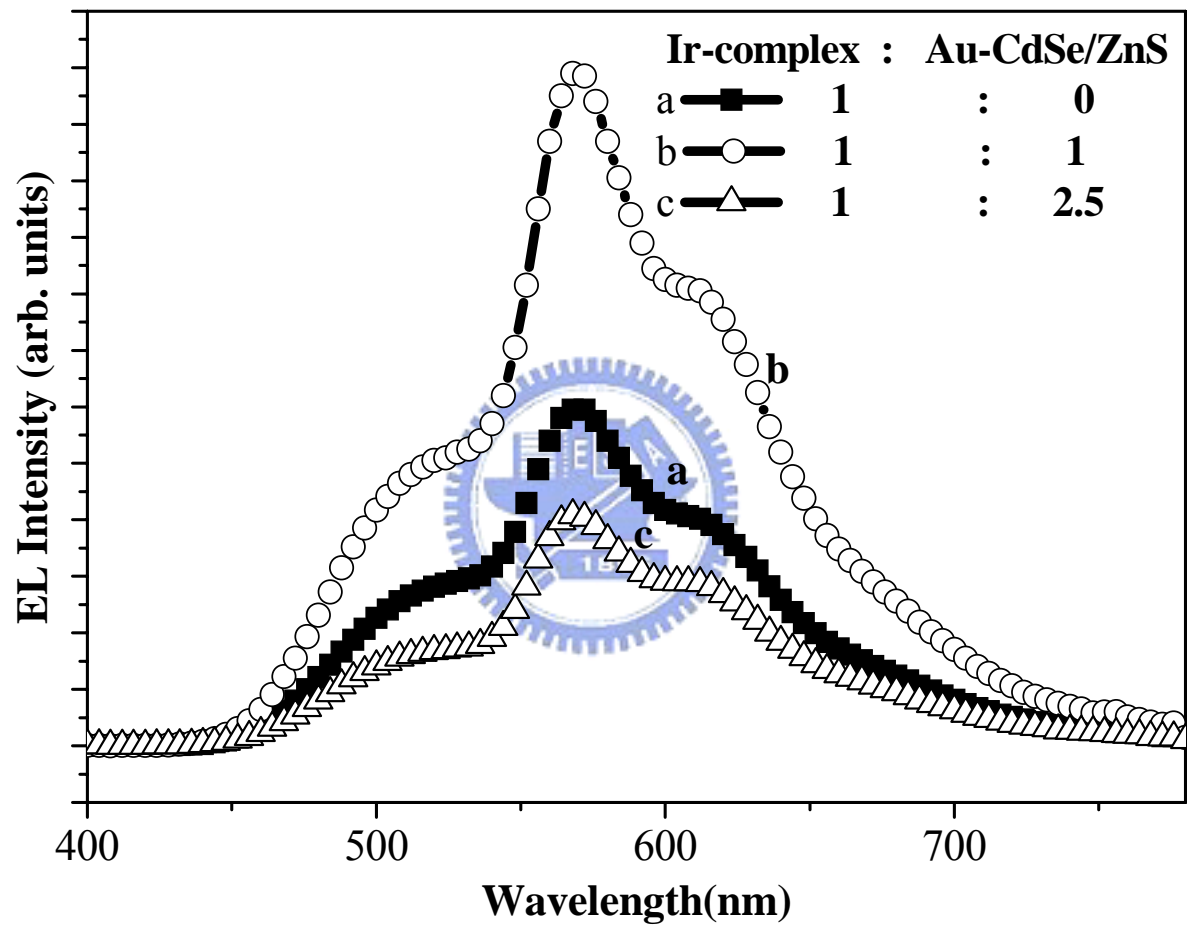
Figure 5.8 EL emission spectra of the fabricated devices with different molar proportions of the Ir-complex and Au-CdSe/ZnS NCs as emitting layer in PVK matrix.

Chapter 6

Conclusions and Future Work

In the present work, we have successfully synthesized a series of high-quality CdSe, CdSe/ZnS QDs and Au-CdSe/ZnS NCs by simple chemical colloid methods. In this study, CdSe/ZnS QDs were applied in OLEDs and biochips. The PL intensity of Au-CdSe/ZnS NCs was found to exceed that of CdSe/ZnS NPs. The optimal fraction of Au NPs incorporated into CdSe NPs was found to be 0.1% Au NPs, which shows the highest PL intensity. The PL quantum efficiency of Au-CdSe/ZnS NCs was found to increase by ~ 70%. The observed drastic increase in luminescence intensity of Au-CdSe/ZnS NPs can probably be attributed to the existence of surface plasma excitation of Au when the PL spectrum for Au-CdSe/ZnS is compared with that of CdSe/ZnS NPs.

Adding CdSe/ZnS NPs and Au-CdSe/ZnS NCs to the cyclometalated iridium (III) complexes greatly enhanced the PL intensity of a triplet emitter. These double-layered EL devices were fabricated and exhibited optimal EL performances as compared to blank device. The PL and EL enhancement of the triplet emitter were also strongly supported by using ZnSe QDs rather than CdSe/ZnS QDs.

By employing a modified synthetic route, we have synthesized high-quality HDA-and MAA-capped (or MSA-capped) CdSe QDs that exhibit decent PL intensity and photostability. To investigate the fluorescent CdSe/ZnS QDs as a potential bio-labeling agent for detecting allergens in immuno-assay, we have bound QDs to streptavidin to form QDs-streptavidin complexes, which were further bioconjugated specifically to form a series QDs-streptavidin-biotin--human-IgE complexes. We report the fluorescence spectra of QDs, dynamic range of fluorescence characteristics for QDs-streptavidin, and laser confocal

imaging for bioconjugated complexes. We have set up models and the empirical dynamic fluorescence calibration curves will be used as a basis to fabricate immuno-assay biosensors.

To obtain high-quality QDs, surface-modification of inorganic QDs is important to prevent the aggregation of QDs. In future work, synthesis and characterization of polymer-capped luminescent quantum dots is an important subject in our research. Enhanced phosphorescence of phosphorescent materials with doped small amounts of QDs was confirmed in our study. According to above results, improving the performance of EL devices is one of our future work. Recently, with the development of magnetization pigments in nanometer size range, the use of advanced metal pigments in flexible technology has expanded dramatically. The other future work of our research is the preparation of magnetic metal pigments (ie., Fe-Co & Sm-Co alloys). These metal alloys are planned to apply in bio-technology in the future.

List of Publications and Presentations

A. Journal Papers:

[1] H. W. Liu, I. R. Laskar, C. P. Huang, J. A. Cheng, S. S. Cheng, T. M. Chen, "Enhanced Phosphorescence and Electroluminescence in Triplet Emitters by Doping Gold into Cadmium Selenide / Zinc Sulfide Nanoparticles", Thin Solid Films, in press, available online, 15 June (2005).

[2] I. R. Laskar, H. W. Liu, C. P. Huang and T. M. Chen , "Observation of Enhanced Phosphorescence from a Triplet Emitter by Quantum Dot Doping", Japanese Journal of Applied Physics, **44 (23)** (2005) L727-L730..

[3] C. P. Huang**,** H. W. Liu**,** C. Y. Tsao, L. T. Yin, S. F. Chiu and T. M. Chen, "Plate-based biochemical assay using quantum dots as a fluorescent labeling agent", Sensors and Actuators B Chemical, **108** (2005) 713.

[4] H. W. Liu, I. R. Laskar, C. P. Huang, J. A. Cheng, S. S. Cheng, T. M. Chen, "Synthesis and Application of Luminescent CdSe Quantun Dots for OLEDs", Chinese Journal of Luminescence, 26(3) (2005) XX-XX..

[5] H. W Liu, C. P. Huang, K. C. Liu, T. M. Chen, "Synthesis, Characterizations and Applications of Surface-Functionalized CdSe Quantum Dots in Immuno-assay", Japanese Journal of Applied Physics, submitted (2005).

B. International Conference Papers and Posters

[1] H. W. Liu, I. R. Laskar, C. P. Huang and T. M. Chen, "Observation of Enhanced Luminescence from Visible Emitter by Quantum Dots Doping", The 71th Meeting of the Chinese Chemical Society, Taoyuan, Taiwan, 2003, In-PA-177.

[2] H. W. Liu, C. P. Huang and T. M. Chen, "Enhanced Photoluminescence Observed in Core-shell Composites of Au/CdSe and Au/CdSe/ZnS Nanocrystals", Taiwan International Conference on Nano Science and Technology, Hsinchu, Taiwan, 2004, poster session II, p. 101-103.

[3] C. P. Huang, H. W. Liu and T. M. Chen, "Development of a Plate-based Biochemical Assay by using Quantum Sots as a Fluorescence Labeling Agent", Taiwan International Conference on Nano Science and Technology, Hsinchu, Taiwan, 2004, poster session II, p. 68-71.

[4] H. W. Liu, I. R. Laskar, C. P. Huang and T. M. Chen, "Synthesis and Application of Luminescent CdSe Quantun Dots for OLEDs", The 10th Annual Chinese Luminescence Conference, Dalian, China, 2004.

[5] H. W. Liu, I. R. Laskar, C. P. Huang and T. M. Chen, "Enhanced Electroluminescence in Triplet Emitters by Doping of Modified CdSe Nanoparticles", The 72th Meeting of the Chinese Chemical Society, Taichung, Taiwan, 2004, ICS-B-166.

[6] C. P. Huang , H. W. Liu, C. Y. Tsao, L. T. Yin, S. F. Chiu and T. M. Chen, "The Fabrication and Characterizations of a Plate-base Biochemical Assay by using Water-soluble Fluorescent Quantum Dots", The 72th Meeting of the Chinese Chemical Society, Taichung, Taiwan, 2004, ICS-B-164.

[7] H. R. Wang, H. W. Liu and T. M. Chen, "Sensitized Photoluminescence of CdSe/ZnS Quantum Dots by Doping Metal Nanoparticles", The 72th Meeting of the Chinese Chemical Society, Taichung, Taiwan, 2004, ICS-B-154.

Appendix
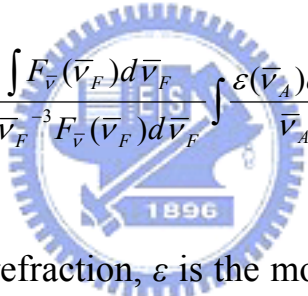
The quanum yield (QY) can be calculated by the equation:

$$QY = \frac{\tau_S}{\tau_R}$$

$_R$: radiative lifetime

$_S$: average decay lifetime

The Strickler-Berg relation is represented as:

$$\frac{1}{\tau_R} = 2.88 \times 10^{-9} n^2 \frac{\int F_{\bar{v}}(\bar{v}_F) d\bar{v}_F}{\int \bar{v}_F^{-3} F_{\bar{v}}(\bar{v}_F) d\bar{v}_F} \int \frac{\varepsilon(\bar{v}_A) d\bar{v}_A}{\bar{v}_A}$$

Where n is the index of refraction, ε is the molar absorption coefficient, $F_{\bar{v}}$ is the intensity corresponding to the emission wavenumber of PL emission, $\bar{v}_F$ is the wavenumber of PL emission, and $\bar{v}_A$ is wavenumber of UV-absorption. The Strickler-Berg equation yields values of τ_R that are often in agreement with experimental ones.

The results of TCSPC data were fitted by a stretched multi-exponential decay model as described in the following:

$$y(\tau) = A_1 \exp(\frac{-\tau_1}{\tau}) + A_2 \exp(\frac{-\tau_2}{\tau}) + A_3 \exp(\frac{-\tau_3}{\tau}) + A_4 \exp(\frac{-\tau_4}{\tau}) \ + \ldots\ldots\ldots$$

When the fluorescence decay of a fluorophore is multi-exponential, the natural way of defining an average decay lifetime (τ_S) is as follow:

$$\tau_s = \sum_{i=1}^{n} f_i \tau_i$$

(Here, $\sum_{i=1}^{n} f_i = 1$, f_i : fractional contribution)

The quanum yield can be calculated by the equation :

$$QY = \frac{\tau_S}{\tau_R}$$